

/SIMULATION STUDIES OF VELOCITY SEDIMENTATION
FOR MIXED ASSOCIATING SYSTEMS/

by

GLEN MICHAEL DELOID

B.S., Kansas State University, 1980

A MASTER'S THESIS

submitted in partial fulfillment of the
requirements for the degree

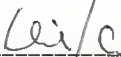
MASTER OF SCIENCE

Graduate Biochemistry Group
Department of Biochemistry

KANSAS STATE UNIVERSITY
Manhattan, Kansas

1984

Approved by:


Major Professor

ACKNOWLEDGEMENTS

I would like to thank Dr. David Cox for the privilege and pleasure of working with him on this project and for his unlimited patience and understanding in encouraging and guiding my progress.

I would also like to thank the members of my committee, Dr. Burkhard, Dr. Mueller and Dr. Roche, for taking the time and effort to wade through this rather cumbersome document on regrettably short notice, and for their helpful suggestions.

In terms of the actual physical construction and production of this thesis a sizable portion of the credit must be given to John Robarge who mediated and facilitated many of our interactions with the computer. As our investigations and their documentation (this thesis) were both heavily computerized John's contribution was an invaluable one.

I would also like to thank John and Kathy King for coming to my rescue when time was fleeting and madness was taking its toll (August, 1983; 110°F in the shade). John typed most of the text into the computer while Kathy decorated and labeled computer generated plots in addition to drawing several original figures for the thesis.

CONTENTS

ACKNOWLEDGEMENTS ii

<u>Chapter</u>	<u>page</u>
I. INTRODUCTION	1
II. THE DISTORTED GRID METHOD	4
Initialization of the Simulation Arrays	5
Simulation of Diffusion	11
Systems not Undergoing Mixed-Association	11
Mixed Associating Systems	15
Computing Gradients at Box Boundaries	19
Computation of Diffusion Coefficients	23
Non-Interacting Systems	23
Self-Associating Systems	24
Mixed-Associating Systems	27
Simulation of Sedimentation	29
Computation of Sedimentation Coefficients	31
Non-Associating Systems	31
Self-Associating Systems	32
Mixed-Associating Systems	34
Computing Local Constituent Concentrations	35
Table Assemblies	36
Self-Associating systems	39
Mixed Associating Systems	45
Table Look-Up	62
Re-Indexing	79
Regulating Box Sizes	82
Box Splitting	83
Box Squashing	87
Time Intervals	90
Sedimentation Transfer Time	90
Diffusion Transfer Time	91
Time Averaging	95
III. EXPERIMENTS AND SIMULATIONS	97
Uncooperative AB _n Systems	97
Effect of K_{1n} on Boundary Shape	105
Comparison of Uncooperative AB _n Boundary Shapes	120
Effect of Constituent Mole Ratio	126
Systems with Non-Identical Monomers	133

Completely Cooperative Systems	148
Effect of Constituent Mole Ratio	173
Cooperative Systems with Nonidentical Monomers	181
General AB_2 Systems	190
Effect of Aggregate Frictional Ratios	213
Effect of Hydrodynamic Dependence	217
Effect of Self Association	233
Effect of Non-Interacting Contaminants	244
Fixed Dimer	245
Crippled Monomer	250
IV. DISCUSSION	257
REFERENCES	261

LIST OF TABLES

<u>Table</u>	<u>page</u>
1. Varieties of Table Assemblies	38
2. Species Transport Coefficients and Positions (at 2155.51sec) for Systems with $W_A=W_B=100Kd$	104
3. Species Transport Coefficients and Positions for Systems with $W_A=140Kd > W_B=60Kd$	139
4. Species Transport Coefficients and Positions for Systems with $W_B=140Kd > W_A=60Kd$	140

LIST OF FIGURES

<u>Figure</u>	<u>page</u>
1. Ultracentrifuge Cell at t_0	5
2. Gradient Interpolation Scheme	20
3. Topologies of Sedimentation Coefficient Tables for an Uncooperative AB_2 System ($K_I=10^6$)	46
4. Topologies of Sedimentation Coefficient Tables for a Completely Cooperative AB_2 System ($K_{2M}=10^{10}$)	48
5. Types of Table Organization	73
6. Boundary Movement	80
7. Box Splitting and Re-indexing	87
8. Box Squashing	89
9. Rectangular Boxes, Equal Box Widths	92
10. Gradient Profiles of Uncooperative AB_n Systems	99
11. Gradient Profiles of AB Systems of Different Strengths	102
12. Gradient Profiles Uncooperative AB_2 Systems of Different Strengths	106
13. Species Concentrations and Average Sedimentation Coefficients for Uncooperative AB_2 Systems	108
14. Gradient Profiles of Uncooperative AB_3 Systems of Different Strengths	112
15. Gradient Profiles Uncooperative AB_4 Systems of Different Strengths	114
16. Species Concentrations and Average Sedimentation Coefficients for Uncooperative AB_3 Systems	116

17.	Species Concentrations and Average Sedimentation Coefficients for Uncooperative AB_4 Systems . . .	118
18.	Leading Boundary Heights (H_L) and Positions (R_L) of Uncooperative AB_n Gradient Profiles . . .	122
19.	Comparison of Uncooperative AB_2 and AB_4 Gradient Profiles	124
20.	Gradient Profiles Uncooperative AB_2 Systems at Different Constituent Mole Ratios	128
21.	Equivalence Mole Ratio vs. $\log_{10} K_I$ for Uncooperative AB_2 and AB_4 Systems	130
22.	Gradient Profiles Uncooperative AB_2 Systems at Different Constituent Mole Ratios	134
23.	Gradient Profiles of Uncooperative AB_2 Systems with Non-Identical Monomers	136
24.	Gradient Profiles of Uncooperative AB_2 Systems of Different Strengths with Non-Identical Monomers ($W_A > W_B$)	141
25.	Gradient Profiles of Uncooperative AB_2 Systems with $W_A > W_B$ at Different Constituent Mole Ratios	144
26.	Gradient Profiles of Uncooperative AB_2 Systems with $W_B > W_A$ at Different Constituent Mole Ratios	146
27.	Gradient Profiles of Completely Cooperative AB_2 Systems of Different Strengths	151
28.	Gradient Profiles of Completely Cooperative AB_4 Systems of Different Strengths	153
29.	Boundary Heights (H_L and H_T) and Leading Boundary Positions (R_L) for Cooperative AB_n Gradient Profiles	155
30.	Species Concentrations and Average Sedimentation Coefficients for Completely Cooperative AB_2 Systems	157
31.	Species Concentrations and Average Sedimentation Coefficients for Completely Cooperative AB_4 Systems	159
32.	Comparison of Boundary Dimensions for Uncooperative and Cooperative AB_n Systems . . .	162

33.	Gradient Profiles of an Uncooperative AB_4 and Completely Cooperative AB_2 System with Similar Leading Boundaries	164
34.	Comparison of Completely Cooperative AB_2 and AB_4 Gradient Profiles	167
35.	Comparison of Completely Cooperative and Uncooperative AB_2 Gradient Profiles	169
36.	Comparison of Completely Cooperative and Uncooperative AB_4 Gradient Profiles	171
37.	Gradient Profiles of a Completely Cooperative AB_2 Systems at Different Constituent Mole Ratios	174
38.	Gradient Profiles of a Weak Completely Cooperative AB_2 Systems at Different Constituent Mole Ratios	176
39.	Gradient Profiles of Completely Cooperative AB_4 Systems at Different Constituent Mole Ratios	178
40.	Gradient Profiles of Completely Cooperative AB_4 Systems of Different Strengths with $w_A > w_B$	183
41.	Gradient Profiles of Cooperative AB_4 Systems with $w_A > w_B$ at Different Constituent Mole Ratios	185
42.	Gradient Profile of a Completely Cooperative AB_4 System With $w_B > w_A$	188
43.	Comparison of Boundary Dimensions for AB_2 Systems with Different Degrees of Cooperativity	193
44.	Gradient Profiles of AB_2 Systems with K'_{1M} and K'_{2M} Varied Independently	195
45.	Changes in Boundary Dimensions with K'_{2M} for AB_2 Systems with K'_{1M} Constant	198
46.	Comparison of Boundary Dimensions for AB_2 Systems with Different values of K'_{2M}	200
47.	Species Concentrations for AB_2 Systems	202
48.	Average Constituent Sedimentation Coefficients for AB_2 Systems	204

49.	Gradient Profiles of Two AB_2 Systems at Two Different Constituent Ratios	206
50.	Changes in Boundary Dimensions With K'_{2M} for AB_2 Systems with K_{1M} Constant	209
51.	Comparison of Boundary Dimensions for AB_2 Systems with Different Values of K_{2M} at a 2:1 Constituent Mole Ratio	211
52.	Gradient Profiles of Uncooperative AB_2 Systems with Different Aggregate Frictional Ratios	215
53.	Effect of Overall Hydrodynamic Dependence on Boundaries of Uncooperative AB_2 Systems	220
54.	Effect of Overall Hydrodynamic Dependence on Bimodality of Uncooperative AB_2 Profiles	223
55.	Effects of Cross Hydrodynamic dependence on Boundaries of Uncooperative AB_2 Systems	226
56.	Effects of Individual Self Hydrodynamic Dependences on Boundaries of Uncooperative AB_2 Systems	228
57.	Effects of Individual Cross Hydrodynamic Dependences on Boundaries of Uncooperative AB_2 Systems	231
58.	Effect of Self Association of A on the Boundary of an Uncooperative AB_2 System at a 1:1 Constituent Ratio	235
59.	Effect of Self Association of B on the Boundary of an Uncooperative AB_2 System at a 1:1 Constituent Ratio	237
60.	Effect of Self Association of A on the Boundary of an Uncooperative AB_2 System at a 2:1 Constituent Ratio	240
61.	Effect of Self Association of B on the Boundary of an Uncooperative AB_2 System at a 2:1 Constituent Ratio	242
62.	Effect of Fixed A_2 on the Boundary of an Uncooperative AB_2 System.	246
63.	Effect of Fixed B_2 on the Boundary of an Uncooperative AB_2 System.	248

64.	Effect of Crippled A Monomer on the Boundary of an Uncooperative AB_2 System.	252
65.	Effect of Crippled B Monomer on the Boundary of an Uncooperative AB_2 System.	254

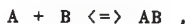
Chapter I

INTRODUCTION

Two very fundamental functional properties of an associating system of macromolecules are: (1) the stoichiometries of the interactions that occur (i.e. the compositions of the molecular species that exist) in solution and (2) the equilibrium constants that govern these interactions¹.

To determine these properties of a system, thermodynamic equilibrium techniques such as osmometry, light scattering, equilibrium sedimentation and small angle X-ray scattering are usually employed. The variations of molecular weight

¹ The Law of Mass Action states that the rate of a reaction at a given time is proportional to the active masses of reacting substances present at the time. Thus, for the reversible reaction:



the speed with which A and B react is proportional to the product of their activities. The rate of the forward reaction, v_1 , is given by $k_1(A)(B)$, and that of the reverse reaction, v_2 , by $k_2(AB)$. At equilibrium, $v_1 = v_2$ and hence, also at equilibrium,

$$k_1(A)(B) = k_2(AB),$$

and therefore,

$$k_1/k_2 = (AB)/(A)(B)$$

averages with the concentrations of the interacting constituents, obtained by these methods, provide diagnostic data which, ideally, would fit only one correct reaction model for the system.² Frequently, however, more than one reaction scheme can fit all of the molecular weight data equally well, and additional experiments are required to eliminate the remaining incorrect reaction models.

One potential source of complementary distinguishing data is the behavior of the system during a mass migration experiment such as velocity sedimentation. If the shape of a system's migrating boundary is a distinctive indicator of its reaction pattern, as it is generally thought to be, then a comparison of the real system's boundary shapes with boundary shapes predicted for different possible model systems should help to eliminate at least some of the ambiguity.

To predict the shapes of migrating boundaries for interacting systems during velocity sedimentation experiments it is necessary to invoke numerical methods, since analytical solutions do not exist for the differential (continuity) equations that describe the behavior of interacting systems during transport. Several such numerical methods have been developed and computerized for simulating velocity sedimentation in the ultracentrifuge (2-38).

This last quantity defines the equilibrium constant, K_{eq} , for the reaction with the stoichiometry given above.

² An overview of equilibrium methods can be found in (1).

If these techniques are to be useful in distinguishing between various possible models for an interacting system then the sedimenting boundaries of significantly different model systems must not be alike. We are thus interested in knowing the extent to which boundaries of different systems may be distinguished from one another.

In the work described herein the distorted-grid method of Cox (29-35) was used to simulate velocity sedimentation of various systems undergoing mixed association reactions (i.e. reactions between dissimilar protein molecules) and an attempt was made to assess the diversity in the resulting simulated gradient profiles. Only AB_n systems were considered, and, within this class of systems, the focus was almost exclusively on AB_2 systems. AB_2 systems are, conceptually and computationally, the simplest systems among AB_n systems (which are the simplest among A_nB_m systems) and therefore represent a convenient and logical starting point for such studies. These studies are described and discussed in chapters three and four.

The theory of the Cox distorted-grid model for simulating velocity sedimentation is presented in chapter two. This was written primarily as an exercise and is presented here for the sake of completeness. More elegant treatments of this theory may be found elsewhere (29-35).

Chapter II

THE DISTORTED GRID METHOD

In the distorted grid model the ultracentrifuge cell is treated as an array of narrow concentric cylindrical sectors (boxes). The distribution of solute in the model cell is described by three arrays: r , \bar{r} , and \bar{c} . Arrays r and \bar{r} contain the values of the distances from the axis of rotation to the box boundaries and box centers, respectively, and the array \bar{c} contains the values of solute concentrations at the box centers. Thus the j th box in the model would have upper (nearer to the axis) and lower boundaries at r_j and r_{j+1} , respectively and a solute concentration, \bar{c}_j , at its center, \bar{r}_j .

When two different constituents (ie. types of monomeric species) are present, the arrays r , \bar{r} and \bar{c} become two dimensional so that the distribution of each constituent is described independently by its corresponding track of r , \bar{r} and \bar{c} values. For example the j th boundary position, the box center position, and the box center concentration of constituent A would be given by $r_{A,j}$, $\bar{r}_{A,j}$, and $\bar{c}_{A,j}$.

Velocity sedimentation is simulated in the model cell by making the appropriate changes in the three simulation arrays (r , \bar{r} and \bar{c}) to describe sedimentation and diffusion in short time intervals.

An ultracentrifuge cell at time zero in a velocity sedimentation experiment is represented in figure 1. The length of the cell is $r_b - r_t$ where r_b and r_t are the distances from the axis of rotation to the bottom and top of the cell. The initial sharp solute boundary (meniscus) is at r_o and the initial plateau region is between r_o and r_b . Typical values for r_t , r_b and r_o are 6.0, 7.0 and 6.1 cm.

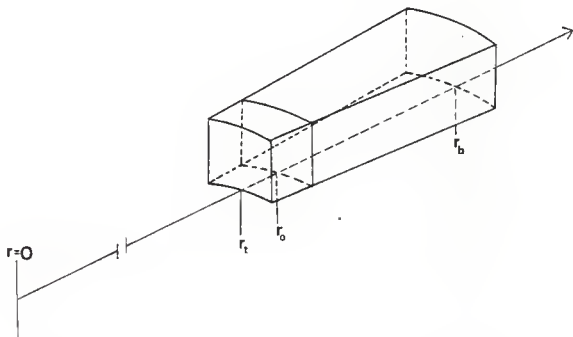


Figure 1: Ultracentrifuge Cell at t_0

2.1 INITIALIZATION OF THE SIMULATION ARRAYS

To simulate a velocity sedimentation experiment, using the distorted grid model, the simulation arrays (r , \bar{r} and \bar{c}) must first be initialized so that they describe the initial conditions in the cell. Array r (box boundary positions) is initialized so that the boundaries are evenly spaced, or otherwise systematically placed, between positions about 0.1

cm above r_0 and the cell bottom³.

To avoid ambiguity in assigning box center concentrations, one of the box boundaries is positioned at the meniscus, r_0 . The initial position of this boundary is then used as a reference point for assigning positions to the boundaries above and below r_0 . For instance if boundaries separated by a constant distance, Δr , are desired and the n th boundary is given the position of r_0 ($r_n = r_0$) then the position of the boundary immediately below r_n is $r_n + \Delta r$ and the position of the boundary immediately above r_n is $r_n - \Delta r$.

The following algorithm illustrates equal box width initialization of boundaries for a 100 box model of a 1.0 cm. cell. Note that the number of box boundaries must always be one greater than the number of boxes and that giving the eleventh boundary the position r_0 places the first ten boxes above r_0 .

³ The upper and lower limits of box boundary positions are not necessarily the same as the positions of the top and bottom of the real cell.

Algorithm

I) number of boxes = 100
 II) cell length = 1.0
 III) $\Delta r = (\text{cell length}) / (\text{num. boxes})$
 IV) $r(11) = r_0$
 V) $j = 11$
 VI) Repeat from $i = 1$ to 10
 A) $j = j - 1$
 B) $r(j) = r(j+1) - \Delta r$
 End Repeat
 VII) Repeat from $j = 12$ to $(\text{num. boxes} + 1)$
 A) $r(j) = r(j-1) + \Delta r$
 End Repeat
 End Algorithm

In some simulation programs the boundaries are not evenly spaced in the initialization routine. Instead they are positioned so that the distance to each boundary from the axis of rotation is greater than that of the boundary immediately above it by a constant factor γ .

$$\gamma = \frac{r_0 + \Delta \bar{r}}{r_0} \quad (1)$$

where $\Delta\bar{r}$ is the average box width. Since r_0 is always much larger than $\Delta\bar{r}$, γ is just slightly greater than one. The following algorithm illustrates initialization of box boundaries using a factor of γ for spacing.

Algorithm

- I) number of boxes = 100
- II) length of cell = 1.0
- III) $\Delta\bar{r} = (\text{length of cell}) / (\text{num. boxes})$
- IV) $\gamma = (r_0 + \Delta r) / r_0$
- V) $r(11) = r_0$
- VI) $j = 11$
- VII) Repeat from $i = 1$ to 10
 - A) $j = j - 1$
 - B) $r(j) = r(j+1) / \gamma$
 - End Repeat.
- VIII) Repeat from $j = 12$ to (num. boxes + 1)
 - A) $r(j) = r(j-1)\gamma$
 - End Repeat.

End Algorithm

The number of boxes used in a simulation is not always 100 but it usually is. Fewer boxes may be used to conserve computer time, but, since a decrease in the number of boxes will result in an increase in the box width, the interpolations of concentrations between box centers that occur dur-

ing the simulation will become less accurate and the simulated result less reliable. On the other hand, very little is usually gained, in terms of precision, by using more than 100 boxes.

With box boundary positions initialized as described above the box center concentrations are initialized to match the situation in the real cell. Boxes below r_0 are given concentrations equal to the initial plateau concentration, C_0 , and boxes above r_0 are assigned initial concentrations of zero. The positions of the box centers are computed from the boundary positions

$$\bar{r}_j = \frac{r_j + r_{j+1}}{2} \quad (2)$$

The algorithm that follows illustrates the initialization of arrays \bar{c} and \bar{r} .

Algorithm

- I) Repeat from $j = 1$ to 10
- A) $\bar{c}_j = 0.0$
- B) $\bar{r}_j = (r_j + r_{j+1})/2$
- End Repeat.
- II) Repeat from $j = 11$ to (nm. boxes)
- A) $\bar{c}_j = C_0$
- B) $\bar{r}_j = (r_j + r_{j+1})/2$
- End Repeat.

End Algorithm

In a two constituent model both constituent tracks are initialized the same way that a single constituent array is initialized. Box boundary positions are given the same values in both tracks ($r_{A,j} = r_{B,j}$). The only difference initially between constituent tracks is in their plateau concentrations $C_{A,0}$ and $C_{B,0}$.

The algorithm above creates a sharp initial boundary, which is the usual choice. It is also possible, and sometimes desirable, to begin with an initial situation in the model cell describing a diffused initial boundary. In this case the initial concentration in each box would either be read directly by the program, or arrived at by subjecting a sharp boundary to a few rounds of simulated diffusion without the corresponding rounds of simulated sedimentation.

Once the arrays have been initialized, the simulation begins, with alternating rounds of sedimentation and diffusion.

2.2 SIMULATION OF DIFFUSION

2.2.1 Systems not Undergoing Mixed-Association

A short interval, Δt_D , of diffusion (without sedimentation) is simulated by computing, for each constituent, the mass of that constituent that would flow upward across each boundary in its track during Δt_D seconds and subsequently computing new constituent concentrations for each box.

In a single constituent system the rate at which constituent mass moves upward in the cell per unit cross sectional area at boundary j is given by Ficks law as:

$$-J = D_j \left[\frac{\partial c}{\partial r} \right]_j \quad (3)$$

where D_j and $(\partial c / \partial r)_j$ are the local average diffusion coefficient and concentration gradient at r_j .

The total flow rate of mass upward at boundary j , F_j , is $-J$ times the cross sectional area of the cell at r_j .

$$F_j = b \theta r_j D_j \left[\frac{\partial c}{\partial r} \right]_j \quad (4)$$

where $b\theta r_j$ is the cross sectional area of the cell at r_j , b and θ are the height and sector angle of the cell.

The mass that would flow past boundary j during the time from t_0 to t_1 , m_j , is given by the following expression.

$$\begin{aligned}
 m_j &= b\theta r_j \int_{t_0}^{t_1} \left[\bar{D}_{o,j} \left[\frac{\partial c}{\partial r} \right]_{o,j} + \frac{\partial \left[\bar{D}_j \left[\frac{\partial c}{\partial r} \right]_j \right]}{\partial t} \right] dt \\
 &\quad (t_0 \leq t \leq t_1) \\
 &= b\theta r_j \int_{t_0}^{t_1} \bar{D}_{o,j} \left[\frac{\partial c}{\partial r} \right]_{o,j} dt + \int_{t_0}^{t_1} \frac{\partial \left[\bar{D}_j \left[\frac{\partial c}{\partial r} \right]_j \right]}{\partial t} dt \\
 &\quad (t_0 \leq t \leq t_1)
 \end{aligned} \tag{5}$$

The second integral in equation 5 cannot be evaluated directly. However, since

$$\bar{D}_{o,j} \left[\frac{\partial c}{\partial r} \right]_{o,j} \gg \frac{\partial \left[\bar{D}_j \left[\frac{\partial c}{\partial r} \right]_j \right]}{\partial t}, \tag{6}$$

the contribution of the second integral can be considered negligible as long as the interval from t_0 to t_1 is very short.

$$\lim_{(\Delta t \rightarrow 0)} m_j = b\theta r_j \int_{t_0}^{t_1} \bar{D}_{o,j} \left[\frac{\partial c}{\partial x} \right]_{o,j} dt \quad (7)$$

($t_0 \leq t \leq t_1$)

Since $\bar{D}_{o,j}$ and $(\partial c/\partial x)_{o,j}$, the average diffusion coefficient and local gradient at t_0 , are constant, evaluation of the last expression gives:

$$m_j = b\theta r_j \bar{D}_{o,j} \left[\frac{\partial c}{\partial x} \right]_{o,j} \Delta t_D \quad (8)$$

where

$$\Delta t_D = t_1 - t_0$$

The mass of solute (constituent) that accumulates in box j during Δt_D , Δm_j , is equal to the mass that flows upward across boundary $j+1$, into the box, minus the mass that flows upward, across boundary j , out of the box.

$$\begin{aligned} \Delta m_j &= m_{j+1} - m_j \\ &= b\theta \left[r_{j+1} \bar{D}_{o,j+1} \left[\frac{\partial c}{\partial x} \right]_{o,j+1} - r_j \bar{D}_{o,j} \left[\frac{\partial c}{\partial x} \right]_{o,j} \right] \Delta t_D \quad (9) \end{aligned}$$

Dividing the change in mass, Δm_j , by the volume of box j ,

$$V_j = b\theta\bar{r}_j(r_{j+1} - r_j), \quad (10)$$

results in the following expression for the change in the concentration of box j during Δt_D .

$$\Delta C_j = \frac{\Delta m_j}{V_j} = \frac{r_{j+1}\bar{D}_{j+1} \left[\frac{\partial c}{\partial r} \right]_{j+1} - r_j\bar{D}_j \left[\frac{\partial c}{\partial r} \right]_j}{\bar{r}_j(r_{j+1} - r_j)} \Delta t_D \quad (11)$$

Finally, the new concentration in box j , $\bar{c}_{new,j}$, at the end of diffusion is equal to the original concentration in box j plus the change in its concentration.

$$\bar{c}_{new,j} = \bar{c}_{o,j} + \Delta C_j \quad (12)$$

Thus, to simulate Δt_D seconds of diffusion (in a one constituent system), equations (11) and (12) are applied to each box in the array.

Expressions analogous to (11) and (12) for the diffusion of constituents A and B in a noninteracting two constituent system are the following.

$$\Delta \bar{c}_{A,j} = \frac{\left[\begin{array}{c} r_{A,j+1} \bar{D}_{A,j+1} \frac{[\partial C_{AT}]}{\partial r} \Big|_{A,j+1} - r_{A,j} \bar{D}_{A,j} \frac{[\partial C_{AT}]}{\partial r} \Big|_{A,j} \end{array} \right] \Delta t_D}{\bar{r}_{A,j} (r_{A,j+1} - r_{A,j})} \quad (13a)$$

$$\Delta \bar{c}_{B,j} = \frac{\left[\begin{array}{c} r_{B,j+1} \bar{D}_{B,j+1} \frac{[\partial C_{BT}]}{\partial r} \Big|_{B,j+1} - r_{B,j} \bar{D}_{B,j} \frac{[\partial C_{BT}]}{\partial r} \Big|_{B,j} \end{array} \right] \Delta t_D}{\bar{r}_{B,j} (r_{B,j+1} - r_{B,j})} \quad (13b)$$

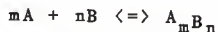
$$C_{\text{new},A,j} = \bar{c}_{A0,j} + \Delta C_{A,j} \quad (14a)$$

$$C_{\text{new},B,j} = \bar{c}_{B0,j} + \Delta C_{B,j} \quad (14b)$$

To simulate diffusion in a two constituent system (not undergoing mixed association reactions) equations (13a) and (14a) are applied to each box in the constituent A track and equations (13b) and (14b) are applied to each box in the constituent B track.

2.2.2 Mixed Associating Systems

A mixed association reaction is one in which constituent monomers of different types associate to produce a heterogeneous (mixed) aggregate.



A system undergoing mixed association may contain a number of different mixed aggregates in addition to constituent monomers and possibly some self association products (A_n , B_m). The distribution of constituents among the various species present is governed by the set of association constants for all aggregate species present,

$$K_{A_m} = \frac{C_{A_m}}{C_A^m}, \quad K_{A_m B_n} = \frac{C_{A_m B_n}}{C_A^m C_B^n} \quad (15)$$

and, for a given set of association constants, will depend on the total concentrations of each of the two constituents.

The flow of a constituent in response to its gradient in such a system is the sum of constituent weight fractions of the flows of the individual species in response to their individual species gradients. The flow of constituent A, for example, is the sum of constituent A weight fractions of the mass flows of all species containing constituent A.

The constituent A gradient is the sum of constituent A weight fractions of the individual species gradients. Since the individual species have different diffusion coefficients, the flow of A depends, not only on the magnitude of the A gradient, but on its composition as well. Whereas the distribution of constituent A among species at any point in the cell depends only on the two constituent concentrations,

the distribution of the A gradient among species gradients at that point, which will determine the average rate of diffusion of constituent A at that point, depends on both of the constituent gradients in addition to the constituent concentrations. Since the gradient of constituent B affects the distribution of the A gradient among gradients in molecular species that have different diffusion coefficients, it must also affect the flow of constituent A. (i.e. a cross diffusion effect) The total flow of constituent A can be expressed as the sum of a self diffusion term (diffusion of constituent A in response to the A gradient) and a cross diffusion term (diffusion of A in response to the B gradient).

$$-J_A = D_{AA} \frac{[\partial C_{AT}]}{[\partial r]} + D_{AB} \frac{[\partial C_{BT}]}{[\partial r]} \quad (16)$$

D_{AA} and D_{AB} in this expression are the direct and cross diffusion coefficients of constituent A.

Similarly, the flow of constituent B would be affected by the A gradient, and its flow is likewise expressed as the sum of a direct and cross diffusion term.

$$-J_B = D_{BB} \frac{[\partial C_{BT}]}{[\partial r]} + D_{BA} \frac{[\partial C_{AT}]}{[\partial r]} \quad (17)$$

Expressions analogous to equations (11) and (12) for the change in box constituent concentrations and resulting new box concentrations after a time, Δt_D , of diffusion in a two constituent (A and B) system undergoing mixed association are obtained by replacing each of the diffusion terms,

$$D_j \frac{[\partial c]}{[\partial r]_j},$$

with the appropriate cross and direct diffusion terms.

$$\Delta \bar{c}_{A,j} = \Delta t_D \times$$

$$\frac{\left[r_{A,j+1} D_{AA,j+1} \frac{[\partial C_{AT}]}{[\partial r]_{j+1}} + D_{AB,j+1} \frac{[\partial C_{BT}]}{[\partial r]_{j+1}} \right]}{\bar{r}_{A,j} (r_{A,j+1} - r_{A,j})} -$$

$$\frac{\left[r_{A,j} D_{AA,j} \frac{[\partial C_{AT}]}{[\partial r]_j} + D_{AB,j} \frac{[\partial C_{BT}]}{[\partial r]_j} \right]}{\bar{r}_{A,j} (r_{A,j+1} - r_{A,j})} \quad (18a)$$

$$\bar{c}_{A,new,j} = \bar{c}_{A,j} + \Delta C_{A,j} \quad (19a)$$

$$\Delta \bar{c}_{B,j} = \Delta t_D \times$$

$$\frac{\left[r_{B,j+1} D_{BB,j+1} \frac{\partial C_{BT}}{\partial x} \Big|_{j+1} + D_{BA,j+1} \frac{\partial C_{AT}}{\partial x} \Big|_{j+1} \right]}{\bar{r}_{B,j} (r_{B,j+1} - r_{B,j})} -$$

$$\frac{\left[r_{B,j} D_{BB,j} \frac{\partial C_{BT}}{\partial x} \Big|_j + D_{BA,j} \frac{\partial C_{AT}}{\partial x} \Big|_j \right]}{\bar{r}_{B,j} (r_{A,j+1} - r_{B,j})} \quad (18b)$$

$$\bar{c}_{B,new,j} = \bar{c}_{B,j} + \Delta C_{B,j} \quad (19b)$$

2.2.3 Computing Gradients at Box Boundaries

The boundary gradients, (dc/dr) , or simply g , used in the diffusion routine (equations 13 and 14 and equations 18 and 19) are computed immediately prior to each round of simulated diffusion.

The gradients, g_j , at the box boundaries, r_j , in a one constituent systems are computed in two steps. In the first step, gradients, g'_j , at positions midway between adjacent box centers, are computed along with the positions, r'_j , to which they correspond.

$$g'_j = \frac{\bar{c}_j - \bar{c}_{j-1}}{\bar{r}_j - \bar{r}_{j-1}} \quad (20)$$

$$r'_j = \frac{\bar{r}_j - \bar{r}_{j-1}}{2} \quad (21)$$

Because the box widths are generally not uniform (sedimentation operations distort the spacing of the grid) the position, r'_j , of the midpoint between \bar{r}_{j-1} and \bar{r}_j is not necessarily the same as the position, r_j , of the boundary between the boxes (figure 2).

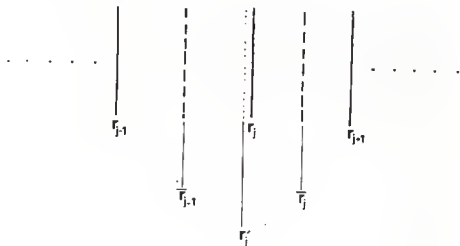


Figure 2: Gradient Interpolation Scheme

The gradients, g_j , at the box boundary positions, r_j , are computed by linear interpolation between the gradients, g' , at the box center midpoints. For instance, the gradient g_j at r_j is interpolated between g'_j at r'_j and g'_{j+1} at r'_{j+1} .

$$g_j = g'_j + \frac{(g'_{j+1} - g'_j)(r_j - r'_j)}{r'_{j+1} - r'_j} \quad (22)$$

Analogous expressions for computing the gradients of each constituent, g_A and g_B , at its own boundary positions in a two constituent model are given below.

$$g'_{A,j} = \frac{\bar{c}_{A,j} - \bar{c}_{A,j-1}}{\bar{r}_{A,j} - \bar{r}_{A,j-1}} \quad (23a) \quad r'_{A,j} = \frac{\bar{r}_{A,j} - \bar{r}_{A,j-1}}{2} \quad (24a)$$

$$g'_{B,j} = \frac{\bar{c}_{B,j} - \bar{c}_{B,j-1}}{\bar{r}_{B,j} - \bar{r}_{B,j-1}} \quad (23b) \quad r'_{B,j} = \frac{\bar{r}_{B,j} - \bar{r}_{B,j-1}}{2} \quad (24b)$$

$$g_{A,j} = g'_{A,j} + \frac{(g'_{A,j+1} - g'_{A,j})(r_{A,j} - r'_{A,j})}{r'_{A,j+1} - r'_{A,j}} \quad (25a)$$

$$g_{B,j} = g'_{B,j} + \frac{(g'_{B,j+1} - g'_{B,j})(r_{B,j} - r'_{B,j})}{r'_{B,j+1} - r'_{B,j}} \quad (25b)$$

The cross gradients required for diffusion in mixed associating systems (ie. the gradients in constituent B at the constituent A boundaries and the gradients in constituent A at the constituent B boundaries) are computed in a similar

fashion. The first step is again to compute gradients midway between box centers. For example, in determining gradients in constituent B at A boundaries, the first step is to calculate $g'_{B,j}$ and $r'_{B,j}$ between each adjacent pair of B box centers (equations 23b and 24b). A complication arises at this point because box boundaries in the two constituent tracks are usually not in register. That is, the position of boundary j in constituent track A is not necessarily the same as the position of the jth boundary in constituent track B. In fact $r_{A,j}$ and $r_{B,j}$ may be separated by several boxes. This lack of correspondence in position between the boxes of the two tracks develops during the sedimentation routine, in which the boundaries of the two tracks are shifted independently.

The second step in finding the B gradient at an A boundary, $r_{A,j}$, is to locate the pair of gradients, $g'_{B,n}$ and $g'_{B,n-1}$, located at positions, $r'_{B,n}$ and $r'_{B,n-1}$, that bracket $r_{A,j}$. This is accomplished by searching from the top of the array through successive values of $r'_{B,j}$ until the first occurrence of $r'_{B,j}$ greater than $r_{A,j}$ is located. The gradient in B at $r_{A,j}$ is then interpolated between the gradient, $g'_{B,n}$, at this position, which is $r'_{B,n}$, and the gradient, $g'_{B,n-1}$, at the position $r'_{B,n-1}$.

$$g_{BA, j} = g'_{B, n-1} + \frac{(g'_{B, n} - g'_{B, n-1})(r_{A, j} - r'_{B, n-1})}{r'_{B, n} - r'_{B, n-1}} \quad (26)$$

2.2.4 Computation of Diffnsion Coefficients

The difficulty involved in computing the appropriate diffusion coefficients for simulated diffusion operations depends on the complexity of the system being studied.

2.2.4.1 Non-Interacting Systems

The simplest systems are those which undergo no association whatsoever. Since the constituent molecules in systems of this type spend all of their time as monomers, the constituent diffusion coefficients are the same as the monomer diffusion coefficients and are concentration independent. For non-associating systems, then, each constituent diffusion coefficient is computed only once.

$$D = \frac{RT}{Nf}, \text{ where } f = f_0 \frac{f}{f_0} \quad (27)$$

f/f_0 is the ratio of the frictional coefficient of the molecule, f , to that of an unhydrated sphere of equal volume, f_0 . f_0 is given by Stokes law.

$$f_0 = 6\pi\eta R_0, \text{ where } R_0 = \frac{[3M\bar{v}]^{1/3}}{[4\pi N]} \quad (28)$$

and η is the solvent viscosity. M and \bar{v} are the molecular weight and partial specific volume of the macromolecular solute.

Alternatively, D may be obtained from the sedimentation coefficient at infinite dilution and the molecular weight, eliminating the need to know f .

$$S_0 = \frac{M(1 - \bar{v}\rho)}{Nf} \quad (29)$$

$$D = \frac{RT}{Nf} = \frac{S_0 RT}{M(1 - \bar{v}\rho)} \quad (30)$$

2.2.4.2 Self-Associating Systems

In self associating systems a constituent molecule spends part of its time as a monomer and part of its time as part of any number of aggregates, diffusing, at any instant, at a rate determined by the diffusion coefficient and local gradient of whichever species it is existing in at that instant. Since the diffusion coefficients of the monomer and aggregate species are not the same, the diffusion coeffi-

cient of a constituent molecule that spends part of its time as one or part of each different species must be an average of some sort over all species present.

The total mass flux of a self associating system is the sum of monomer and aggregate species fluxes in response to their respective species gradients.

$$-J_T = \sum D_j \frac{\partial C_j}{\partial x} \quad (1 \leq j \leq n) \quad (31)$$

Thus the contribution, to the total flux, of each species is proportional to its species gradient and the average diffusion coefficient, \bar{D} , is a species gradient weighted average.

$$-J_T = \bar{D} \frac{\partial C_T}{\partial x} \quad (32)$$

$$\bar{D} = \frac{\sum D_j \frac{\partial C_j}{\partial x}}{\sum \frac{\partial C_j}{\partial x}} \quad (1 \leq j \leq n) \quad (33)$$

The species gradients ($\partial c_j / \partial r$), in equation 33 can be re-expressed in terms of the monomer concentration C_1 , and the species association constants, K_j , as follows.

$$K_j = \frac{c_j}{C_1^j} \quad (34)$$

$$c_j = K_j C_1^j \quad (35)$$

$$\frac{\partial(c_j)}{\partial r} = \frac{\partial(K_j C_1^j)}{\partial r} \quad (36)$$

If the association constants are pressure-independent then equation 36 may be rewritten as:

$$\frac{\partial(c_j)}{\partial r} = K_j \frac{[\partial C_1^j]}{[\partial r]} \quad (37)$$

$$\frac{\partial(c_j)}{\partial r} = K_j \frac{[\partial C_1^j] [\partial C_1]}{[\partial C_1] [\partial r]} \quad (38)$$

Partially differentiating with respect to C_1 and substituting the result for the species gradients in equation 33 gives

$$\bar{D} = \frac{\sum_j D_j K_j C_1^{j-1} \frac{[\partial c]}{\partial r}}{\sum_j K_j C_1^{j-1} \frac{[\partial c]}{\partial r}} \quad (39)$$

which is equivalent to

$$\bar{D} = \frac{\sum_j D_j C_1^j}{\sum_j C_1^j} \quad (40)$$

2.2.4.3 Mixed-Associating Systems

The derivation of the following expressions for the average diffusion coefficients in a mixed associating system, in terms of the monomer concentrations, C_A and C_B , though straight-forward, is quite cumbersome and will not be presented here. A detailed derivation of these expressions may be found elsewhere. (35)

$$\begin{aligned} \bar{D}_{AA} &= (d_{AA}^q{}_{BB} - d_{AB}^q{}_{BA}) / dq \\ \bar{D}_{AB} &= (d_{AB}^q{}_{AA} - d_{AA}^q{}_{AB}) / dq \\ \bar{D}_{BB} &= (d_{BB}^q{}_{AA} - d_{BA}^q{}_{AB}) / dq \\ \bar{D}_{BA} &= (d_{BA}^q{}_{BB} - d_{BB}^q{}_{BA}) / dq \end{aligned} \quad (41)$$

where

$$\begin{aligned}
 dq &= q_{BB}q_{AA} - q_{AB}q_{BA} \\
 d_{AA} &= \sum_i \sum_j D_{ij} f_{A,ij} K_{ij} C_A^{i-1} C_B^j \\
 &\quad (0 \leq i \leq m) \quad (1 \leq j \leq n) \\
 d_{AB} &= \sum_j \sum_i D_{ij} f_{A,ij} K_{ij} C_A^i C_B^{j-1} \\
 &\quad (0 \leq i \leq m) \quad (1 \leq j \leq n) \\
 d_{BB} &= \sum_j \sum_i D_{ij} f_{A,ij} K_{ij} C_A^i C_B^{j-1} \\
 &\quad (0 \leq i \leq m) \quad (1 \leq j \leq n) \\
 d_{BA} &= \sum_i \sum_j D_{ij} f_{A,ij} K_{ij} C_A^{i-1} C_B^j \\
 &\quad (1 \leq i \leq m) \quad (0 \leq j \leq n)
 \end{aligned} \tag{42}$$

and

$$\begin{aligned}
 q_{AA} &= \sum_i \sum_j f_{A,ij} K_{ij} C_A^{i-1} C_B^j, \\
 &\quad (0 \leq i \leq m, 1 \leq j \leq n) \\
 q_{AB} &= \sum_i \sum_j f_{A,ij} K_{ij} C_A^i C_B^{j-1}, \\
 &\quad (1 \leq i \leq m, 0 \leq j \leq n) \\
 q_{BB} &= \sum_i \sum_j f_{B,ij} K_{ij} C_A^i C_B^{j-1}, \\
 &\quad (1 \leq i \leq m, 0 \leq j \leq n) \\
 q_{BA} &= \sum_i \sum_j f_{B,ij} K_{ij} C_A^{i-1} C_B^j, \\
 &\quad (0 \leq i \leq m, 1 \leq j \leq n)
 \end{aligned} \tag{43}$$

The summations in these expressions are over all species $A_i B_j$ that are present in the system with i and j equal to or greater than the values given below each expression. The summation limits, m and n , are the largest numbers of A and B monomers occurring in any of the aggregates. $f_{A,ij}$ and

$f_{B,ij}$ are the weight fractions, in species A_iB_j , of constituent A and constituent B, respectively, D_{ij} is the diffusion coefficient of species A_iB_j and K_{ij} is the association constant for A_iB_j .

$$f_{A,ij} = \frac{iM_A}{iM_A + jM_B}, \quad f_{B,ij} = \frac{jM_B}{iM_A + jM_B} \quad (44)$$

$$K_{ij} = \frac{C_{A_iB_j}}{C_A^i C_B^j} \quad (45)$$

2.3 SIMULATION OF SEDIMENTATION

Sedimentation is simulated by shifting box boundaries downward in the array and away from the axis of rotation. In the time interval for one simulated sedimentation shift, Δt_s , which corresponds to Δt_s seconds of real experimental time, a boundary initially at r_j will move to a new position, $r_{new,j}$, so that

$$r_{new,j} = r_j e^{(\bar{S}_j \omega^2 \Delta t_s)} \quad (46)$$

where

ω is the rotor speed in radians per second and S_j is the local average sedimentation coefficient at r_j .

Solute does not cross boundaries in the model during a sedimentation shift; all solute initially contained between boundaries r_{j+1} and r_j will be contained between boundaries $r_{new,j+1}$ and $r_{new,j}$ at the end of the sedimentation shift. Because the boundaries move at different rates, however, the box volumes and box center concentrations will be changed⁴. The initial volume of box j , V_j , and the volume of box j at the end of a sedimentation shift, $V_{j,new}$, are given by the following expressions.

$$V_j = \frac{b\theta(r_{j+1}^2 - r_j^2)}{2} \quad (47)$$

$$V_{j,new} = \frac{b\theta(r_{new,j+1}^2 - r_{new,j}^2)}{2} \quad (48)$$

Thus if the initial concentration in box j was c_j (box center concentration) then the concentration at the end of the sedimentation shift, $c_{new,j}$, would be as follows

⁴ Because the cell is sector shaped, the movement of two adjacent boundaries away from the axis of rotation will result in a change in the volume and concentration of the intervening box even when the boundaries move at the same rate.

$$c_{\text{new},j} = \frac{c_j (r_{j+1}^2 - r_j^2)}{r_{\text{new},j+1}^2 - r_{\text{new},j}^2} \quad (49)$$

For a two constituent system the equations for sedimentation, analogous to equations 46 and 49, are written as follows.

$$r_{\text{new},A,j} = r_{A,j} \exp(\bar{S}_{A,j} \omega^2 \Delta t_s) \quad (50a)$$

$$C_{\text{new},A,j} = \frac{c_{A,j} (r_{A,j+1}^2 - r_{A,j}^2)}{r_{\text{new},A,j+1}^2 - r_{\text{new},A,j}^2} \quad (51a)$$

$$r_{\text{new},B,j} = r_{B,j} \exp(\bar{S}_{B,j} \omega^2 \Delta t_s) \quad (50b)$$

$$C_{\text{new},B,j} = \frac{c_{B,j} (r_{B,j+1}^2 - r_{B,j}^2)}{r_{\text{new},B,j+1}^2 - r_{\text{new},B,j}^2} \quad (51b)$$

where $\bar{S}_{A,j}$ and $\bar{S}_{B,j}$ are the local average sedimentation coefficients of constituents A and B.

2.3.1 Computation of Sedimentation Coefficients

2.3.1.1 Non-Associating Systems

The local average sedimentation coefficients are generally concentration dependent. In non-associating systems only

the hydrodynamic dependence of \bar{S} needs to be considered. In this case, \bar{S}_j is obtained directly from S_o , the sedimentation coefficient at infinite dilution.

$$\bar{S}_j = \frac{S_o}{1 + kC_j} \quad (52)$$

where C_j is the concentration at boundary j and k is the hydrodynamic constant. For a two constituent non-associating system

$$\bar{S}_{A,j} = \frac{S_{A,o}}{1 + k_{AA}C_{AT,j} + k_{AB}C_{BT,j}} \quad (53a)$$

$$\bar{S}_{B,j} = \frac{S_{B,o}}{1 + k_{BB}C_{BT,j} + k_{BA}C_{AT,j}} \quad (53b)$$

where $C_{AT,j}$ and $C_{BT,j}$ are the concentrations of constituents A and B at boundary j and k_{AA} , k_{AB} , k_{BB} , and k_{BA} are the appropriate hydrodynamic constants.

2.3.1.2 Self-Associating Systems

If constituent A self associates then its average sedimentation coefficient will depend upon its distribution

among aggregate species and monomer. The average sedimentation coefficient of constituent A is a weight average over all species in which constituent A participates. An appropriate expression for the average sedimentation coefficients of a self associating constituent A at indefinite dilution (not corrected for hydrodynamic dependence), $S_{A,0}$, is the following.

$$S_{A,0} = \frac{\sum S_{A_i,0} C_{A_i}}{\sum C_{A_i}} \quad (54)$$

where $S_{A_i,0}$ is the ideal sedimentation coefficient of species A_i (ie., in the absence of hydrodynamic effects) and C_{A_i} is its concentration.

Since

$$C_{A_i} = K_{A_i} C_A^i \quad (55)$$

equation 54 can be reexpressed in terms of the monomer concentration, C_A , and the association constants, K_{A_i} .

$$S_{A,0} = \frac{\sum S_{A_i,0} K_{A_i} C_A^i}{\sum K_{A_i} C_A^i} \quad (56)$$

2.3.1.3 Mixed-Associating Systems

The appropriate expression for $\bar{S}_{A,o}$ in a mixed associating system is similar to equation 54 but in this case the summations are two dimensional and each term in the summation includes an additional factor, $f_{A,ij}$, the weight fraction of A in species A_iB_j .

$$\bar{S}_{A,o} = \frac{\sum \sum S_{ij,o} f_{A,ij} C_{ij}}{\sum \sum f_{A,ij} C_{ij}} \quad (57)$$

(0 ≤ i ≤ m, 1 ≤ j ≤ n)

where $S_{ij,o}$ and C_{ij} are the sedimentation coefficient and concentration of A_iB_j .

Equation 57 can also be re-expressed in terms of the monomer concentrations, C_A and C_B , and association constants K_{ij} as follows.

$$\bar{S}_{A,o} = \frac{\sum \sum S_{ij,o} f_{A,ij} C_A^i C_B^j}{\sum \sum f_{A,ij} C_A^i C_B^j} \quad (58)$$

(1 ≤ i ≤ m, 1 ≤ j ≤ n)

The average sedimentation coefficients, $\bar{S}_{A,o}$, in equations 54-58 are infinite dilution coefficients. The correction for hydrodynamic dependence is the same as in nonassociating systems (equation 52-53). Thus, for instance,

$$S_A = \frac{S_{A,0}}{1 + k_{AA} C_{AT} + k_{AB} C_{BT}} \quad (59)$$

2.3.2 Computing Local Constituent Concentrations

The boundary monomer concentrations needed to compute local average transport coefficients are extracted from boundary constituent concentrations. Boundary constituent concentrations which are also needed for computing the hydrodynamic dependence of the local average sedimentation coefficients, are interpolated from box center constituent concentrations. The concentrations of a constituent at its own boundaries are computed directly by linear interpolation.

$$C_{AT,j} = \bar{c}_{AT,j-1} + \frac{(\bar{c}_{AT,j} - \bar{c}_{AT,j-1})(r_{A,j} - \bar{r}_{A,j-1})}{(\bar{r}_{A,j} - \bar{r}_{A,j-1})} \quad (60)$$

The concentration, at a boundary in one constituent track, of the other constituent (eg. C_{BT} at $r_{A,j}$) is interpolated between the two box centers in the other constituent track that bracket the position of the boundary being considered.

$$c_{BT}(A, j) = \bar{c}_{BT, n-1} + \frac{(\bar{c}_{BT, n} - \bar{c}_{BT, n-1})(r_{A, j} - \bar{r}_{B, n-1})}{(\bar{r}_{B, n} - \bar{r}_{B, n-1})} \quad (61)$$

where

$$\bar{r}_{B, n-1} > r_{A, j} > \bar{r}_{B, n}$$

2.4 TABLE ASSEMBLIES

In all but a few simple cases the calculation of transport coefficients from local constituent concentrations, which is essentially a problem of extracting monomer concentrations from constituent concentrations, is fairly complex and expensive in terms of computer time. A typical two constituent 100 box model simulation consisting of 100 sedimentation transfers⁵ and 500 diffusion transfers would require $100 \times 600 \times 2 = 120,000$ such calculations which would consume a considerable block of computer time.

An alternative approach which greatly reduces the number of calculations is to assemble a table, prior to the simulation, containing transport coefficients at a number of constituent concentrations over an appropriate range, and to then interpolate transport coefficients from the table as they are needed during the simulation. The tables are produced by table assembly programs, of which there are several types, each designed to create tables as efficiently as possible.

⁵ The maximum allowable diffusion transfer time (Δt_D) is usually about 1/5 as long as the sedimentation transfer time. Five diffusion transfers are thus required for each sedimentation transfer (see p. 94).

sible for a particular class of systems. (See table 1.)

TABLE 1

Varieties of Table Assemblies

- I) Self Association ($nA \Leftrightarrow A_n$)
- A) A_2 only ($n=2$).
 - B) One A_n aggregate ($n>2$).
 - C) Multiple A_n aggregates ($n = \text{any positive integer}$).
- II) Mixed Association ($mA + nB \Leftrightarrow A_m B_n$).
- A) $A_1 B_1$ only ($n = m = 1$)
 - B) One or more $A_1 B_n$ aggregates ($n = \text{any positive integer}$).
 - C) One or more $A_2 B_n$ aggregates ($n = \text{any positive integer}$).
 - D) One or more $A_m B_n$ aggregates ($m = \text{any positive integer}$, $n = \text{any positive integer}$).

2.4.1 Self-Associating systems

In preparing tables for self associating systems entries are made at regular intervals in either c_t , \bar{D} , or S_o , all of which are functions of the monomer concentrations:

$$c_t = c_1 + \sum K_j c_1^j \quad (1 \leq j \leq n) \quad (62)$$

$$S_o = \frac{S_{A_o} + \sum S_{j,o} K_j c_1^{j-1}}{1 + \sum K_j c_1^{j-1}} \quad (2 \leq j \leq n) \quad (63)$$

$$\bar{D}_o = \frac{D_{A_o} + \sum j D_{j,o} K_j c_1^{j-1}}{1 + \sum j K_j c_1^{j-1}} \quad (2 \leq j \leq n) \quad (64)$$

With one of the three variables, c_t , \bar{D} , or S_o , fixed at each point in the table, the other two are computed using equations 62-64. This involves finding the value of c_1 that corresponds to the value of the fixed variable and then computing the other two variables from c_1 . Equation 62 can be solved directly for c_1 , as long as no aggregates higher than dimer are present, in which case equation 62 is a quadratic.

$$c_1 = \frac{-1 + [1 + 4K_2 c_t]^{1/2}}{2K_2} \quad (65)$$

Equations (63) and (64) can be solved for c_1 as long as only one aggregate (A_j where j is any integer) is present.

$$c_1 = \frac{[S_{A,o} - \bar{S}_o - 1]^{1/(j-1)}}{[S_o - S_{A_j,o} - K_j]} \quad (j \geq 2) \quad (66)$$

$$c_1 = \frac{[D_{A,o} - \bar{D} - 1]^{1/(j-1)}}{[\bar{D} - D_{A_j} - jK_j]} \quad (j \geq 2) \quad (67)$$

Finding c_1 from c_t when aggregates beyond dimer are present, or from \bar{S}_o or \bar{D} when two or more aggregates are present, requires a binary search, whereby the correct value of c_1 is approached through a logical trial and error procedure. The general scheme of the binary search is illustrated in the algorithm below. The first test value of c_1 is that midway between its maximum and minimum values. The maximum possible value of c_1 is c_t when the search is for c_1 at some value of c_t , and c_o when the search is for c_1 at some value of \bar{S}_o or \bar{D} . The scheme shown below is general; y may represent either c_t , \bar{S}_o or \bar{D} , y_{test} is the value of either c_t , \bar{S}_o , or \bar{D} computed from the test value of c_1 , and y_o is the value of that variable for which c_1 is being sought. The exact value of c_1 corresponding to y_o is usually not found. What is found is a value of c_1 that corresponds to a value of y_{test} that is acceptably close to y_o . The values

of y and c_1 stored in the table are the final values of y_{test} and $c_{1,\text{test}}$ ($y_{\text{test}} \approx y_0$). y_0 is not stored. The pairs of c_1 and y , ($y = c_t, \bar{D}$, or \bar{S}_0), stored in the table are thus in exact agreement. The acceptable difference between y_{test} and y_0 is arbitrary but should be small. For most of our programs an acceptable difference of $C_{\text{max}}/10,000$ is used.

Algorithm

- I) $C_{\text{top}} = C_{\text{max}}$
- II) $C_{\text{bot}} = C_{\text{min}} = 0$
- III) $c_{1,\text{test}} = (C_{\text{top}} + C_{\text{bot}}) / 2$
- IV) $y_{\text{test}} = f(c_{1,\text{test}})$
- V) If $|y_{\text{test}} - y_0| \leq C_{\text{max}} / 10,000$
 - A) Then begin
 1. $c_1 = c_{1,\text{test}}$
 2. $y = f(c_1) = y_{\text{test}}$
 End.
 - B) Else If $y_{\text{test}} > y_0$
 1. Then begin
 - a) $C_{\text{top}} = c_{1,\text{test}}$
 - b) Go to III
 End.
 2. Else begin
 - a) $C_{\text{bot}} = c_{1,\text{test}}$
 - b) Go to III
 End.

End Algorithm

The operations involved in creating a table with regular intervals in \bar{S}_0 are outlined below.

Algorithm

I) Determine $\bar{S}_{0, \max}$ (\bar{S}_0 at C_{\max}) The largest value of \bar{S}_0 that will occur during a simulation is the value of \bar{S}_0 when $c_t = C_{\max}$

A) Find c_1 at C_{\max}

1. Only one aggregate (A_j).

a) If $j = 2$ Then Begin

$$i) \quad c_t = c_1 + K_2 c_1^2$$

ii)

$$c_1 = \frac{-1 + (1 + 4K_2 c_t)^{1/2}}{2K_2}$$

End

b) If $j > 2$ Then Begin

i) Requires a binary search.

$$c_t = c_1 + K_j c_1^j$$

$$\text{ii) } y = c_t = f(c_1) = \sum K_j c_1^j$$

End

2. More than one aggregate.

Requires a binary search.

$$\text{a) } c_t = c_1 + \sum K_j c_1^j$$

$$\text{b) } y = c_t = f(c_1) = \sum K_j c_1^j$$

B) Compute $S_{0, \max}$ from c_1 at C_{\max} .

$$S_{\max} = \frac{S_{A0} + \sum S_{Aj, 0} K_j c_1^{j-1}}{1 + \sum K_j c_1^{j-1}}$$

II) Compute ΔS_0 , the increment in S_0 between adjacent table entries.

$$\Delta S_0 = \frac{S_{0, \max} - S_{0, A}}{n-1}$$

where n is the number of table entries. ($n = 100$ is usually sufficient.)

III) Compute $c_1(i)$ at each $S_0(i)$ in the table for ($1 \leq i \leq n$).

$$S_0(i) = S_{A0} + (i-1)\Delta S_0$$

A) Only one aggregate.

1.

$$\bar{S}_0(i) = \frac{S_{A0} + S_{Aj0} K_{Aj} c_1^{j-1}(i)}{1 + K_{Aj} c_1^{j-1}(i)}$$

2.

$$c_1(i) = \frac{[S_{A0} - \bar{S}_0(i) \quad 1]^{1/(j-1)}}{[\bar{S}_0(i) - S_{A,j,0} \quad K_j]}$$

B) More than one aggregate.

Requires binary search.

$$y = \bar{S}_0 = f(c_1) = \frac{S_{A0} + \sum S_{Aj,0} K_j c_1^{j-1}(i)}{1 + \sum K_j c_1^{j-1}(i)}$$

IV) Compute c_t and $\bar{D}(i)$ for each $c_1(i)$.

A) $c_t(i) = c_1(i) + \sum K_j c_1^j(i)$

B)

$$\bar{D}(i) = \frac{\sum_j K_j D_j c_1^j(i)}{\sum_j K_j c_1^j(i)}$$

End Algorithm

2.4.2 Mixed Associating Systems

Tables for systems undergoing mixed association are two dimensional. Within a given row of the table C_{AT} is held constant and C_{BT} is incremented. Within a given column C_{BT} is constant and C_{AT} is incremented. Each position (row i , column j) in the table corresponds to a constituent A concentration $C_{AT,ij}$, a constituent B concentration $C_{BT,ij}$ and the average transport coefficients of the system at those concentrations $\bar{D}_{AA,ij}$, $\bar{D}_{BB,ij}$, $\bar{D}_{AB,ij}$, $\bar{D}_{BA,ij}$, $\bar{S}_{Ao,ij}$, $\bar{S}_{Bo,ij}$. Surface diagrams of some sample sedimentation coefficient tables for mixed associating systems are shown in figures 3 and 4

The constituent concentrations and all of the transport coefficients are functions of the monomer concentrations C_A and C_B .

$$C_{AT} = \sum \sum f_{A,ij} K_{ij} C_A^i C_B^j \quad (68a)$$

$$C_{BT} = \sum \sum f_{B,ij} K_{ij} C_A^i C_B^j \quad (68b)$$

(0 ≤ i ≤ m) (0 ≤ j ≤ n)

$$\bar{S}_{Ao} = \frac{\sum \sum f_{A,ij} K_{ij} S_{ij,o} C_A^i C_B^j}{\sum \sum f_{A,ij} K_{ij} C_A^i C_B^j} \quad (69a)$$

(0 ≤ i ≤ m) (0 ≤ j ≤ n)

Figure 3: Topologies of Sedimentation Coefficient Tables for an Uncooperative AB_2 System ($K_I=10^6$)

See p.97 for description of Uncooperative AB_n systems.

a. S_A vs. C_{AT} and C_{BT}

b. S_B vs. C_{AT} and C_{BT}

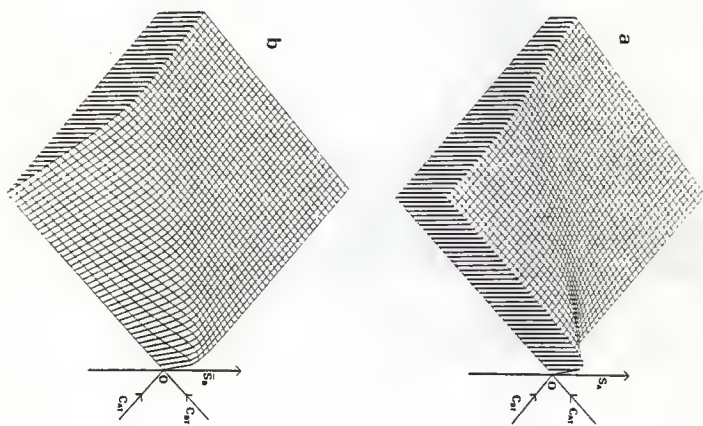
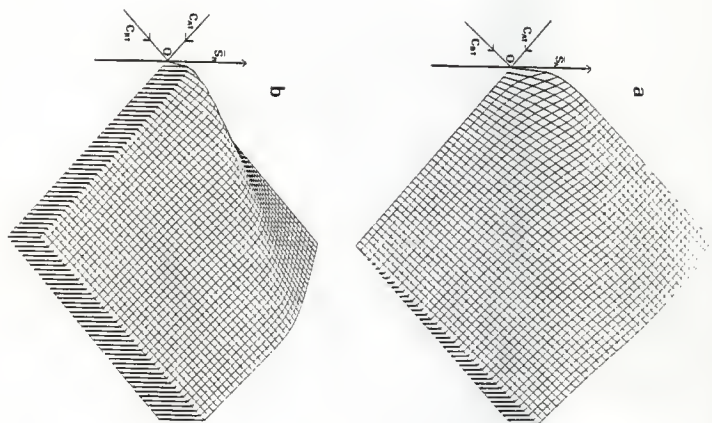
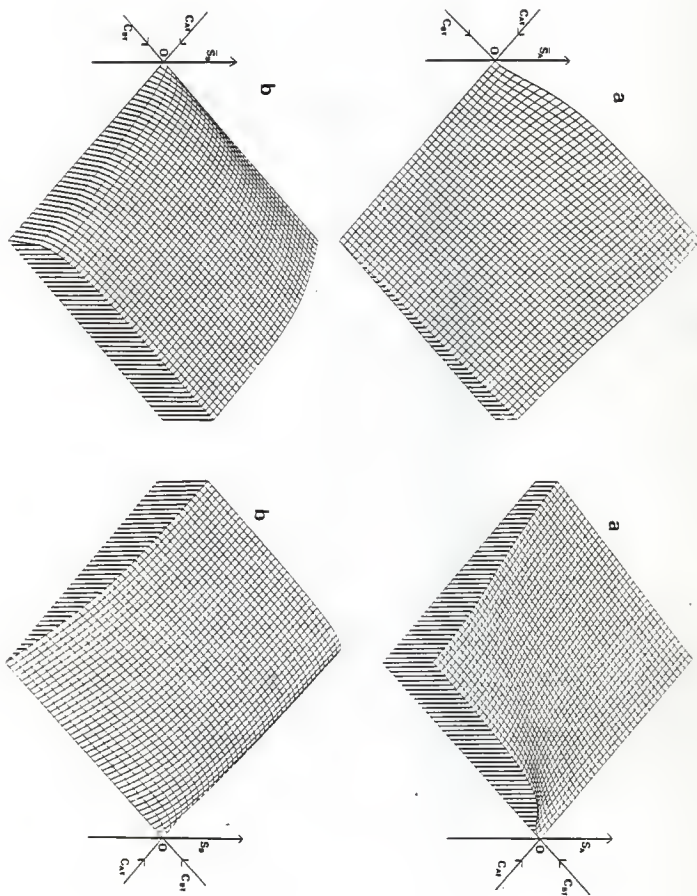


Figure 4: Topologies of Sedimentation Coefficient Tables
for a Completely Cooperative AB_2 System
($K_{2M}=10^{10}$)

See p.148 for description of Cooperative AB_n
systems.

a. S_A vs. C_{AT} and C_{BT}

b. S_B vs. C_{AT} and C_{BT}



$$S_{Bo} = \frac{\sum \sum f_{B,ij} K_{ij} S_{ij,0} C_A^i C_B^j}{\sum \sum f_{B,ij} K_{ij} C_A^i C_B^j} \quad (69a)$$

(0 ≤ i ≤ m) (0 ≤ j ≤ n)

$$\begin{aligned} D_{AA} &= (d_{AA} q_{BB} - d_{AB} q_{BA}) / dq \\ D_{AB} &= (d_{AB} q_{AA} - d_{AA} q_{AB}) / dq \\ D_{BB} &= (d_{BB} q_{AA} - d_{BA} q_{AB}) / dq \\ D_{BA} &= (d_{BA} q_{BB} - d_{BB} q_{BA}) / dq \end{aligned} \quad (70)$$

where

$$dq = q_{BB} q_{AA} - q_{AB} q_{BA}$$

and

$$\begin{aligned} d_{AA} &= \sum \sum i D_{ij} f_{A,ij} K_{ij} C_A^{i-1} C_B^j \\ &\quad (0 \leq i \leq m) (1 \leq j \leq n) \\ d_{AB} &= \sum \sum j D_{ij} f_{A,ij} K_{ij} C_A^i C_B^{j-1} \\ &\quad (0 \leq i \leq m) (1 \leq j \leq n) \\ d_{BB} &= \sum \sum j D_{ij} f_{A,ij} K_{ij} C_A^i C_B^{j-1} \\ &\quad (0 \leq i \leq m) (1 \leq j \leq n) \\ d_{BA} &= \sum \sum i D_{ij} f_{A,ij} K_{ij} C_A^{i-1} C_B^j \\ &\quad (1 \leq i \leq m) (0 \leq j \leq n) \end{aligned} \quad (71)$$

and

$$\begin{aligned}
 q_{AA} &= \sum \sum f_{A,ij} i K_{ij} C_A^{i-1} C_B^j, \\
 &\quad (0 \leq i \leq m, 1 \leq j \leq n) \\
 q_{AB} &= \sum \sum f_{A,ij} j K_{ij} C_A^i C_B^{j-1}, \\
 &\quad (1 \leq i \leq m, 0 \leq j \leq n) \\
 q_{BB} &= \sum \sum f_{B,ij} j K_{ij} C_A^i C_B^{j-1}, \\
 &\quad (1 \leq i \leq m, 0 \leq j \leq n) \\
 q_{BA} &= \sum \sum f_{B,ij} i K_{ij} C_A^{i-1} C_B^j, \\
 &\quad (0 \leq i \leq m, 1 \leq j \leq n)
 \end{aligned} \tag{72}$$

$$\begin{aligned}
 f_{A,ij} &= i M W_A / (i M W_A + j M W_B) \\
 f_{B,ij} &= j M W_B / (i M W_A + j M W_B)
 \end{aligned} \tag{73}$$

$$\begin{aligned}
 f_A(0,1) &= f_B(1,0) = 0 \\
 f_A(1,0) &= f_B(0,1) = 1 \\
 K_{ij} &= C_{A_i B_j} / C_A^i C_B^j \\
 K(0,1) &= K(1,0) = 1
 \end{aligned} \tag{74}$$

Here, i and j refer to the numbers of A monomers and B monomers, respectively, in each aggregate species, and should not be confused with indices of table entries or simulation array elements.

The summations in these expressions are over all species $A_i B_j$ present in the system with i and j equal to or greater than the values given below each equation. For example,

suppose we are considering a system which contains, in addition to the monomers, A and B, the two associated species, A_1B_2 and A_2B_4 . The summations in this case include only four terms:

1. $i = 0, j = 1$, corresponding to monomer B (A_0B_1).
2. $i = 1, j = 0$, corresponding to monomer A (A_1B_0).
3. $i = 1, j = 2$, corresponding to species A_1B_2 .
4. $i = 2, j = 4$, corresponding to species A_2B_4 .

In some of the summations, one of the monomer species is excluded by the lower limits indicated. For instance, $(1 \leq i \leq m) (0 \leq j \leq n)$ indicates that i is greater than one in all of the species to be included in the summation, which means that the monomer B term ($i=0, j=1$) is not included in the summation.

Thus, for example, d_{AA} for an $A+B+AB_2+A_2B_4$ system could be written as follows.

$$d_{AA} = \sum \sum i D_{A_i B_j} f_{A, ij} K_{ij} C_A^{i-1} C_B^j =$$

$$(1 \leq i \leq m) (0 \leq j \leq n)$$

$$D_A f_A(1,0) K(1,0) + D_{AB_2} f_A(1,2) K(1,2) C_B^2$$

$$+ 2 D_{A_2 B_4} f_A(2,4) K(2,4) C_A C_B^4 \quad (75)$$

In constructing these tables, C_{AT} and C_{BT} are fixed at each table entry, C_A and C_B are computed from C_{AT} and C_{BT} using equation (68a) and (68b), (this usually involves bina-

ry search) and \bar{S}_{A_0} , \bar{S}_{B_0} , \bar{D}_{AA} , \bar{D}_{AB} , \bar{D}_{BB} , and \bar{D}_{BA} are computed from the monomer concentrations using (69-74).

The complexity of a mixed association table assembly, which is related to the number of binary searches involved, depends upon the types of species present. When only one aggregate, AB, is present, (68a) and (68b) become simply:

$$\begin{aligned} C_{AT} &= C_A + f_A(AB)K_{AB}C_A C_B \\ &= C_A (1 + f_A(AB)K_{AB}C_B) \end{aligned} \quad (76)$$

and

$$\begin{aligned} C_{BT} &= C_B + f_B(AB)K_{AB}C_A C_B \\ &= C_B (1 + f_B(AB)K_{AB}C_A) \end{aligned} \quad (77)$$

Solving (76) for C_A and substituting for C_A in (77) gives:

$$C_A = \frac{C_{AT}}{1 + f_A(AB)K_{AB}C_B} \quad (78)$$

$$C_{BT} = C_B + \frac{C_{AT}f_B(AB)K_{AB}C_B}{1 + f_A(AB)K_{AB}C_B} \quad (79)$$

(79) can be written as a quadratic in terms of C_B as follows:

$$C_{BT}(1 + f_A K_{AB} C_B) = C_B(1 + f_A K_{AB} C_B) + C_{AT} f_B K_{AB} C_B \quad (80)$$

$$C_{BT} + C_{BT} f_A K_{AB} C_B = C_B + C_B f_A K_{AB} C_B + C_{AT} f_B K_{AB} C_B \quad (81)$$

$$0 = f_A K_{AB} C_B^2 + [1 + C_{AT} f_B K_{AB} - C_{BT} f_A K_{AB}] C_B - C_{BT} \quad (82)$$

where $f_A = f_A(AB) = M_A/M_{AB}$ and $f_B = f_B(AB) = M_B/M_{AB}$.

Thus, C_B can be determined directly from C_{AT} and C_{BT} , using the quadratic formula.

$$C_B = - \frac{(1 + C_{AT} f_B K_{AB} + C_{BT} f_A K_{AB})}{2 f_A K_{AB}} \pm \frac{[(1 + C_{AT} f_B K_{AB} + C_{BT} f_A K_{AB})^2 - 4 f_A K_{AB} C_{BT}]^{1/2}}{2 f_A K_{AB}} \quad (82)$$

C_A can then be computed directly from equation (78).

The following algorithm outlines the table assembly program for mixed association with the only aggregate species present being $A_1 B_1$.

Algorithm

- I) $n = \text{number of rows and columns.}$
- II) $\Delta C_{AT} = C_{ATmax} / (n-1)$
- III) $\Delta C_{BT} = C_{BTmax} / (n-1)$
- IV) $C_{AT} = 0$
- V) Repeat from $i = 1$ to $(n+1)$.
- A) $C_{AT} = C_{AT} + (i-1)\Delta C_{AT}$
- B) $C_{BT} = 0$
- C) Repeat from $j = 1$ to $(n+1)$.
1. $C_{BT} = C_{BT} + (j-1)\Delta C_{BT}$
 2. Compute $C_{B,ij}$ using eq. 83.
 3. Compute $C_{A,ij}$ using eq. 78.
 4. Compute $\bar{S}_{A,o,ij}$, $\bar{S}_{B,o,ij}$, $\bar{D}_{AA,ij}$, $\bar{D}_{AB,ij}$,
 $\bar{D}_{BB,ij}$, $\bar{D}_{BA,ij}$, using equations 69-74.
- End repeat.
- End repeat.

End Algorithm

A binary search for monomer concentrations is needed to construct tables for systems with two or more mixed association products. If all of the mixed aggregates present contain only one subunit of one of the constituents (i.e., if all mixed aggregates are from A_1B_n , where n is any integer), and if there are no self association products in constituent A then $i=1$ in every term in equation (68a), which can then be rewritten as follows:

$$C_A = \frac{C_{AT}}{\sum f_A(1, j) K(1, j) C_B^j} \quad (0 \leq j \leq n) \quad (84)$$

Substituting the right hand side of (84) for C_A in equation (68b) gives:

$$C_{BT} = \sum \sum f_B(i, j) K(i, j) C_B^j \left[\frac{C_{AT}}{\sum f_A(1, j) K(1, j) C_B^j} \right]^j \quad (85)$$

(0 ≤ i ≤ 1) (0 ≤ j ≤ n)

If there are no self association species in B, equation (85) can be simplified as follows:

$$C_{BT} = C_B + \sum f_B(1, j) \frac{C_{AT}}{\sum f_A(1, j) K(1, j) C_B^j} \quad (86)$$

(0 ≤ j ≤ n)

Whether using equations (85) or (86), a binary search is required to determine C_B at a given C_{AT} and C_{BT} . The object of the binary search is to find a value of C_B which corresponds to a value of C_{BT} that is very close to, but not necessarily equal to a target value of C_{BT} . The target values of C_{BT} are not stored in the table, but serve as guidelines

for constructing a table that is nearly evenly spaced in C_{BT} . The values of C_{BT} that are finally stored in the table are those which correspond exactly to the final values of C_B .

Once C_B is found, C_A is computed directly from (84). The general scheme of an A_1B_n table assembly with a binary search is illustrated below.

Algorithm

I) Compute increments for C_{AT} and $C_{BT, target}$.

A)

$$\Delta C_{AT} = \frac{C_{AT, max}}{\text{number of rows} - 1}$$

B)

$$\Delta C_{BT} = \frac{C_{BT, max}}{\text{number of columns} - 1}$$

II) Repeat from $k = 0$ to (number of rows).

A) $C_{AT, k} = k\Delta C_{AT}$

B) Repeat from $m = 0$ to (number of columns).

1. $C_{BT, target} = m\Delta C_{BT}$

2. Compute initial test value of C_B

a) $C_{B, bot} = 0$

b) $C_{B, top} = C_{BT, target}$

c) $C_{B, test} = (C_{B, top} + C_{B, bot}) / 2$

3. Compute test value of C_{BT} from the test value of C_B using equations (85) or (86).

$$C_{BT, \text{test}} = \frac{\sum \sum f_B(i, j) K(i, j) C_B^j}{\sum f_A(1, j) K(1, j) C_B^j} \frac{C_{AT}}{C_{B, \text{test}}^j}$$

(0 ≤ i ≤ m) (0 ≤ j ≤ n)

4.

Compare $C_{BT, \text{test}}$ and $C_{BT, \text{target}}$. If $C_{BT, \text{test}}$ is close enough to $C_{BT, \text{target}}$, store $C_{BT, \text{test}}$ and $C_{B, \text{test}}$ as $C_{BT}(k, m)$ and $C_B(k, m)$, respectively, and compute and store $C_A(k, m)$.

If $|C_{BT, \text{target}} - C_{BT, \text{test}}| < C_{BT, \text{target}} / 10^3$
Then begin

a) $C_{BT}(k, m) = C_{BT, \text{test}}$

b) $C_B(k, m) = C_{B, \text{test}}$

$$c) C_A(k, m) = \frac{C_{AT}}{\sum f_A(1, j) K(1, j) C_B^j(k, j)}$$

(0 ≤ j ≤ m)

End

5. If $C_{BT, \text{test}}$ is too large, set $C_{B, \text{top}}$ equal to $C_{B, \text{test}}$ and compute a new $C_{B, \text{test}}$.

Else If $C_{BT, \text{test}} > C_{BT, \text{target}}$

Then Begin

a) $C_{B, \text{top}} = C_{B, \text{test}}$

b) Go to 2c.

End.

6. If $C_{BT, \text{test}}$ is too small, set $C_{B, \text{bot}}$ equal to $C_{B, \text{test}}$ and compute a new $C_{B, \text{test}}$.

Then Begin

a) $C_{B, \text{bot}} = C_{B, \text{test}}$

b) Go to 2c.

End.

7. Compute $\bar{S}_{AO, km}$, $\bar{S}_{Bo, km}$, $\bar{S}_{AA, km}$, $\bar{S}_{BB, km}$, $\bar{S}_{AB, km}$, $\bar{S}_{BA, km}$ using equations 69-74.

End Repeat.

End Repeat.

End Algorithm

If species containing 2 subunits of A (A_2 and A_2B_n) are present, equation (68a) is a quadratic.

$$C_{AT} = C_A \sum f_A(1, j) K(1, j) C_B^j + C_A^2 \sum f_A(2, j) K(2, j) C_B^j$$

$$(0 \leq j \leq n) \quad (87)$$

and

$$C_A = \frac{-\sum f_A(1,j)K(1,j)C_B^j}{2\sum f_A(1,j)K(2,j)C_B^j} + \frac{[(\sum f_A(1,j)K(1,j)C_B^j)^2 + 4C_{AT}\sum f_A(1,j)K(2,j)C_B^j]^{1/2}}{2\sum f_A(1,j)K(2,j)C_B^j} \quad (0 \leq j \leq n) \quad (88)$$

Substituting the right hand side of this expression for C_A in equation (68b) gives.

$$C_{BT} = \sum \sum f_B(i,j)K(i,j)C_B^j \frac{[-\sum f_A(1,j)K(1,j)C_B^j]}{[2\sum f_A(1,j)K(2,j)C_B^j]} \quad (0 \leq i \leq m) \quad (1 \leq j \leq n)$$

$$+ \frac{[(\sum f_A(1,j)K(1,j)C_B^j)^2 + 4\sum f_A(1,j)K(2,j)C_B^j C_{AT}]^{1/2}}{2\sum f_A(1,j)K(2,j)C_B^j} \quad (0 \leq j \leq n) \quad (89)$$

A table assembly program for this type of system differs from that for an A_1B_n system only in that equations (88) and (89) are used in place of equations (84) and (85). The A_2B_n assembly program is suitable for systems including A_1B_n species and self associating species in constituent B_n , as well as A_2 and A_2B_n species, but cannot be used for systems

that include self association products in A beyond the dimer.

In dealing with more complex systems ($A_m B_n$, $m > 2$) it is not possible, as it is with simpler systems, to simplify or combine equations (68a) and (68b) in any way that will allow a direct computation of one of the monomer concentrations. A binary search must therefore be employed to find C_A and C_B that simultaneously satisfy equations (68a) and (68b) at a given C_{AT} and C_{BT} . In this case target values are used for both C_{AT} and C_{BT} at each position in the table. Values of C_A and C_B that correspond to values of C_{AT} and C_{BT} that are acceptably close to the target values are located and stored along with the constituent concentrations to which they correspond directly. The target constituent concentrations are not stored in the table.

The organization of the search is such that for each trial value of C_A a value of C_B is found (though a binary search like that used in simpler assembly programs) that satisfies equation (68b). This value of C_B and the trial value of C_A are then tested in equation (68a). If equation (68a) is not satisfied the trial value of C_A is adjusted appropriately and the preceding steps are repeated. This process continues until values for C_A and C_B that satisfy both equations (68a) and (68b) have been located.

It should be noted that this table assembly is capable of dealing with $A_1 B_n$ and $A_2 B_n$ systems as well as more complex

cases. Simpler assembly programs, however, are preferred whenever possible to save computing time.

2.5 TABLE LOOK-UP

In order for a simulation program to extract transport coefficients from a table, it must be equipped with a table look-up routine. The lookup routine consists of (1) a search routine which locates the table entries with constituent concentrations that bracket the boundary constituent concentration(s), and (2) an interpolation routine which computes the local average boundary transport coefficients by linear interpolation(s) between the bracketing table values.

For single constituent (self associating) systems the table search and interpolation routines are fairly simple. To obtain \bar{S}_O , \bar{D} at a boundary where $C_t = C_t(j)$, the search routine inspects each successive value of C_t in the table until it finds a value, $C_t(h)$, greater than or equal to $C_t(j)$. The local average transport coefficients at boundary j are then computed by linear interpolation between the values of the transport coefficients at $C_t(h-1)$ and $C_t(h)$ which bracket $C_t(j)$.

The following algorithm illustrates the table search and interpolation procedure for single constituent (self associating) systems.

Algorithm

- I) Search Routine
- A) $h = 2$
- B) If $C_t(h) \geq C_t(j)$ go to II
- C) $h = h + 1$
- D) go to B
- II) Interpolation ($T \equiv \bar{S}_o$ or \bar{D})
- $T(j) = T(h-1) +$

$$\frac{(T(h) - T(h-1)) (C_t(j) - C_t(h-1))}{(C_t(h) - C_t(h-1))}$$

End Algorithm

The table look-up for a two constituent system not undergoing mixed association is the same, for each constituent, as the single constituent system look-up described above. For example, $\bar{S}_{A,o}(A, j)$, the local average sedimentation coefficient of constituent A at boundary j of constituent track A, is obtained by interpolating between table values $\bar{S}_{A,o}(h)$ and $\bar{S}_{A,o}(h-1)$, which correspond to constituent A concentrations $C_{AT}(h)$ and $C_{AT}(h-1)$, where $C_{AT}(h-1) < C_{AT}(A, j) \leq C_{AT}(h)$.

$$\bar{S}_{A,o}(A, j) = \bar{S}_{A,o}(h-1) + \frac{(\bar{S}_{A,o}(h) - \bar{S}_{A,o}(h-1)) (C_{AT}(A, j) - C_{AT}(h-1))}{(C_{AT}(h) - (C_{AT}(h-1)))}$$

$$\bar{D}_A(A, j) = \bar{D}_A(h-1) + \frac{(\bar{D}_A(h) - \bar{D}_A(h-1)) (C_{AT}(A, j) - C_{AT}(h-1))}{(C_{AT}(h-1)) - (C_{AT}(A, j))} \quad (91)$$

$$\bar{S}_{B, o}(B, j) = \bar{S}_{B, o}(h-1) + \frac{(\bar{S}_{B, o}(h) - \bar{S}_{B, o}(h-1)) (C_{BT}(B, j) - C_{BT}(h-1))}{(C_{BT}(h-1)) - (C_{BT}(B, j))} \quad (92)$$

$$\bar{D}_B(B, j) = \bar{D}_B(h-1) + \frac{(\bar{D}_B(h) - \bar{D}_B(h-1)) (C_{BT}(B, j) - C_{BT}(h-1))}{(C_{BT}(h) - C_{BT}(h-1))} \quad (93)$$

When mixed associations are involved the table look-up procedures become more complex. The table transport coefficient arrays, \bar{S}_A , \bar{S}_B , \bar{D}_{AA} , \bar{D}_{AB} , \bar{D}_{BB} and \bar{D}_{BA} , are all two dimensional. Each member, (i, j) , of these arrays corresponds to a pair of constituent concentrations in the C_{AT} and C_{BT} arrays.

For the simplest mixed associating system, (AB), it may be recalled that the construction of the table does not require a binary search, and that the values of constituent concentrations (C_{AT} and C_{BT}) for each table entry may therefore be selected to create a table with rows varying by ex-

act increments in C_{AT} and columns varying by exact increments in C_{BT} . C_{AT} is constant within a given row and C_{BT} is constant within a given column. The C_{AT} and C_{BT} arrays in a table of this type are one dimensional.

The following algorithm outlines, in general form, the procedure used by the table look-up routine to extract a local average transport coefficient, $T_{A,j}$ or $T_{B,j}$. ($T_{A,j}$ denotes a transport coefficient at boundary j in the constituent A track and $T_{B,j}$ denotes a transport coefficient at boundary j in the constituent B track (ie. $T_{A,j} = \bar{S}_A(A,j)$, $\bar{D}_{AA}(A,j)$ or $\bar{D}_{AB}(A,j)$ and $T_{B,j} = \bar{S}_B(B,j)$, $\bar{D}_{BB}(B,j)$ or $\bar{D}_{BA}(B,j)$), corresponding to boundary constituent concentrations, $C_{AT}(A,j)$ and $C_{BT}(A,j)$ or $C_{AT}(B,j)$ and $C_{BT}(B,j)$, from a table of the type described above.

Algorithm

I) Table search routine

- A) Locate the two members of the C_{AT} table array ($C_{AT}(h-1)$ and $C_{AT}(h)$) whose values bracket the boundary j constituent A concentration ($C_{AT}(j)$).
1. $h = 2$
 2. If $C_{AT}(h) \geq C_{AT}(j)$ go to B
 3. $h = h + 1$
 4. go to 2
- B) Locate members of the table C_{BT} array ($C_{BT}(k-1)$ and $C_{BT}(k)$) whose values bracket the boundary constituent B concentration $C_{BT}(j)$.

1. $k = 2$
2. if $C_{BT}(k) \geq C_{BT}(j)$ go to II
3. $k = k + 1$
4. go to 2

II) Interpolation routine

- A) Interpolate the value of the transport coefficient at $C_{AT} = C_{AT}(h-1)$ and $C_{BT} = C_{BT}(j)$, $T(h-1, j)$, between $T(h-1, k-1)$ and $T(h-1, k)$.

$$T(h-1, j) = T(h-1, k-1) + \frac{(T(h-1, k) - T(h-1, k-1)) (C_{BT}(j) - C_{BT}(k-1))}{(C_{BT}(k) - C_{BT}(k-1))}$$

- B) Interpolate the value of the transport coefficient at $C_{AT} = C_{AT}(h)$ and $C_{BT} = C_{BT}(j)$, $T(h, j)$, between $T(h, k-1)$ and $T(h, k)$.

$$T(h, j) = T(h, k-1) + \frac{(T(h, k) - T(h, k-1)) (C_{BT}(j) - C_{BT}(k-1))}{(C_{BT}(k) - C_{BT}(k-1))}$$

- C) Interpolate the value of the transport coefficient at $C_{AT} = C_{AT}(j)$ and $C_{BT} = C_{BT}(j)$, $T(j)$, between $T(h-1, j)$ and $T(h, j)$.

$$T(j) = T(h-1, j) + \frac{(T(h, j) - T(h-1, j)) (C_{AT}(j) - C_{AT}(h-1))}{(C_{AT}(h) - C_{AT}(h-1))}$$

End Algorithm

It will be recalled that the construction of tables for systems with mixed aggregates of the form AB_n , where n is an integer greater than one, requires a binary search to find corresponding pairs of C_{BT} and C_B , and that therefore, while the target values of C_{BT} are exactly incremented in each row and constant within each column, the values of C_{BT} that are finally stored in the table, those that correspond exactly to the stored transport coefficients, being only close to the target values, are not exactly incremented within rows or constant within columns. The value of C_{BT} is thus unique at each position, (h, k) , in the table so that C_{BT} requires a two dimensional array.

As long as no mixed aggregates containing more than one molecule of constituent A (and no self aggregates of A larger than A_2) are present, a binary search is not required for C_{AT} and the C_{AT} array can be kept one dimensional.

The following algorithm illustrates the general procedure for extracting transport coefficients from tables of this type (ie. a two dimensional C_{BT} array and a one dimensional C_{AT} array).

Algorithm

I) Search routine

A) Locate members of the table C_{AT} array ($C_{AT}(h-1)$ and $C_{AT}(h)$) whose values bracket the boundary constituent A concentration, $C_{AT}(j)$.

1. $h = 2$
2. if $C_{AT}(h) \geq C_{AT}(j)$ go to B
3. $h = h + 1$
4. go to 2

B) Locate members of the C_{BT} array in row h , ($C_{BT}(h, a-1)$ and $C_{BT}(h, a)$, whose values bracket the boundary j constituent B concentration ($C_{BT}(j)$).

1. $a = 2$
2. If $C_{BT}(h, a) \geq C_{BT}(j)$ go to C
3. $a = a + 1$
4. go to 2

C) Locate members of the C_{BT} array in row $h-1$, ($C_{BT}(h-1, b-1)$ and $C_{BT}(h-1, b)$, whose values bracket $C_{BT}(j)$.

1. $b = 2$
2. if $C_{BT}(h-1, b) \geq C_{BT}(j)$ go to II
3. $b = b + 1$
4. go to 2

II) Interpolation routine

- A) Interpolate the value of the transport coefficient at $C_{AT} = C_{AT}(h-1)$ and $C_{BT} = C_{BT}(j)$, $T(h-1, j)$, between $T(h-1, b-1)$ and $T(h-1, b)$.

$$T(h-1, j) = T(h-1, b-1) + \frac{(T(h-1, b) - T(h-1, b-1)) (C_{BT}(j) - C_{BT}(h-1, b-1))}{(C_{BT}(h-1, b) - C_{BT}(h-1, b-1))}$$

- B) Interpolate the value of the transport coefficient at $C_{AT} = C_{AT}(h)$ and $C_{BT} = C_{BT}(j)$, $T(h, j)$, between $T(h, a-1)$ and $T(h, a)$.

$$T(h, j) = T(h, a-1) + \frac{(T(h, a) - T(h, a-1)) (C_{BT}(j) - C_{BT}(h, a-1))}{(C_{BT}(h, a) - C_{BT}(h, a-1))}$$

- C) Interpolate the value of the transport coefficient at $C_{AT} = C_{AT}(j)$ and $C_{BT} = C_{BT}(j)$, $T(j)$, between $T(h-1, j)$ and $T(h, j)$.

$$T(j) = T(h-1, j) + \frac{(T(h, j) - T(h-1, j)) (C_{AT}(j) - C_{AT}(h-1))}{(C_{AT}(h) - C_{AT}(h-1))}$$

End Algorithm

Generating tables for more complex mixed associating systems (ie. systems with mixed aggregates of the form $A_m B_n$,

where $m > 1$ and $n > 1$, or systems with only AB_n mixed aggregates but with one or more A_m aggregates with $m > 2$) involves a binary search for $C_{AT} - C_A$ pairs as well as for $C_{BT} - C_B$ pairs. As a result the values of both C_{AT} and C_{BT} are unique at each position in the table and two dimensional tables are necessary for both constituent concentrations.

Because of the irregularity of tables of this type, the look-up routine that is required is somewhat more involved than those required for simpler systems and the transport coefficients extracted from them are likely to be slightly more erroneous than those extracted from the more orderly tables.

As with simpler mixed associating systems, four points are located in the table for interpolation, and these four points define a quadrilateral which contains the point $(C_{AT}(j), C_{BT}(j))$, where the interpolation is to take place. However, whereas with simpler tables it is always possible to select points which allow interpolation (as opposed to extrapolation) along all four sides of the quadrilateral, this is not the case with the doubly irregular tables.

Portions of each type of mixed association table are shown in figure 5. In the first two types of tables (AB and AB_n) any point, $(C_{AT}(j), C_{BT}(j))$, will lie within a quadrilateral in such a way that (1) $C_{BT}(j)$ will fall between the C_{BT} values of the two points that define the top of the quadrilateral, (2) $C_{BT}(j)$ will fall between the C_{BT} values

of the two points that define the bottom of the quadrilateral, (3) $C_{AT}(j)$ will fall between the C_{AT} values of the two points that define the left side of the quadrilateral and (4) $\beta_{CAT}(j)$ will fall between the C_{AT} values of the two points that define the right side of the quadrilateral. Furthermore, these four conditions can always be satisfied (in the simpler tables) without extending any edge of the quadrilateral over more than one table division in either constituent concentration. (eg. in figure 5-b these conditions are met by selecting table points (2,3), (2,4), (3,3) and (3,2).

Figure 5-c depicts a situation which can arise while interpolating from the double irregular table of an A_nB_m system. The point $C_{AT}(j), C_{BT}(j)$ is included in the quadrilateral (2,3), (2,4), (3,4), (3,3). However, $C_{BT}(j)$ is less than $C_{BT}(2,3)$ so that the first condition listed above is violated and an extrapolation will be necessary along this side of the quadrilateral with respect to C_{BT} . Moreover, there are no four points which satisfy all four conditions without extending an edge of the quadrilateral through two table divisions in one constituent concentration or the other. Although the irregularity of the table in figure 5 has been greatly exaggerated for illustration (in a typical table the deviation from rectangularity would be barely noticeable) this problem is real and will occur in a small percentage of the interpolations. However, since the

irregularity is very small in relation to the distance between adjacent table entries, it is not a serious problem and a sufficiently accurate "interpolation" should always be possible.

The A_{nB_m} search routine is responsible for locating an appropriate "rectangular" quadrilateral for interpolation at $C_{AT}(j)$, $C_{BT}(j)$ (rhombic quadrilaterals are not considered⁶). A first guess is made by locating the table entries in the first row whose C_{BT} values bracket $C_{BT}(j)$, and the entries in the first column whose C_{AT} values bracket $C_{AT}(j)$. For instance, if $C_{BT}(1,k-1) < C_{BT}(j) < C_{BT}(1,k)$, and $C_{AT}(h-1,1) < C_{AT}(j) < C_{AT}(h,1)$, then since the table is irregular, but only slightly so, $(C_{AT}(j), C_{BT}(j))$ should be included either within the quadrilateral $(h-1,k-1)$, $(h-1,k)$, (h,k) , $(h,k-1)$ or within one of eight quadrilaterals surrounding it.

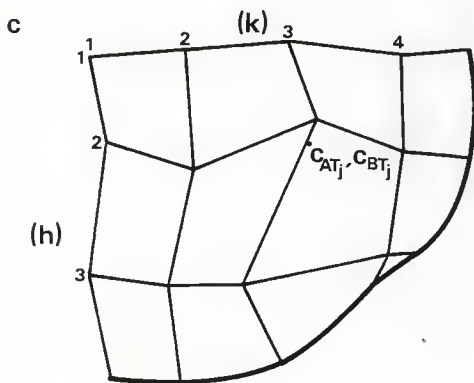
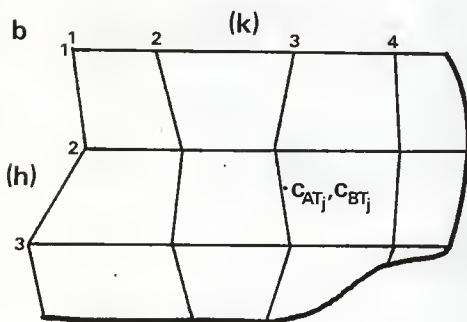
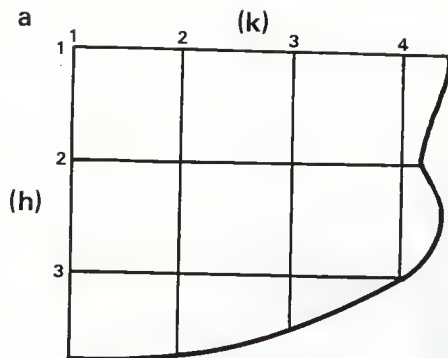
The search routine then sequentially checks each edge of the test quadrilateral to determine whether the point $C_{AT}(j)$, $C_{BT}(j)$ lies on the inside or outside of the quadrilateral along that edge. If $C_{AT}(j)$, $C_{BT}(j)$ lies outside of

6

In addition to the rectangular quadrilateral(s) several (4-12) rhombic quadrilaterals may contain the point $C_{AT}(j)$, $C_{BT}(j)$. Although one or more of these rhomboids may be more optimal for interpolation than the rectangular quadrilateral (the most ambitious table extraction procedure might be to average the interpolated values from all (as many as 16) of the quadrilaterals containing $C_{AT}(j)$, $C_{BT}(j)$) the "first rectangular quadrilateral" method should give adequately accurate results, is much simpler, and would consume less computer time than procedures that consider other quadrilaterals.

Figure 5: Types of Table Organization

- a. Regular Table: AB systems only
 C_{AT} and C_{BT} evenly spaced.
- b. Irregular Table: AB_n systems only
 C_{AT} evenly spaced, C_{BT} spaced unevenly.
- c. Double Irregular Table: A_nB_m systems
 C_{AT} and C_{BT} both spaced unevenly.



the quadrilateral on a given edge then the test quadrilateral is moved, horizontally or vertically, one table division in the appropriate direction. Checking and repositioning continue until the correct quadrilateral is located.

The following algorithm illustrates the procedure used by the search routine to locate a rectangular quadrilateral, in an $A_n B_m$ table, that includes the point $(C_{AT}(j), C_{BT}(j))$.

Algorithm

I) Search Routine.

A) Locate table entries in column 1 whose C_{AT} values bracket $C_{AT}(j)$ (ie. $C_{AT}(h-1,1)$ and $C_{AT}(h,1)$):

$$C_{AT}(h-1,1) < C_{AT}(j) \leq C_{AT}(h,1)$$

1. $h = 2$

2. If $C_{AT}(h,1) \geq C_{AT}(j)$ Then Proceed

Else Begin

a) $h = h + 1$

b) Go to 2.

End

B) Locate table entries in row 1 whose C_{BT} values bracket $C_{BT}(j)$ (ie. $C_{BT}(1,k-1)$ and $C_{BT}(1,k)$):

$$C_{BT}(1,k-1) < C_{BT}(j) \leq C_{BT}(1,k)$$

1. $k = 2$

2. If $C_{BT}(1,k) \geq C_{BT}(j)$ Then Proceed

;Else Begin

a) $k = k + 1$

b) Go to 2

End

C) Inspect each edge of the quadrilateral $(h, k-1)$, $(h-1, k-1)$, $(h-1, k)$, (h, k) and adjust h and k , if necessary, until a suitable quadrilateral is located.

1. If $C_{AT}(j) \leq C_{AT}(h, k-1) +$

$$(C_{BT}(j) - C_{BT}(h, k-1)) \frac{C_{AT}(h, k) - C_{AT}(h, k-1)}{C_{BT}(h, k) - C_{BT}(h, k-1)}$$

Then Proceed

Else Begin

a) $h = h + 1$

b) Go to 3

End

2. If $C_{AT}(j) \geq C_{AT}(h-1, k) +$

$$(C_{BT}(j) - C_{BT}(h-1, k-1)) \frac{C_{AT}(h-1, k) - C_{AT}(h-1, k-1)}{C_{BT}(h-1, k) - C_{BT}(h-1, k-1)}$$

Then Proceed

Else Begin

a) $h = h - 1$

b) Proceed.

End

3. If $C_{BT}(j) \geq C_{BT}(h-1, k-1) +$

$$(C_{AT}(j) - C_{AT}(h-1, k-1)) \frac{C_{BT}(h, k-1) - C_{BT}(h-1, k-1)}{C_{AT}(h, k-1) - C_{AT}(h-1, k-1)}$$

Then Proceed

Else Begin

a) $k = k - 1$

b) Go to C

End

4. If $C_{BT}(j) \leq C_{BT}(h-1, k) +$

$$(C_{AT}(j) - C_{AT}(h-1, k)) \frac{C_{BT}(h, k) - C_{BT}(h-1, k)}{C_{AT}(h, k) - C_{AT}(h-1, k)}$$

Then Proceed
Else Begin

a) $k = k + 1$

b) Go to C

End

End Algorithm

The following algorithm illustrates the interpolation procedure for $A_n B_m$ systems.

Algorithm

I) Interpolate the values of the transport coefficient and C_{BT} at C_{AT} , along line $(h-1, k-1)$, $(h, k-1)$.

A) $T(j, k-1) = T(h-1, k-1) +$

$$(T(h, k-1) - T(h-1, k-1)) \frac{C_{AT}(j) - C_{AT}(h-1, k-1)}{C_{AT}(h, k-1) - C_{AT}(h-1, k-1)}$$

B) $C_{BT}(j, k-1) = C_{BT}(h-1, k-1) +$

$$(C_{BT}(h, k-1) - C_{BT}(h-1, k-1)) \frac{C_{AT}(j) - C_{AT}(h-1, k-1)}{C_{AT}(h, k-1) - C_{AT}(h-1, k-1)}$$

II) Interpolate the values of the transport coefficient and C_{BT} at $C_{AT}(j)$ along line $(h-1, k)$, (h, k)

$$A) T(j, k) = T(h-1, k) +$$

$$(T(h, k) - T(h-1, k)) \frac{C_{AT}(j) - C_{AT}(h-1, k)}{C_{AT}(h, k) - C_{AT}(h-1, k)}$$

$$B) C_{BT}(j, k) = C_{BT}(h-1, k) +$$

$$(C_{BT}(h, k) - C_{BT}(h-1, k)) \frac{C_{AT}(j) - C_{AT}(h-1, k)}{C_{AT}(h, k) - C_{AT}(h-1, k)}$$

III) Interpolate transport coefficients at $C_{AT}(j)$,

$$C_{BT}(j).$$

$$T(j) = T(j, k-1) +$$

$$(T(j, k) - T(j, k-1)) \frac{C_{BT}(j) - C_{BT}(j, k-1)}{C_{BT}(j, k) - C_{BT}(j, k-1)}$$

A) End.

End Algorithm

2.6 RE-INDEXING

When the boundaries are shifted in a sedimentation transfer, the entire array of boxes, the simulation's frame of reference, is displaced downward in the cell. Space is created between the initial top of the array, r_0 , and the first boundary while the last boundary migrates past the initial bottom, r_{bot} (see figure 6).

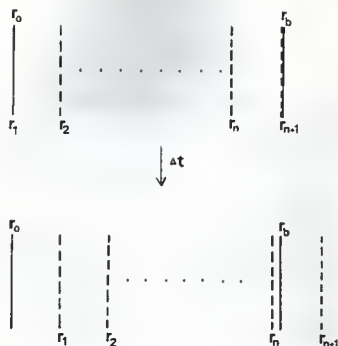


Figure 6: Boundary Movement

If this process were allowed to continue, unchecked, through a large number of sedimentation transfers, a large part of the array would wind up outside the cell.

To keep the simulation arrays from sliding out of the cell, new boxes are usually (but not always⁷) added to the top of the array as space becomes available. A constant number of boxes is maintained by eliminating one box from the bottom of the array for every box added to the top.

When the space between r_0 and r_1 is large enough (ie. when $r_1 - r_0 \geq \Delta\bar{r}$), a new box, $\Delta\bar{r}$ wide, is created at the top by inserting a new boundary. The new boundary becomes the first in the array and is assigned a position

⁷ Occasionally it is desirable to use a very short, finely divided array (especially for simulating systems with large species that generate sharp boundaries). In these cases simulation arrays are allowed to slide and re-indexing is bypassed.

$$r_{\text{new},1} = r_1 - \Delta\bar{r} \quad (94)$$

In most cases the initial solute boundary is far enough below the top of the array that the concentration of the new box can safely be set to zero ($c_{\text{new},1} = 0.0$).

To accommodate a new box at the top, the old boxes below must be re-indexed, and the last box discarded. To avoid propagating r_1 and c_1 to the bottom of the array, reindexing must be carried out in two steps:

1. The new r and c values are stored with the appropriate new indices in "temporary holding arrays" (r_{new} and c_{new}).
2. The r and c array members are assigned the values of the r_{new} and c_{new} array members.

The following algorithm adds a box to the top and reindexes the simulation arrays (if and only if there is room).

Algorithm

- I) If $r(1) - r_0 \geq \Delta\bar{r}$
Then Begin
 - A) $C_{\text{new}}(1) = 0.0$
 - B) $r_{\text{new}}(1) = r(1) - \Delta\bar{r}$
 - C) Repeat from $i = 2$ to $n+1$
 1. $r_{\text{new}}(i) = r(i-1)$
 2. $C_{\text{new}}(i) = C(i-1)$
 End Repeat.

D) Repeat from $i = 1$ to $n+1$

$$1. \quad r(i) = r_{\text{new}}(i)$$

$$2. \quad C(i) = C_{\text{new}}(i)$$

End Repeat;

End

Else Continue

End Algorithm

2.7 REGULATING BOX SIZES

Because the boundaries sediment at different rates, the original box sizes will change during the sedimentation routine. Some boxes may become much wider than $\Delta \bar{r}$, others much narrower. Boundary spreading can be expected with associating systems in areas where the gradient profile is steep and will be most pronounced when the concentration there corresponds to a rapidly rising region of the S vs. C curve for the system. Compression of boxes occurs when the concentration gradient is steep and the sedimentation coefficient is decreasing with concentration (due to hydrodynamic dependence).

Boxes that are too wide lead to serious errors in interpolation. Boxes that are too narrow are overly sensitive to small errors in shifting the boundaries. In a very narrow box, the error in volume that would result from a slight error in moving one of its boundaries would represent a significant fraction of the boxes total volume and would therefore lead to a sizeable error in the concentration.

In order to avoid these problems box sizes must be regulated. Thus, following each sedimentation event, the sizes of all of the boxes are examined, and any boxes that are narrower than $0.8 \Delta \bar{r}$ or wider than $2 \Delta \bar{r}$ are eliminated.

2.7.1 Box Splitting

If a box is found to be too large it is split at its midpoint into two halves. The concentrations in the upper and lower half-boxes, C_{top} and C_{bot} , are calculated using expressions that incorporate conservation of mass. According to the Law of Conservation of Mass:

$$c_j (r_{j+1}^2 - r_j^2) = C_{bot} (r_{j+1}^2 - \bar{r}_j^2) + C_{top} (\bar{r}_j^2 - r_j^2) \quad (95)$$

where c_j is the concentration of the original box, of which r_{j-1} and r_j are the upper and lower boundaries, and \bar{r}_j is the midpoint.

Assuming a linear gradient within box j , the concentrations (at the midpoints) of the upper and lower box halves are related to one another as follows.

$$C_{bot} = C_{top} + \bar{g}_j \Delta r \quad (96)$$

⁸ \bar{g}_j is interpolated between g_{j+1}^j at r_{j+1}^j and g_j^j at r_j^j as

where \bar{g}_j is the gradient at the midpoint of box j ⁸ and Δr is the distance between the midpoints of the two box halves.

Substituting the right hand side of equation 96 for C_{bot} in equation 95 gives

$$c_j(r_{j+1}^2 - r_j^2) = (C_{top} + \bar{g}_j \Delta r)(r_{j+1}^2 - \bar{r}_j^2) + C_{top}(\bar{r}_j^2 - r_j^2) \quad (98)$$

Factoring this gives

$$\begin{aligned} c_j(r_{j+1} + r_j)(r_{j+1} - r_j) = \\ (C_{top} + \bar{g}_j \Delta r)(r_{j+1} + \bar{r}_j)(r_{j+1} - \bar{r}_j) + \\ C_{top}(\bar{r}_j + r_j)(\bar{r}_j - r_j) \end{aligned} \quad (99)$$

Then, since

follows:

$$\bar{g}_j = g_j' + (g_{j+1}' - g_j') \frac{(\bar{r}_j - r_j')}{(r_{j+1}' - r_j')} \quad (97)$$

where g_j' and g_{j+1}' are the gradients at the midpoints between adjacent box centers (see eq 20-21).

$$r_{j+1} - \bar{r}_j = \bar{r}_j - r_j = \frac{r_{j+1} - r_j}{2} \quad (100)$$

equation 99 can be simplified to give

$$2c_j(r_{j+1} + r_j) = (C_{top} + \bar{g}_j \Delta r)(r_{j+1} + \bar{r}_j) + C_{top}(\bar{r}_j + r_j) \quad (101)$$

Re-grouping and re-arranging gives

$$C_{top} = \frac{2c_j(r_{j+1} + r_j) - \bar{g}_j \Delta r(r_{j+1} + \bar{r}_j)}{r_{j+1} + r_j + 2\bar{r}_j} \quad (102)$$

Since $2\bar{r}_j = r_{j+1} + r_j$, the denominator in equation 102 can be rewritten as $2(r_{j+1} + r_j)$. Making this substitution and simplifying gives

$$C_{top} = c_j - \bar{g}_j \frac{\Delta r(r_{j+1} + \bar{r}_j)}{2(r_{j+1} + r_j)} \quad (103)$$

Finally, since

$$r_{j+1} + \bar{r}_j = 2\bar{r}_j + \Delta r$$

and

$$r_{j+1} + r_j = 2\bar{r}_j,$$

equation (103) can be rewritten as

$$C_{top} = C_j - \frac{\bar{g}_j \Delta r}{4} \left[2 + \frac{\Delta r}{\bar{x}_j} \right]. \quad (104)$$

Equation (104) is used to calculate C_{top} which is then used in equation (96) to compute C_{bot} . The arrays are then re-indexed to include the new boundary. The top half of the split box becomes box j with a concentration of $c_{new}(j) = C_{top}$. The bottom half becomes box $j+1$ with $c_{new}(j+1) = C_{bot}$ and an upper boundary, the new boundary, at $r_{new}(j+1)$. The indices of the concentration and boundary position arrays are incremented by one. The last members of the original arrays are not copied into the re-indexed arrays and are thereby discarded. Figure 7 illustrates box splitting and reindexing.

The following algorithm reindexes the r and c arrays when a box is split.

Algorithm

- I) $c_{new}(j) = C_{top}$
- II) $c_{new}(j+1) = C_{bot}$

before box splitting:



after splitting box j:



Figure 7: Box Splitting and Re-indexing

$$\text{III) } r_{\text{new}}(j+1) = [(r(j) + r(j+1)]/2$$

IV) Repeat from $i = (j+2)$ to $(n+1)$

$$\text{A) } r_{\text{new}}(i) = r(i-1)$$

$$\text{B) } c_{\text{new}}(i) = c(i-1)$$

End repeat.

V) Repeat from $i = 1$ to $(n+1)$

$$\text{A) } r(i) = r_{\text{new}}(i)$$

$$\text{B) } c(i) = c_{\text{new}}(i)$$

End repeat.

End Algorithm

2.7.2 Box Squashing

When a box is found to be too narrow, it is also split at its midpoint and the concentrations in the two halves are computed as described above (equation (104) and (96)). In this case however, the upper and lower halves are added to

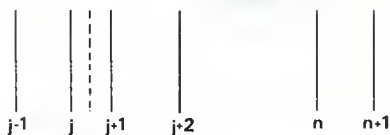
the boxes immediately above and below them, and the original boundaries of the undersized box are dissolved, ie. three boxes become two, (see figure 8). The concentrations of the resulting combined boxes are computed directly from the conservation of mass expressions:

$$c_{\text{new}(j-1)} = \frac{(c_{\text{top}})(\bar{r}_j^2 - r_j^2) + c_{j-1}(r_j^2 - r_{j-1}^2)}{(\bar{r}_j^2 - r_{j-1}^2)} \quad (105)$$

$$c_{\text{new}(j)} = \frac{(c_{\text{bot}})(r_{j+1}^2 - \bar{r}_j^2) + c_{j+1}(r_{j+2}^2 - r_{j+1}^2)}{(r_{j+2}^2 - \bar{r}_j^2)} \quad (106)$$

The arrays are then re-indexed. The boundary that was added at the center of the original undersized box becomes boundary j since the original boundary j , the upper boundary of the undersized box, was eliminated. Since the original boundary $j+1$ was also removed, the indices of all array members below the new boundary j must be reduced by one. Also, because there was a net loss of one boundary (and one box) in this transaction, a new boundary must be added to the bottom of the array. The new box is usually given the same width and concentration as the box immediately above it. Figure 8 illustrates box squashing and re-indexing. The following algorithm re-indexes r and c arrays following box squashing.

before box squashing:



after squashing box j :



Figure 8: Box Squashing

Algorithm

- I) $r_{\text{new}}(j) = [r(j) + r(j+1)]/2$
- II) Repeat from $i = j+1$ to $n-1$
 - A) $r_{\text{new}}(i) = r(i+1)$
 - B) $c_{\text{new}}(i) = c(i+1)$

End Repeat.
- III) $r_{\text{new}}(n) = r(n+1)$
- IV) $r_{\text{new}}(n+1) = r_{\text{new}}(n) + (r_{\text{new}}(n) - r_{\text{new}}(n-1))$
- V) $c_{\text{new}}(n) = c_{\text{new}}(n-1)$
- VI) Repeat from $i = 1$ to n
 - A) $r(i) = r_{\text{new}}(i)$
 - B) $c(i) = c_{\text{new}}(i)$

End Repeat.
- VII) $r(n+1) = r_{\text{new}}(n+1)$

End Algorithm

Splitting an oversized box in two does not guarantee that the two daughter boxes will be smaller than $2\Delta\bar{r}$. If the original box is greater than $4\Delta\bar{r}$, the the two new boxes will be oversized as well. Also, eliminating an undersized box by dividing its volume and contents between its neighbors could cause either or both of its neighbors to become oversized where they had not been before. Thus the box splitting routine must re-check the sizes of the boxes that were altered before proceeding further in the array.

2.8 TIME INTERVALS

2.8.1 Sedimentation Transfer Time

The time for a sedimentation transfer, Δt_S , is usually chosen so that each sedimentation transfer will create a space at the top of the array that is exactly sufficient for the addition of one box.

$$r_{\text{new}}(1) = r(1) + \Delta\bar{r} = r(1)\exp[S(1)\omega^2\Delta t_S] \quad (107)$$

$$\Delta t_S = \frac{1}{S(1)\omega^2} \ln \frac{[r(1) + \Delta\bar{r}]}{r(1)} \quad (108)$$

$S(1)$ is the sedimentation coefficient at the first boundary and is usually taken as the sedimentation coefficient of the monomer at infinite dilution (the concentration at the

first boundary is usually zero). When two or more constituents are present the sedimentation coefficient of the fastest sedimenting monomer is used to calculate Δt_S .

2.8.1.1 Diffusion Transfer Time

Complete simulation of velocity sedimentation during the interval Δt_S includes simulation of diffusion for an equal time. Thus a convenient time interval for diffusion operations, Δt_D , might be simply Δt_S . However, Δt_S is usually too long for a single diffusion operation. It was noted earlier that diffusion times must be short because the simulation expressions for diffusion do not account for gradient changes during the diffusion time interval. The most serious error resulting from a long diffusion time would occur at the initial sharp solute boundary. There the steep gradient would result in an initial rapid diffusion of solute from the first box containing solute into the empty box immediately above it. In a real cell the initial diffusion would rapidly deplete the initially steep gradient continuously decreasing the rate of diffusion at the initial sharp boundary position. In the discontinuous simulation operation, however, the gradient and rate of diffusion are constant throughout Δt_D . If Δt_D is too long, then, an inappropriately large amount of solute would be transferred in the first diffusion operation from the first full box to the empty box above it.

The choice of a maximum value for Δt_D is based on the flow of solute at the initial sharp boundary in a rectangular cell with equal box widths (Δr) (see figure 9).

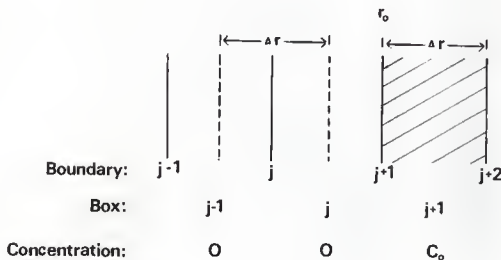


Figure 9: Rectangular Boxes, Equal Box Widths

The mass of solute that will pass from box $i+1$ to box i in Δt_D is

$$\Delta m_2 = DA\Delta t_D \frac{c_{i+1} - c_i}{\Delta r} = DA\Delta t_D \frac{C_0}{\Delta r} \quad (109)$$

where A is the cross sectional area, D is the diffusion coefficient and $(C_{i+1} - C_i)/\Delta r$ is the gradient at boundary $i+1$.

The mass of solute that will flow from box i into box $i+1$ in Δt_D is

$$\Delta m_1 = D A \Delta t \frac{c_i - c_{i-1}}{\Delta r} = 0. \quad (110)$$

The change in the concentration of box i , the first box above the initial sharp boundary, is then

$$\Delta c_i = \frac{\Delta m_2 - \Delta m_1}{A \Delta r} = \frac{\Delta m_2}{A \Delta r} \quad (111)$$

Substituting the right side of (109) for Δm_2 and simplifying gives

$$\Delta c_i = \frac{D \Delta t C_0}{\Delta r^2} \quad (112)$$

or

$$\Delta c_i = a C_0 \quad \text{where } a = \frac{D \Delta t}{\Delta r^2} \quad (113)$$

a is the fraction of solute initially in box $i+1$ that is transferred to the empty box, i , in the first diffusion operation. Obviously, a cannot be greater than 0.5 since if it were, then the sign of the gradient at boundary $i+1$ would be reversed, implying that some of the solute from box $i+1$ had travelled into box i against a positive gradient. An arbitrary maximum value for a has thus been set at 0.2.

$$\alpha = \frac{D\Delta t_D}{\Delta r^2} \leq 0.2 \quad (114)$$

Δt_D is thus limited as follows:

$$\Delta t_D \leq \frac{0.2D_{\max}}{\Delta r_{\min}^2} \quad (115)$$

D_{\max} is the largest diffusion coefficient that could occur in the system - usually that of the smallest species present. Δr_{\min} is the smallest allowable box width ($0.8 \Delta r_{Ave}$). D_{\max} and Δr_{\min} are used to ensure that α will not be greater than 0.2 under any circumstances at any time or place in the cell during the simulation.

To simulate diffusion for a time equal to Δt_S it is necessary to find a Δt_D smaller than $0.2D_{\max} / \Delta r_{\min}^2$ that is an integral factor of Δt_S :

$$\Delta t_S = n_D \Delta t_D \quad (116)$$

The simulated transport corresponding to a total time of Δt_S consists of n_D rounds of diffusion for Δt_D seconds each followed by one sedimentation operation corresponding to Δt_S seconds of sedimentation. Δt_D and n_D can be computed as follows:

$$I) \quad \Delta t_{D_{\max}} = \frac{0.2 D_{\max}}{\Delta r_{\min}^2} \quad (117)$$

$$II) \quad n_D = \frac{|\Delta t_S|}{|\Delta t_{D_{\max}}|} + 1 \quad (118)$$

III)

$$\Delta t_D = \frac{\Delta t_S}{n_D} \quad (119)$$

2.9 TIME AVERAGING

In two constituent systems the boundaries of the two constituent tracks will often sediment at different rates so that during Δt_S a boundary in one of the constituent tracks will move through a range of concentrations in the other constituent. If, as is usually the case, the local sedimentation coefficient of each constituent depends on the local concentration of the other constituent, then the sedimentation coefficients at the boundaries will change during Δt_S . Thus new boundary positions computed from the initial local

sedimentation coefficients will be systematically in error. This error can be largely eliminated by computing boundary sedimentation coefficients from local constituent concentrations that are time-averaged over the interval Δt_s . The time-averaged boundary conditions are obtained as follows.

- I) Initial boundary constituent concentrations are calculated in the usual way (eq. 60-61) and are stored.
- II) The initial conditions in I are used to compute sedimentation coefficients for each boundary.
- III) The sedimentation coefficients in II are used to make a "provisional shift" of the boundaries. (The provisional shift provides approximate end-of-shift conditions)
- IV) The boundary conditions at the end of the provisional shift are computed and stored.
- V) Boundary constituent concentrations from I and IV are averaged.
- VI) The time averaged boundary conditions in V are used to compute time averaged sedimentation coefficients at each boundary.
- VII) The boundaries are returned to their initial positions and new boundary positions are computed using the averaged sedimentation coefficients in VI.

Chapter III
EXPERIMENTS AND SIMULATIONS

3.1 UNCOOPERATIVE AB_N SYSTEMS

We begin by looking at uncooperative AB_n systems in which the binding of a molecule of B to one of the binding sites on A is independent of the occupancy of the other sites on A. For these systems the mole-scale step wise association constants, K_i (where i=1,2...n), are related to the intrinsic association constant, K_I, as follows:

$$K_i = \frac{[AB_i]}{[B][AB_{i-1}]} = K_I \frac{(n-i+1)}{i}$$

where n is the number of binding sites (on A for B) and

$$K_I = \frac{[AB_i]_j}{[B][AB_{i-1}]_j}$$

the association constant for the formation of a particular species of AB_i, (AB_i)_j, by the binding of a molecule of B to a particular binding site, j, on A.

The simulated gradient profile (schlieren pattern; (dc/dr) vs r) of an uncooperative AB₂ system is shown in figure 10a. In this particular hypothetical system the intrinsic association constant, K_I, is 1.0x10⁵ (fairly tight), the mo-

lecular weights of both monomers (A and B) are the same (100Kd), and the frictional ratios (f/f_0) of all species (A, B, AB, AB_2) are equal. The initial constituent concentrations, C_{AT} and C_{BT} , are both 5 mg/ml or $5 \times 10^{-5} M$ (1:1 constituent mole ratio)

The theoretical gradient in figure 10a, produced by the COXMIX distorted-grid simulation program (for systems undergoing mixed association with rapid equilibration) with the SBABN table assembly program (for AB_n systems),⁹ represents the situation in the ultracentrifuge cell after 2155.5 seconds of velocity sedimentation at 60,000 rpm. (241,170xg at $r_0 = 6.00 \text{ cm.}$).

The migrating boundary of this system is clearly bimodal¹⁰. The trailing boundary migrates at the sedimentation rate of free monomer. The position of the trailing boundary (R_T) is the same as that predicted for free monomer with no hydrodynamic dependence. (The predicted positions of individual species with minimum and maximum hydrodynamic dependence are given in table 2). The individual constituent gradients (see fig. 10) indicate that the trailing boundary consists of excess A monomer - in agreement with its sedi-

⁹ The simulation and table assembly programs used throughout this work can be found with Dr. David J. Cox, Department of Biochemistry, Kansas State University.

¹⁰ In general, AB_n systems with $n > 1$ give bimodal boundaries, provided the association is not too weak (see fig. 10). Weakly associating AB_n systems with $n > 1$ have skewed boundaries. $AB (n=1)_n$ boundaries are not bimodal (fig. 11), provided that the initial molar ratio of constituents is 1:1.

Figure 10: Gradient Profiles of Uncooperative AB_n Systems

$$W_A = 100\text{Kd}$$

$$W_B = 100\text{Kd}$$

$$C_{AT} = 5.0 \text{ mg/ml}$$

$$C_{BT} = 5.0 \text{ mg/ml}$$

$$[A] = 5 \times 10^{-5}$$

$$[B] = 5 \times 10^{-5}$$

$$[B]/[A] = 1.0$$

Frictional ratios (f/f_0) for all species = 1.1

All self and cross hydrodynamic constants (k) = 0.01

Species transport coefficients are given in table 2.

Rotor speed = 60,000 rpm.

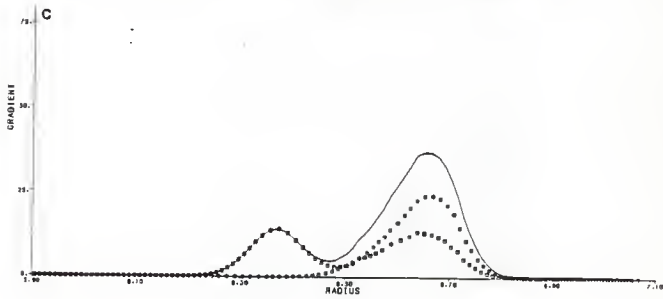
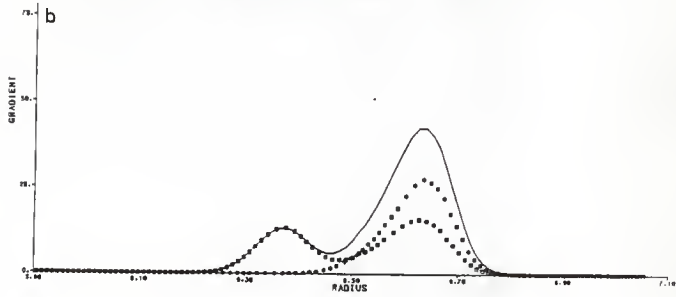
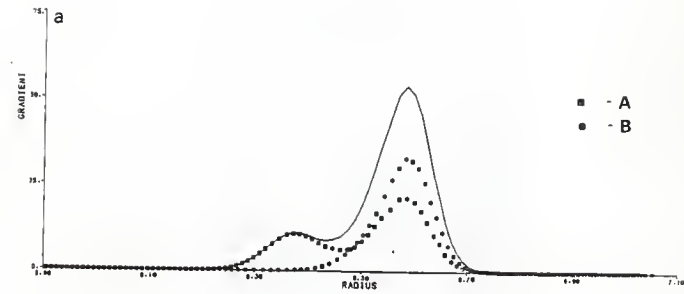
Initial sharp boundary position (r_0) = 6.0 cm.

$\Delta t = 2155.51 \text{ sec.}$

a. $AB_2, K_I = 10^5$

b. $AB_3, K_I = 10^5$

c. $AB_4, K_I = 10^5$



mentation rate. However, the concentration of constituents at the trailing boundary are not negligible (particularly not at earlier times), and, therefore, if the trailing boundary were migrating as free monomer throughout the simulation its final position would be expected to reflect significant hydrodynamic effects.

That the trailing boundary moves at an average rate greater than that of free monomer with a plausible concentration dependence is probably due to participation of material in the trailing boundary (excess A) in aggregated species (AB , AB_2) at earlier times in the experiment.

The position of the leading boundary, R_L , corresponds to an average sedimentation rate greater than that of AB_1 (at $C_{AT,0}$ and $C_{BT,0}$), but considerably less than that of AB_2 (at $C_{AT,0}$ and $C_{BT,0}$), i.e.

$$R_{\min AB} = 6.54 \text{ (cm.)} < R_L = 6.59 < R_{\min AB_2} = 6.72.$$

Gradient profiles for uncooperative AB_3 and AB_4 systems are also shown in figure 10. As with the AB_2 system the profiles of the AB_3 and AB_4 systems are bimodal, the individual constituent gradients show that the trailing boundaries consist almost entirely of constituent A and the trailing boundaries migrate at average rates somewhat faster than would be expected for concentration dependent sedimentation of free monomer. Although $R_L(AB_4) > R_L(AB_3) > R_L(AB_2)$ leading boundary positions for both of these systems still fall between $R_{\min AB}$ and $R_{\min AB_2}$.

Figure 11: Gradient Profiles of AB Systems of Different Strengths

$$W_A = 100\text{Kd}$$

$$W_B = 100\text{Kd}$$

$$C_{AT} = 5.0 \text{ mg/ml}$$

$$C_{BT} = 5.0 \text{ mg/ml}$$

$$[A] = 5 \times 10^{-5}$$

$$[B] = 5 \times 10^{-5}$$

$$[B]/[A] = 1.0$$

Frictional ratios (f/f_0) for all species = 1.1

All self and cross hydrodynamic constants (k) = 0.01

Species transport coefficients are given in table 2.

Rotor speed = 60,000 rpm.

Initial sharp boundary position (r_0) = 6.0 cm.

$\Delta t = 2155.51 \text{ sec}$

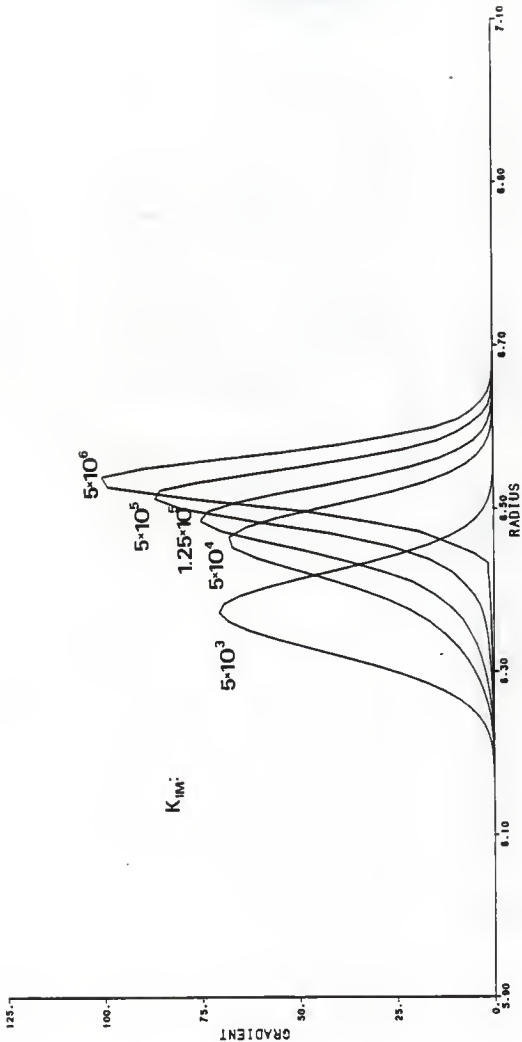


TABLE 2

Species Transport Coefficients and Positions (at 2155.51 sec)
for Systems with $W_A = W_B = 100 \text{Kd}$.

Species	S_o ($\times 10^{13}$ sec)	D ($\times 10^7$ cm^2/sec)	r_{\max}^* (cm)	r_{\min}^* (cm)
A	7.0446	6.3558	6.371	6.336
B	7.0446	6.3558	6.371	6.336
AB	11.183	5.0446	6.599	6.542
AB ₂	14.653	4.4069	6.797	6.720
AB ₃	17.752	4.0041	6.978	6.883
AB ₄	20.598	3.7168	7.149	7.036

$$\bar{v} = 0.73 \text{ cm}^3/\text{mg}$$

$$\rho = 1.0 \text{ g/cm}^3$$

$$\eta = 0.01 \text{ poise}$$

$$r_{\max} = r_o \exp(S_o \omega^2 \Delta t)$$

$$r_{\min} = r_o \exp(S_o \omega^2 \Delta t / (1 + k_{\text{ave}}(C_{\text{AT}} + C_{\text{BT}})))$$

where

$$\omega = 2000\pi \text{ radians/sec}$$

$$\Delta t = 2155.51 \text{ sec}$$

$$k_{\text{ave}} = 0.01 \text{ ml/mg}$$

$$C_{\text{AT}} = 5.0 \text{ mg/ml}$$

$$C_{\text{BT}} = 5.0 \text{ mg/ml}$$

3.1.1 Effect of K_I on Boundary Shape

As one would expect, K_I is an important determinant of boundary shape. Gradient profiles of several noncooperative AB_2 systems with different K_I s are shown in figure 12.

With weakly associating AB_2 systems ($K_I < 2.5 \times 10^4$) bimodal behavior is not observed. At $K_I = 1 \times 10^3$ nearly all of the material in the initial plateau is monomer (see figure 13). The resulting boundary (figure 12a) is nearly symmetrical and sediments at an average rate just slightly greater than that of free monomer (at C_{ATo} and C_{BTo}). As K_I is increased, up to ca. 2.5×10^4 , the boundaries become more noticeably skewed (fig 12b) and an obvious trailing shoulder develops in the constituent A gradient, paralleling an increase in C_{AB} and C_{AB_2} and the appearance of a relative excess of free A monomer (ie. relative to free B monomer) in the initial plateau (fig. 13). A trailing shoulder appears in the total boundary at $K_I = 5 \times 10^4$ and at $K_I = 10^5$ (fig. 12c) the boundary is fully bimodal.

The position of the leading (reaction) boundary¹¹ increases steadily as K_I is increased from 10^3 to about 10^7 . A further increase in K_I has no effect on the shape of the boundary. The increase in reaction boundary sedimentation rate with K_I is related to an increase in associated species concentrations in the initial mixture. Beyond $K_I = 10^7$ the initial species concentrations do not change signifi-

¹¹ The unimodal boundaries of weak systems were considered to be the reaction boundaries of these systems.

Figure 12: Gradient Profiles Uncooperative AB_2 Systems of Different Strengths

$$W_A = 100Kd$$

$$W_B = 100Kd$$

$$C_{AT} = 5.0 \text{ mg/ml}$$

$$C_{BT} = 5.0 \text{ mg/ml}$$

$$[A] = 5 \times 10^{-5} \text{ M}$$

$$[B] = 5 \times 10^{-5} \text{ M}$$

$$[B]/[A] = 1.0$$

Frictional ratios (f/f_0) for all species = 1.1

All self and cross hydrodynamic constants (k) = 0.01

Species transport coefficients are given in table 2.

Rotor speed = 60,000 rpm.

Initial sharp boundary position (r_0) = 6.0 cm.

$\Delta t = 2155.51 \text{ sec}$

$$K_I \quad (M^{-1})$$

- a. 1.0×10^3
- b. 1.0×10^4
- c. 1.0×10^5
- d. 1.0×10^7

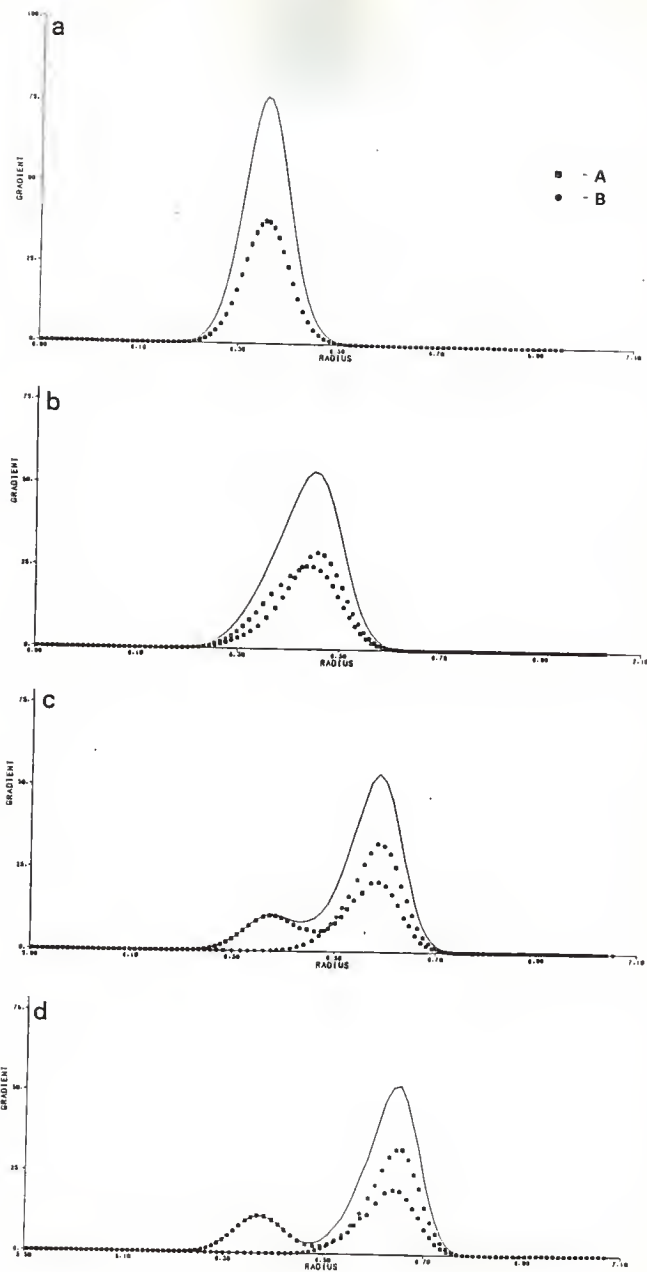


Figure 13: Species Concentrations and Average Sedimentation Coefficients for Uncooperative AB_2 Systems

$$W_A = 100\text{Kd}$$

$$W_B = 100\text{Kd}$$

$$C_{AT} = 5.0 \text{ mg/ml}$$

$$C_{BT} = 5.0 \text{ mg/ml}$$

$$[A] = 5 \times 10^{-5} \text{ M}$$

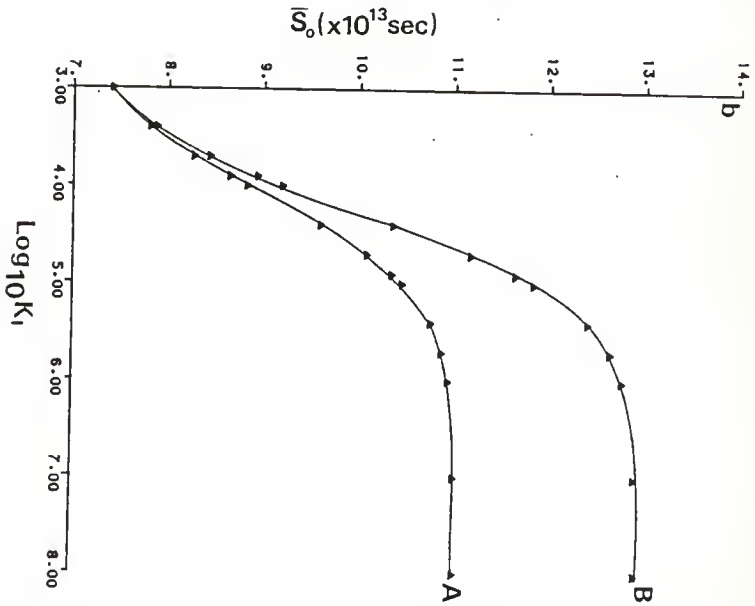
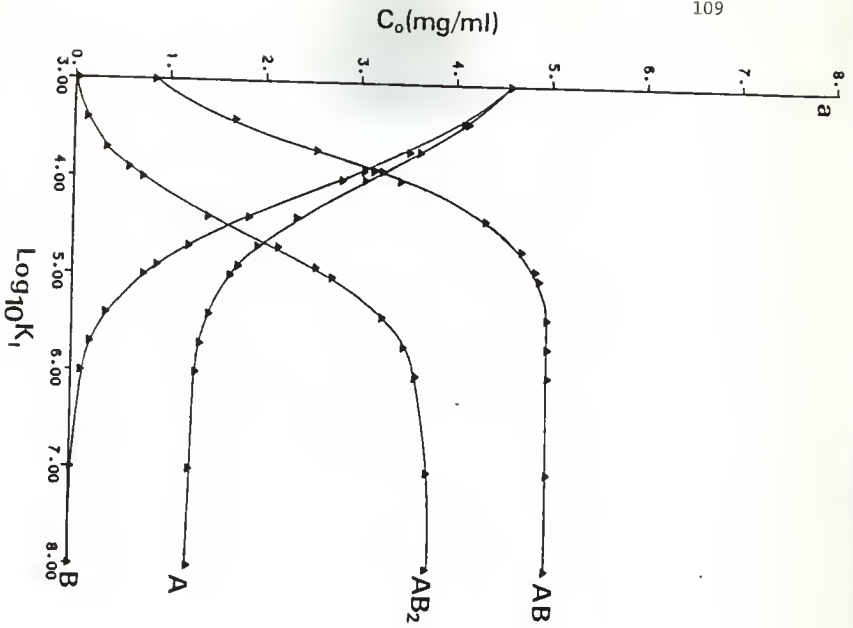
$$[B] = 5 \times 10^{-5} \text{ M}$$

$$[B]/[A] = 1.0$$

Frictional ratios (f/f_0) for all species = 1.1

Species transport coefficients are given in table 2.

- a. Species concentrations vs. $\log_{10} K_I$ for uncooperative AB_2 systems
- b. Average constituent sedimentation coefficients vs. $\log_{10} K_I$ for uncooperative AB_2 systems



cantly. The initial average constituent sedimentation coefficients also approach maximum values at $K_I \sim 10^7$ (fig. 13b)

With systems that are not very tight ($K_I < 10^5$) the size of the leading boundary also depends on K_I . In the AB_2 series (fig. 12) leading boundary height (H_L) decreases as K_I is increased up to about 2.5×10^4 where H_L passes through a minimum (see fig 18b). H_L increases slightly with K_I from ca. 2.5×10^4 to ca. 10^5 and is constant at higher values.

The height and position of the trailing boundary, when there is a trailing boundary (ie. when $K_I > 5 \times 10^4$), are constant.

The changes in gradient profiles of AB_3 and AB_4 systems with K_I (figures 14 and 15) follow the same general pattern as in the AB_2 systems:

- I) AB_3 and AB_4 boundaries are bimodal at $K_I > \text{ca. } 2.5 \times 10^4$ and ca. 1.5×10^4 , respectively, and skewed at lower values.
- II) Reaction boundary position, R_L , increases (sigmoidally with $\log_{10} K_I$ - see fig. 18b) to a maximum at $K_I \sim 10^6$ and remains constant at higher values. As with AB_2 systems this is related to increases in the concentrations of associated species and in the average constituent sedimentation coefficients (fig. 16 and 17)
- III) Leading boundary size decreases as K_I is increased. However, in the AB_3 and AB_4 systems, H_L does not

pass through a minimum as it does with AB_2 systems. Instead it decreases steadily to $K_I = \text{ca. } 10^5$ and remains constant at higher values.

- IV) Trailing boundary height, H_T , and position, R_T , are constant.

Figure 14: Gradient Profiles of Uncooperative AB_3 Systems of Different Strengths

$$W_A = 100Kd$$

$$W_B = 100Kd$$

$$C_{AT} = 5.0 \text{ mg/ml}$$

$$C_{BT} = 5.0 \text{ mg/ml}$$

$$[A] = 5 \times 10^{-5} \text{ M}$$

$$[B] = 5 \times 10^{-5} \text{ M}$$

$$[B]/[A] = 1.0$$

Frictional ratios (f/f_0) for all species = 1.1

All self and cross hydrodynamic constants (k) = 0.01

Species transport coefficients are given in table 2.

Rotor speed = 60,000 rpm.

Initial sharp boundary position (r_0) = 6.0 cm.

$\Delta t = 2155.51 \text{ sec}$

$K_I \text{ (M}^{-1}\text{)}$

a. 1.0×10^3

b. 5.0×10^3

c. 1.0×10^5

d. 1.0×10^6

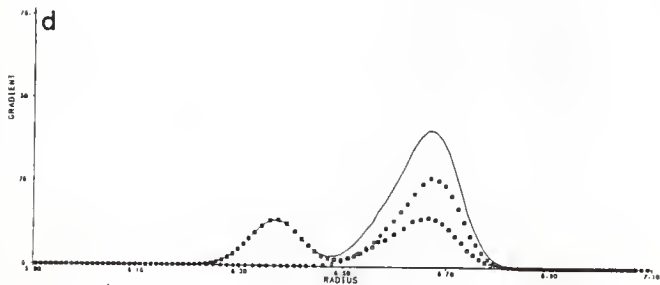
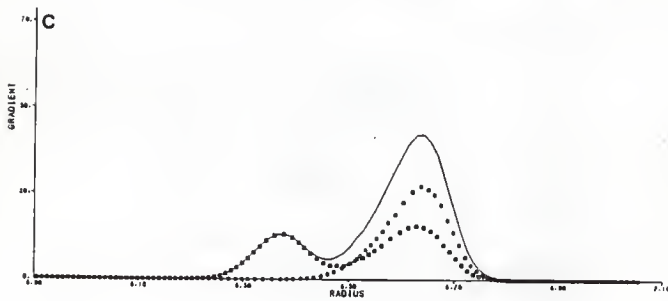
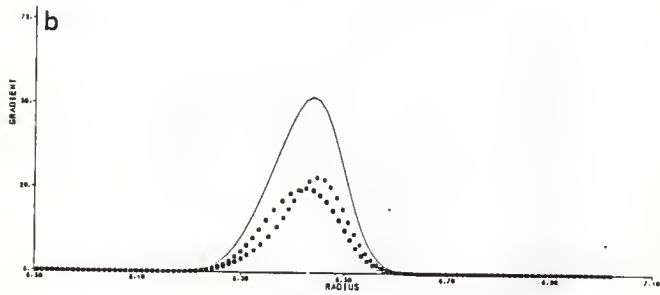
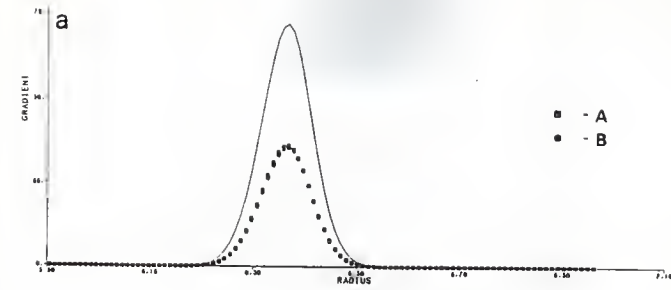


Figure 15: Gradient Profiles Uncooperative AB_4 Systems of Different Strengths

$$W_A = 100Kd$$

$$W_B = 100Kd$$

$$C_{AT} = 5.0 \text{ mg/ml}$$

$$C_{BT} = 5.0 \text{ mg/ml}$$

$$[A] = 5 \times 10^{-5} \text{ M}$$

$$[B] = 5 \times 10^{-5} \text{ M}$$

$$[B]/[A] = 1.0$$

frictional ratios (f/f_0) for all species = 1.1

all self and cross hydrodynamic constants (k) = 0.01

Species transport coefficients are given in table 2.

rotor speed = 60,000 rpm.

initial sharp boundary position (r_0) = 6.0 cm.

$\Delta t = 2155.51 \text{ sec}$

$$K_I \text{ (M}^{-1}\text{)}$$

a. 1.0×10^3

b. 5.0×10^3

c. 5.0×10^4

d. 1.0×10^6

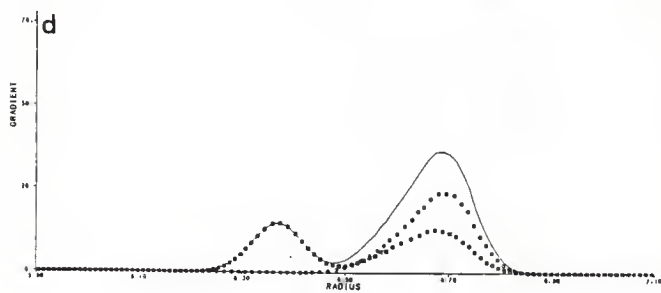
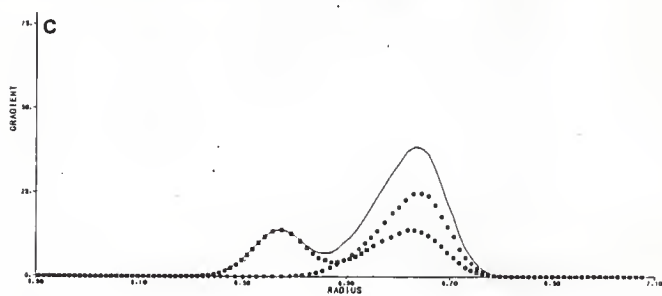
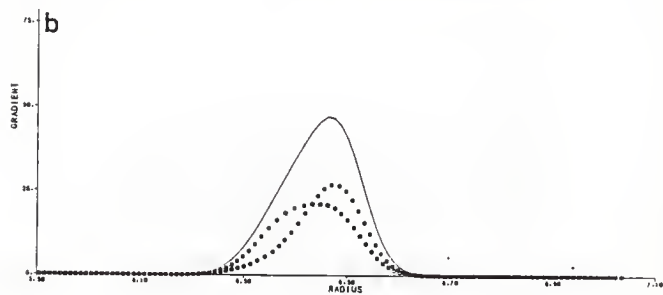
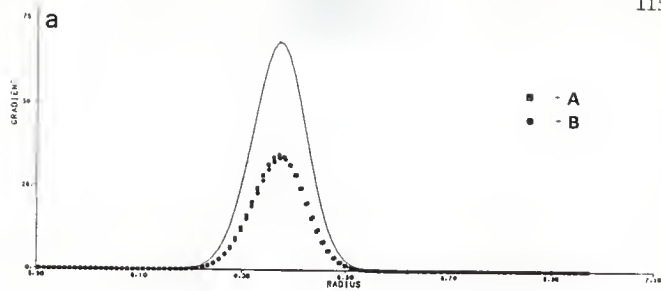


Figure 16: Species Concentrations and Average Sedimentation Coefficients for Uncooperative AB_3 Systems

$$W_A = 100\text{Kd}$$

$$W_B = 100\text{Kd}$$

$$C_{AT} = 5.0 \text{ mg/ml}$$

$$C_{BT} = 5.0 \text{ mg/ml}$$

$$[A] = 5 \times 10^{-5} \text{ M}$$

$$[B] = 5 \times 10^{-5} \text{ M}$$

$$[B]/[A] = 1.0$$

Frictional ratios (f/f_0) for all species = 1.1

Species transport coefficients are given in table 2.

a. Species concentrations vs. $\log_{10} K_I$ for uncooperative AB_3 systems

b. Average constituent sedimentation coefficients vs. $\log_{10} K_I$ for uncooperative AB_3 systems

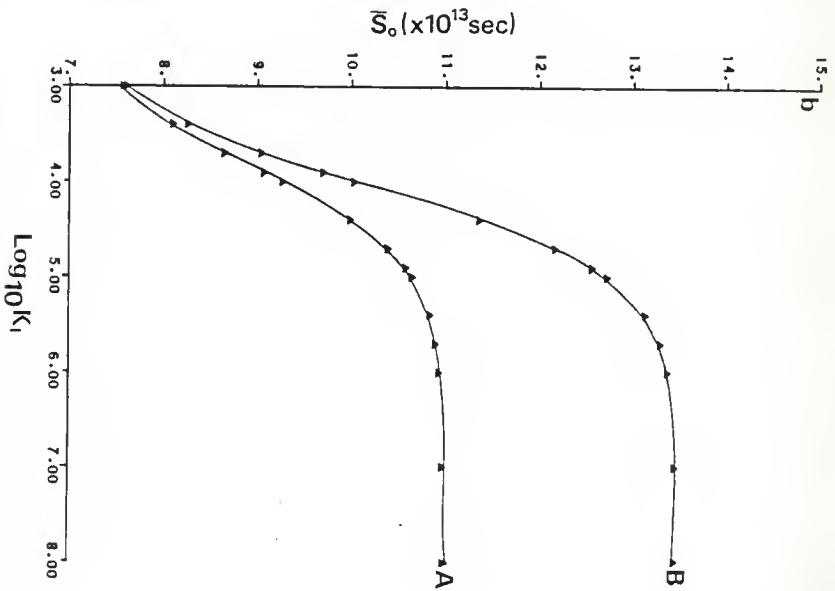
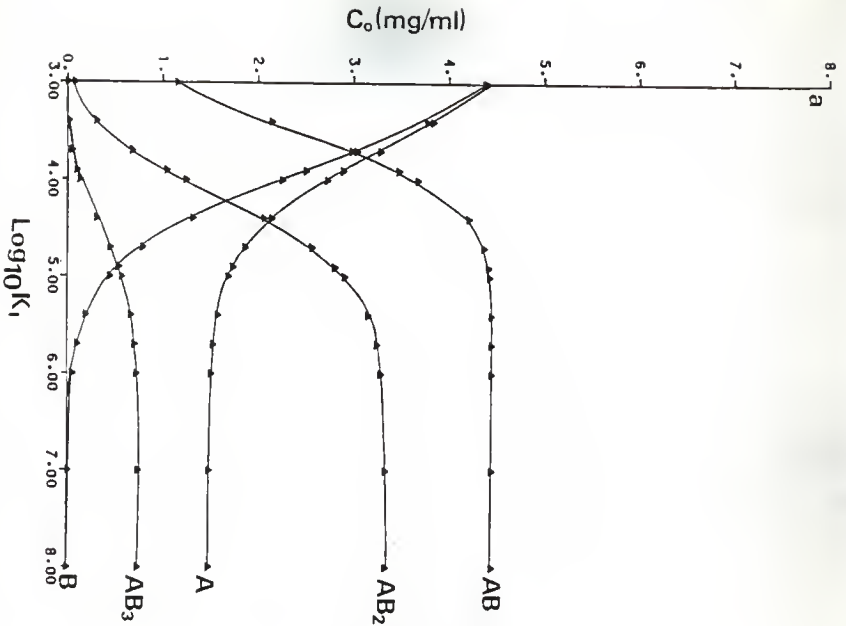


Figure 17: Species Concentrations and Average Sedimentation Coefficients for Uncooperative AB_4 Systems

$$W_A = 100Kd$$

$$W_B = 100Kd$$

$$C_{AT} = 5.0 \text{ mg/ml}$$

$$C_{BT} = 5.0 \text{ mg/ml}$$

$$[A] = 5 \times 10^{-5} \text{ M}$$

$$[B] = 5 \times 10^{-5} \text{ M}$$

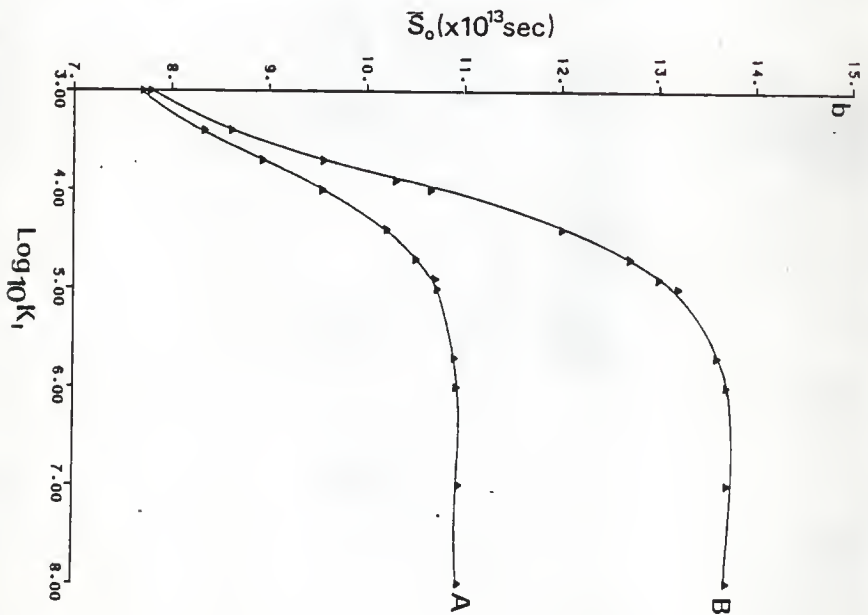
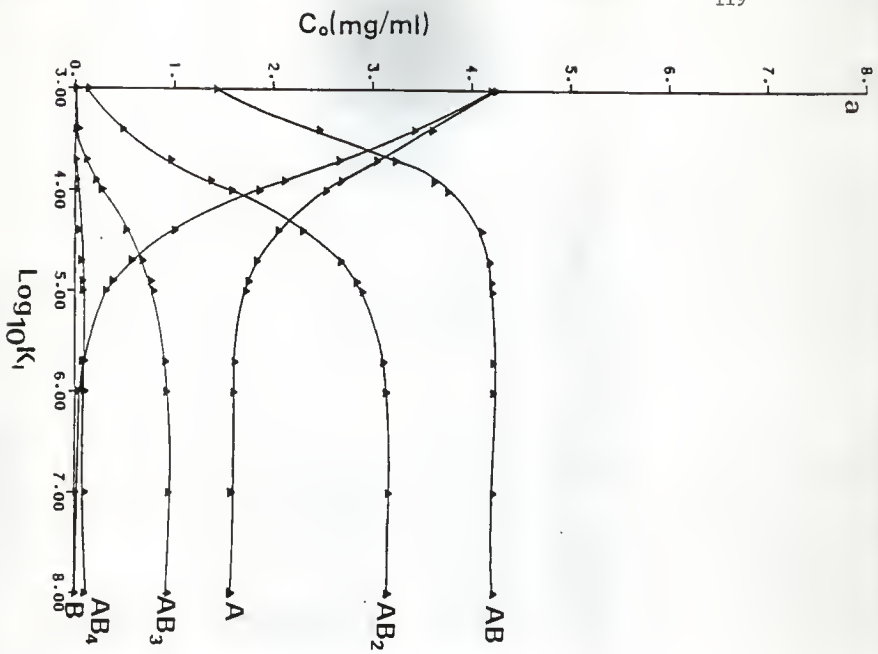
$$[B]/[A] = 1.0$$

frictional ratios (f/f_0) for all species = 1.1

Species transport coefficients are given in table 2.

a. Species concentrations vs. $\log_{10} K_I$ for uncooperative AB_4 systems

b. Average constituent sedimentation coefficients vs. $\log_{10} K_I$ for uncooperative AB_4 systems



3.1.2 Comparison of Uncooperative AB_n Boundary Shapes

Since sedimenting boundary shapes of uncooperative AB_n systems vary systematically with K_I it should not be difficult to distinguish between, say, two (uncooperative) AB₂ systems of different strengths - as long as everything else about the system pertinent to its transport behavior is known. That is, if K_I is the only unknown (which it rarely is) then modelling will give an unambiguous solution. A comparison of boundary shapes of the three families of uncooperative AB_n systems, AB₂, AB₃, and AB₄, suggests that it might also be possible to obtain an unambiguous solution when both stoichiometry and K_I are unknown. First, the three stoichiometries give rise to leading boundaries with distinctly different heights at values of K_I greater than ca. 10^4 (figure 18-a). That is, the leading boundary height of a system with one of these three stoichiometries and $K_I > ca. 10^4$ is different than the leading boundary height of any system with one of the other two stoichiometries and $K_I > 10^4$. Further, since systems with any of these stoichiometries and $K_I < 1.5 \times 10^4$ are not bimodal (AB₂ systems are bimodal at $K_I > 5 \times 10^4$, AB₃ at $K_I > 2.5 \times 10^4$, and AB₄ at $K_I > 1.5 \times 10^4$) it follows that systems giving rise to bimodal boundaries have K_I s greater than 10^4 and therefore have "unique" boundary shapes. Thus, for example, the bimodal boundary of an uncooperative AB₃ system would not look like the boundary of any AB₂ or AB₄ system.

In addition, since trailing boundary heights differ among systems with different stoichiometries, but are constant, or very nearly constant, among systems with the same stoichiometry ($H_T(AB_2) = 11.0-11.7(\text{mg}/\text{cm}^4)$, $H_T(AB_3) = 13.0-13.8$, $H_T(AB_4) = 14.2-14.8$), the trailing boundary height of a bimodal AB_n gradient profile could allow one to distinguish between various stoichiometries.

For weaker systems (not bimodal) boundary size by itself cannot be used to distinguish between stoichiometries (eg. from fig. 18a, an AB_4 system with $K_I = 2.5 \times 10^3$, an AB_3 system with $K_I = 4 \times 10^3$, and an AB_2 system with $K_I = 8 \times 10^3$ all give rise to boundaries of identical height.). Similarly, reaction boundary position alone is not diagnostic for stoichiometry and K_I . Combinations of H_L and R_I , however, appear to be unique for AB_n systems that are not very weak. A plot of H_L vs. R_L for AB_2 , AB_3 , and AB_4 systems shows that systems with leading boundary heights less than ca. $67(\text{mg}/\text{cm}^4)$ (corresponding to AB_2 systems with $K_I > 1 \times 10^3$, AB_3 systems with $K_I > 1.5 \times 10^3$, and AB_4 systems with $K_I > 1 \times 10^3$) have unique combinations of boundary height and position, meaning that they have unique boundary shapes (fig 18-c). Thus, for example, an AB_2 system with $K_I > 2 \times 10^3$ will have a boundary shape unlike that of any AB_3 or AB_4 system.

The superimposed gradients of AB_2 and AB_4 (uncooperative) systems in figure 19 clearly demonstrate the differences between these two families of boundary profiles.

Figure 18: Leading Boundary Heights (H_L) and Positions (R_L) of Uncooperative AB_n Gradient Profiles

$$W_A = 100Kd$$

$$W_B = 100Kd$$

$$C_{AT} = 5.0 \text{ mg/ml}$$

$$C_{BT} = 5.0 \text{ mg/ml}$$

$$[A] = 5 \times 10^{-5} \text{ M}$$

$$[B] = 5 \times 10^{-5} \text{ M}$$

$$[B]/[A] = 1.0$$

Frictional ratios (f/f_0) for all species = 1.1

All self and cross hydrodynamic constants (k) = 0.01

Species transport coefficients are given in table 2.

Rotor speed = 60,000 rpm.

Initial sharp boundary position (r_0) = 6.0 cm.

$\Delta t = 2155.51 \text{ sec}$

- a. H_L vs. $\log_{10} K_I$ for uncooperative AB_2 ,
 AB_3 and AB_4 profiles
- b. R_L vs. $\log_{10} K_I$ for uncooperative AB_2 ,
 AB_3 and AB_4 profiles
- c. H_L vs. R_L for uncooperative AB_2 ,
 AB_3 and AB_4 profiles

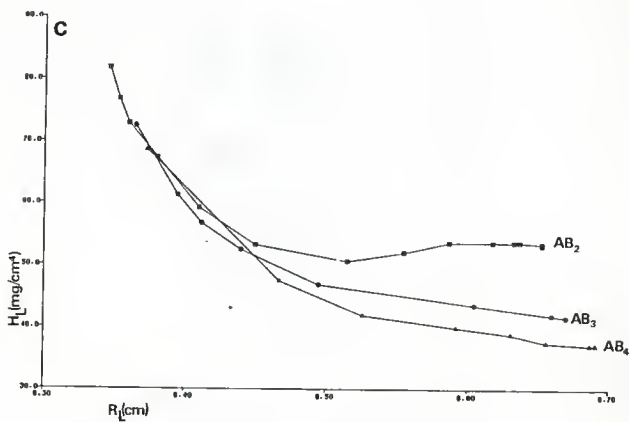
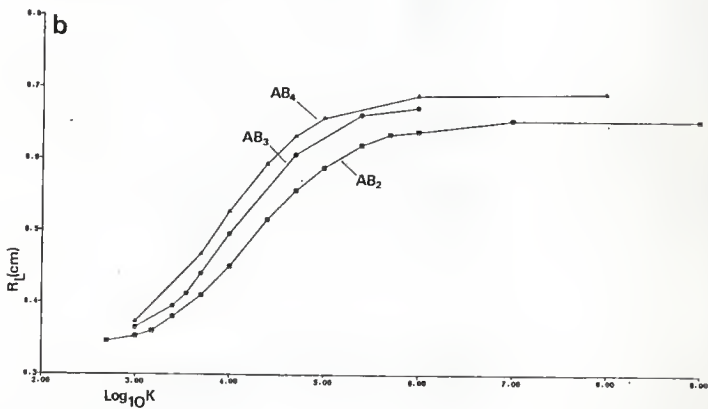
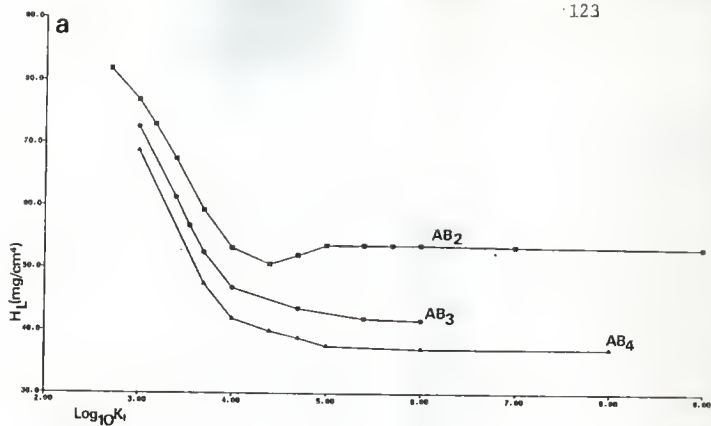


Figure 19: Comparison of Uncooperative AB_2 and AB_4 Gradient Profiles

$$W_A = 100\text{Kd}$$

$$W_B = 100\text{Kd}$$

$$C_{AT} = 5.0 \text{ mg/ml}$$

$$C_{BT} = 5.0 \text{ mg/ml}$$

$$[A] = 5 \times 10^{-5} \text{ M}$$

$$[B] = 5 \times 10^{-5} \text{ M}$$

$$[B]/[A] = 1.0$$

Frictional ratios (f/f_0) for all species = 1.1

All self and cross hydrodynamic constants (k) = 0.01

Species transport coefficients are given in table 2.

Rotor speed = 60,000 rpm.

Initial sharp boundary position (r_0) = 6.0 cm.

$\Delta t = 2155.51 \text{ sec}$

Solid Lines: AB_2 , K_I from left to right

$$1.0 \times 10^3 \text{ (M}^{-1}\text{)}$$

$$1.0 \times 10^3$$

$$1.0 \times 10^5$$

$$1.0 \times 10^7$$

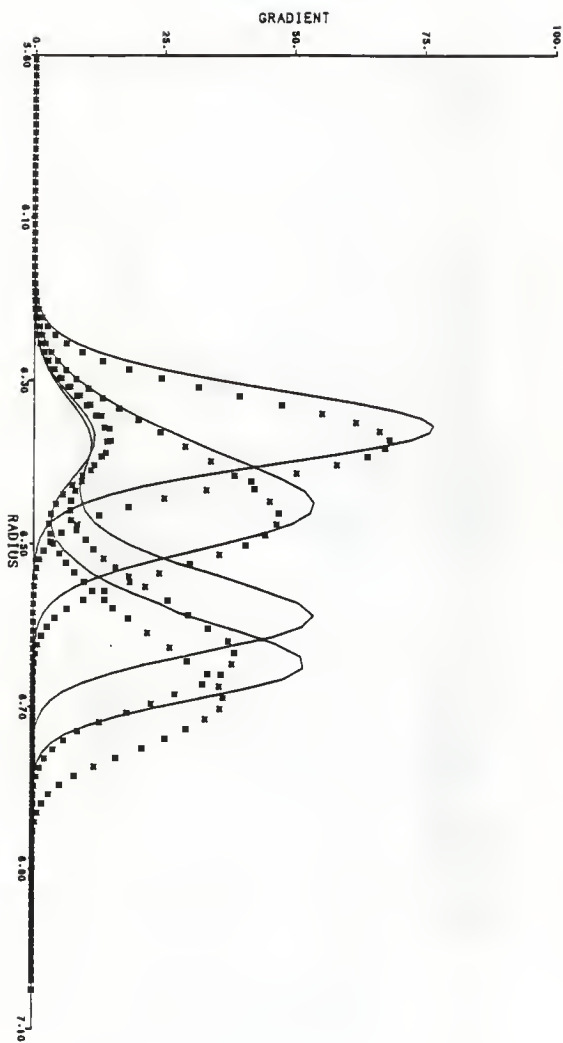
Asterisks : AB_4 , K_I from left to right

$$1.0 \times 10^3$$

$$5.0 \times 10^3$$

$$5.0 \times 10^4$$

$$1.0 \times 10^6$$



While it may be possible to distinguish among AB_2 , AB_3 , and AB_4 systems the apparent tendency of the H_T vs. R_L curves to lie closer together for higher stoichiometries (AB_3 and AB_4) than they do for lower stoichiometries (AB_2 and AB_3) suggests that the boundary shapes of noncooperative systems of higher stoichiometries would be more similar to one another than the AB_2 , AB_3 , and AB_4 systems are to one another and that modeling of velocity sedimentation would probably give more ambiguous results for such systems.

3.1.3 Effect of Constituent Mole Ratio

All of the gradient profiles discussed so far have been for systems at equal initial constituent concentrations ($5 \times 10^{-5} M$) or a constituent mole ratio ($MR = [B]/[A]$) of 1:0. In every case where there was a trailing boundary or shoulder the individual constituent gradient profiles demonstrated that it was due to trailing A monomer, probably reflecting a relative excess of constituent A in the initial mixture. Thus one might expect that if the initial concentration of A were decreased relative to that of B, while keeping the total constituent concentration constant, the excess in A, and the trailing boundary or shoulder, would be reduced. A series of profiles for the uncooperative AB_2 system with $K_I = 10^5$ at various mole ratios (fig. 20) shows that this is exactly what happens. As MR is increased, the trailing boundary of A shrinks, closes in on the edge of the

leading boundary until it becomes a shoulder at the trailing edge of the leading boundary and then disappears altogether. As MR is increased beyond this point a trailing boundary of B develops (first as a shoulder then a boundary)

The mole ratio at which there is no excess of either A or B, the equivalence mole ratio (MR_{eq}), depends on the strength (K_I) and stoichiometry of the association. In general, tightly associating systems have equivalence points at higher mole ratios than weakly associating systems. MR_{eq} for a number of AB_2 and AB_4 systems were determined by examining simulated profiles for each system at several mole ratios. The equivalence point (MR_{eq}) was taken as the mole ratio at which the trailing edges of the constituent A and B boundaries coincided. A plot of MR_{eq} vs. $\log_{10}K_I$ is shown in figure 21. Like H_L and R_L at $MR=1$, MR_{eq} discriminates well among systems with the same stoichiometry and different values of K_I . Moreover, whereas H_L and R_L (at $MR=1$) are essentially constant among tightly associating systems ($K_I > ca. 5 \times 10^5$), MR_{eq} continues to increase beyond $K_I = 10^7$ and may therefore be most useful for modeling relatively tight systems. As with H_L and R_L , however, MR_{eq} can have the same value for two systems, or possibly several systems, with different stoichiometries. Thus MR_{eq} by itself is not an unambiguous indicator of both stoichiometry and K_I . However, combinations of MR_{eq} and H_T (at $MR=1$) or of MR_{eq} and R_L (at $MR=1$), may be.

Figure 20: Gradient Profiles Uncooperative AB_2 Systems at Different Constituent Mole Ratios

$$K_I = 1.0 \times 10^5$$

$$W_A = 100 \text{Kd}$$

$$W_B = 100 \text{Kd}$$

$$C_{AT} + C_{BT} = 10.0 \text{ mg/ml}$$

$$[B]_T + [A]_T = 1.0 \times 10^{-4} \text{ M}$$

Frictional ratios (f/f_o) for all species = 1.1

All self and cross hydrodynamic constants (k) = 0.01

Species transport coefficients are given in table 2.

Rotor speed = 60,000 rpm.

Initial sharp boundary position (r_o) = 6.0 cm.

$$\Delta t = 2155.51 \text{ sec}$$

[B]/[A]

- | | |
|----|------|
| a. | 1.00 |
| b. | 1.38 |
| c. | 1.56 |
| d. | 2.03 |

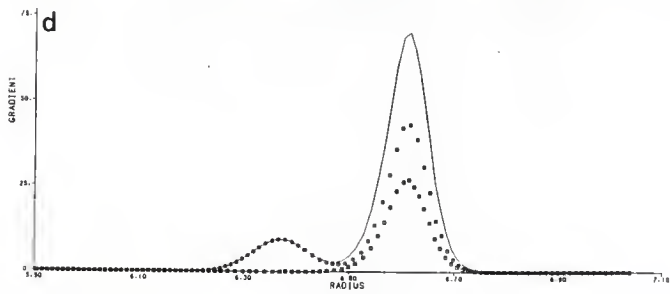
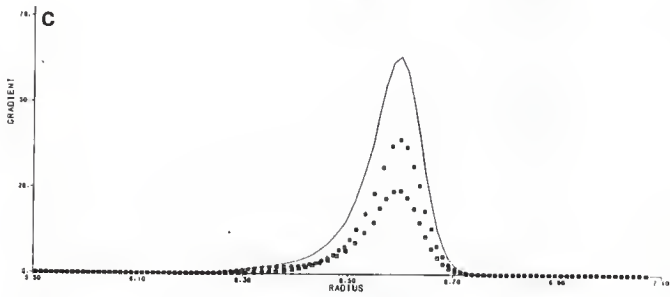
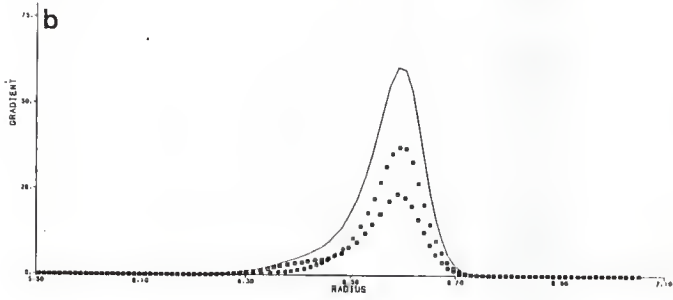
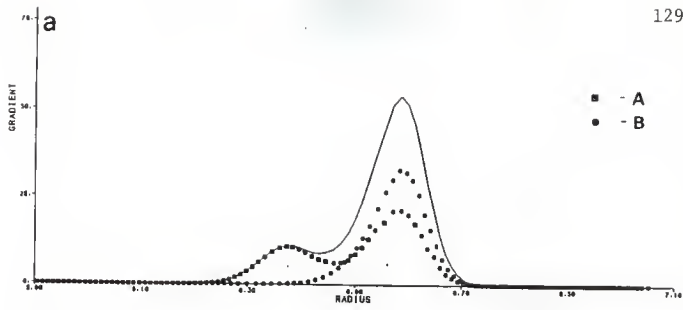


Figure 21: Equivalence Mole Ratio vs. $\log_{10} K_I$ for
Uncooperative AB_2 and AB_4 Systems

$$W_A = 100Kd$$

$$W_B = 100Kd$$

Frictional ratios (f/f_0) for all species = 1.1

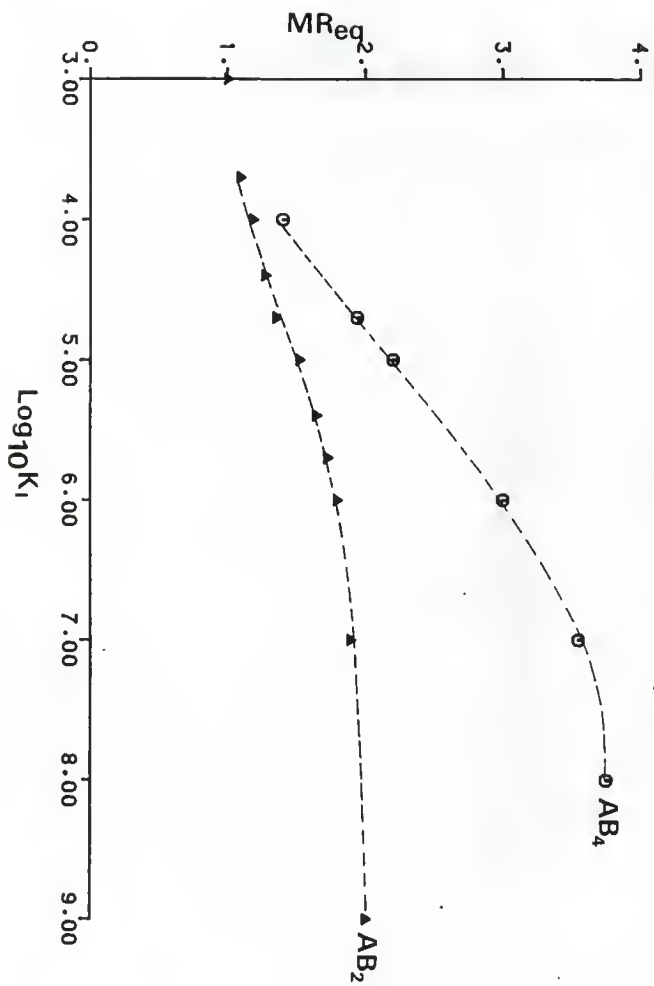
All self and cross hydrodynamic constants (k) = 0.01

Species transport coefficients are given in table 2.

Rotor speed = 60,000 rpm.

Initial sharp boundary position (r_0) = 6.0 cm.

$\Delta t = 2155.51$ sec



While MR_{eq} could be helpful in some instances for distinguishing among various model systems, there are some problems that restrict the usefulness of this type of analysis. First, in order to obtain a value of MR_{eq} for a real system, it would be necessary to run the system in the ultracentrifuge at several mole ratios and to make accurate reproductions or tracings of the schlieren patterns for each run. This would be very time consuming. Second, even if the number of possible models were small, many costly simulations would be required to determine MR_{eq} for each of them. Finally, in many cases it will not be possible to accurately determine MR_{eq} for the experimental system. The MR_{eq} 's in fig. 21 were determined by inspecting the simulated constituent gradients at various mole ratios with MR_{eq} being taken as the mole ratio at which the trailing edges of the two constituent gradients coincided. For a real system only the total gradient profile is available and while with moderately tight and tighter systems the trailing aspect of the total boundary does pass through a detectable minimum at MR_{eq} (see fig. 21) this is not the case for weaker systems. For the AB_2 system with K_I of 10^4 , for instance, the trailing edges of the total boundaries are essentially identical between mole ratios of 1.0 and 1.5, despite the obvious differences, over the same range of mole ratios, in the individual constituent gradients (fig. 22).

3.1.4 Systems with Non-Identical Monomers

So far we have looked only at systems with identical monomers (both 100Kd).

Gradient profiles of noncooperative AB_2 systems ($K_I=10^5$, $MR=1.0$) with monomers of different molecular weights are shown in figure 23

$$(a:W_A=140Kd, W_B=60Kd, b:W_A=60Kd, W_B=140Kd)^{12}.$$

The boundaries of both systems with unequal monomers, like boundaries of systems of comparable strength ($K_I=10^5$) with identical monomers, are bimodal at a constituent mole ratio of 1.0. However, while the trailing boundaries (at $MR=1$) of systems with identical (100Kd) monomers and of the systems with W_B (140K) larger than W_A (60K) consist of excess constituent A, it is constituent B that is in excess and present in the trailing boundary (at $MR=1$) of the system with W_A (140K) larger than W_B (60K).

As with systems with identical monomers ($W_A=W_B$) the trailing boundaries of both of these systems ($W_A>W_B$ and $W_B>W_A$) move at about the rates predicted for pure monomer (the monomer in excess). (Transport coefficients and predicted final positions of the pure species in these systems are given in table 3 and 4.) Thus, in the $W_B>W_A$ system,

¹² The sedimentation and diffusion transfer times and the total time simulated were shorter here than in the previous simulations. Δt_S is computed (by the COXMIX simulation program) as the time it takes for the pure monomer with the largest sedimentation coefficient to move through a distance equal to the average box width. (see p. 90)

Figure 22: Gradient Profiles Uncooperative AB_2 Systems at Different Constituent Mole Ratios

$$K_I = 1.0 \times 10^4$$

$$W_A = 100 \text{Kd}$$

$$W_B = 100 \text{Kd}$$

$$C_{AT} + C_{BT} = 10.0 \text{ mg/ml}$$

$$[B]_T + 1bk1.A]_T = 1.0 \times 10^{-4}$$

Frictional ratios (f/f_o) for all species = 1.1

All self and cross hydrodynamic constants (k) = 0.01

Species transport coefficients are given in table 2.

Rotor speed = 60,000 rpm.

Initial sharp boundary position (r_o) = 6.0 cm.

$$\Delta t = 2155.51 \text{ sec}$$

[B]/[A]

- | | |
|----|------|
| a. | 1.00 |
| b. | 1.08 |
| c. | 1.22 |

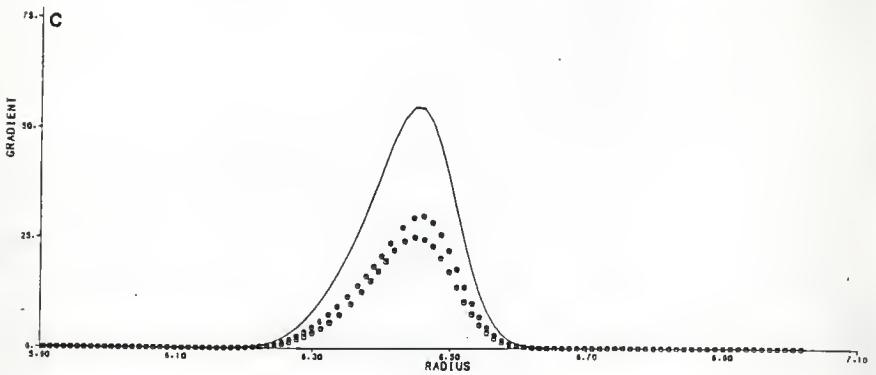
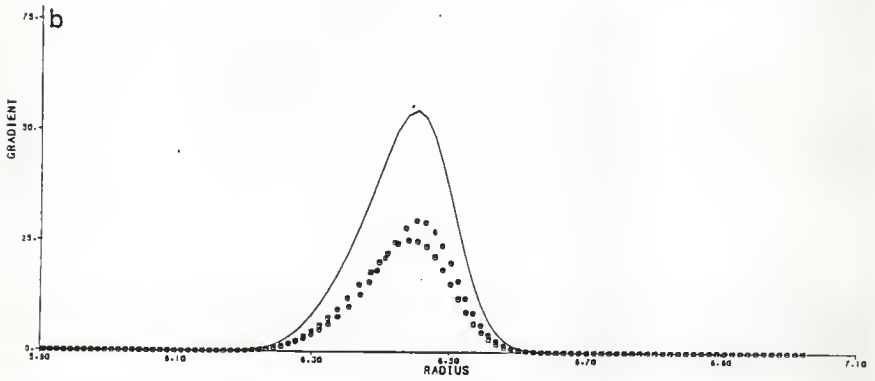
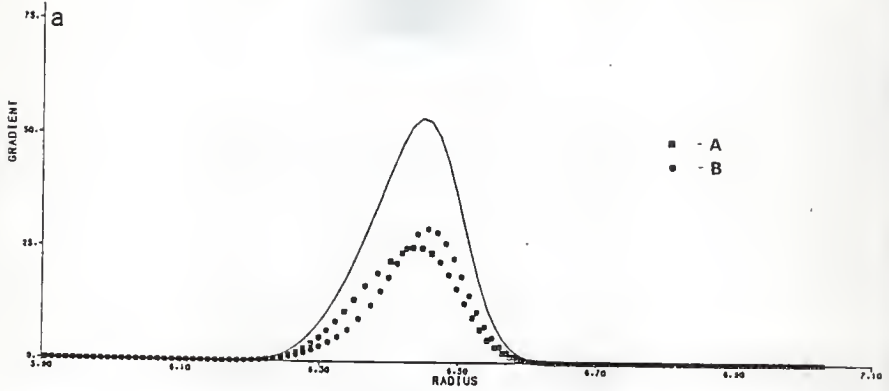


Figure 23: Gradient Profiles of Uncooperative AB_2 Systems with Non-Identical Monomers

$$K_I = 1.0 \times 10^5$$

Frictional ratios (f/f_0) for all species = 1.1

All self and cross hydrodynamic constants (k) = 0.01

Rotor speed = 60,000 rpm.

Initial sharp boundary position (r_0) = 6.0 cm.

$\Delta t = 1722.50$ sec

a. $W_A = 140Kd$

$$W_B = 60Kd$$

$$C_{AT} = 7.0 \text{ mg/ml}$$

$$[A] = 5.0 \times 10^{-5} \text{ M}$$

$$C_{BT} = 3.0 \text{ mg/ml}$$

$$[B] = 5.0 \times 10^{-5} \text{ M}$$

$$[B]/[A] = 1.0$$

Species transport coefficients are given in table 3.

b. $W_A = 60Kd$

$$W_B = 140Kd$$

$$C_{AT} = 3.0 \text{ mg/ml}$$

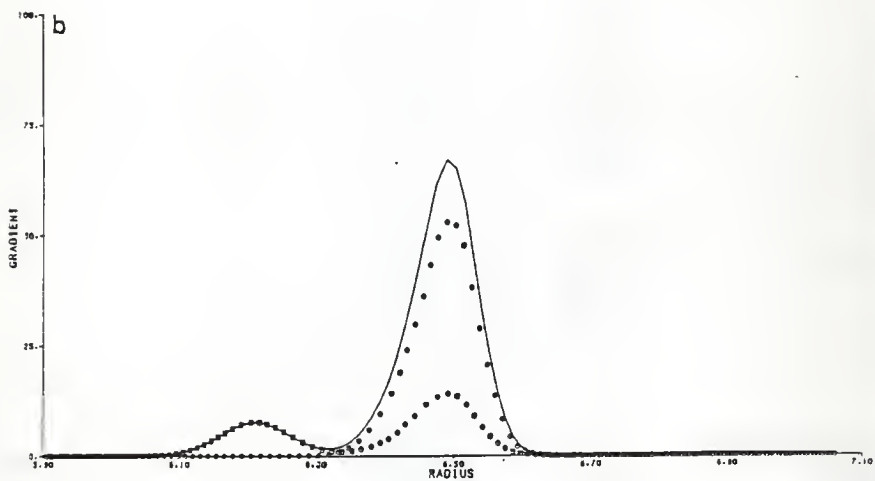
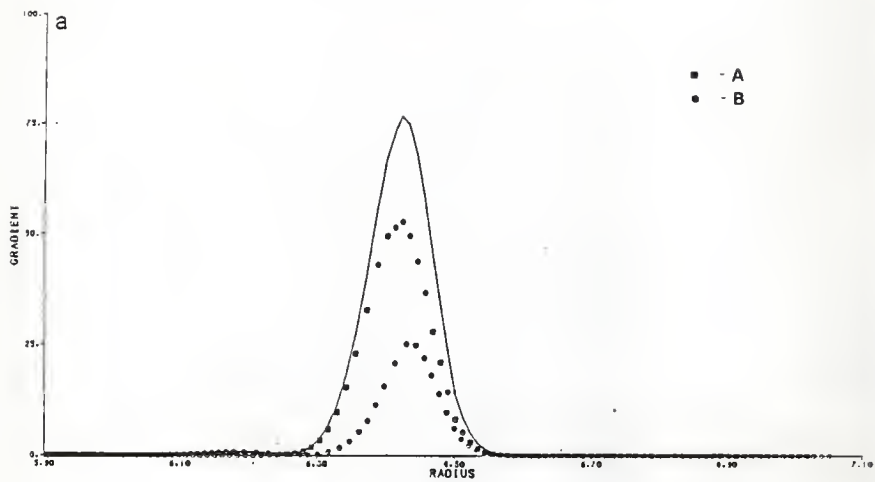
$$[A] = 5.0 \times 10^{-5} \text{ M}$$

$$C_{BT} = 7.0 \text{ mg/ml}$$

$$[B] = 5.0 \times 10^{-5} \text{ M}$$

$$[B]/[A] = 1.0$$

Species transport coefficients are given in table 4.



where constituent A is in excess,

$$R_{\min A} = 6.19(\text{cm.}) < R_T = 6.20 < R_{\max A} = 6.21,$$

and in the $W_A > W_B$ system, where constituent B is in excess,

$$R_{\min B} = R_{\max B} = 6.19$$

For $W_A > W_B$ systems the shape of the gradient profile seems to depend on K_I in about the same way that it does with $W_A = W_B$ systems (fig. 24): Increasing K_I decreases the height and increases the average sedimentation rate of the leading boundary. However, the trailing boundary heights of the $W_A > W_B$ systems decrease with K_I (fig. 24), whereas among $W_A = W_B$ (AB_2 , uncooperative) systems those strong enough to give a bimodal profile under the conditions simulated had trailing boundaries of the same size.

A possible explanation for this difference might be that the sedimentation coefficients of the monomer in excess and the aggregate species are more different in the $W_A > W_B$ systems ($S_{AB}/S_B = 2.232$) than in the $W_A = W_B$ systems ($S_{AB}/S_A = 1.587$) so that $W_A > W_B$ systems give rise to bimodal boundaries at lower values of K_I where the amount of excess trailing monomer varies more strongly with K_I .

The dependence of boundary shape on mole ratio is, in general, qualitatively the same for $W_A > W_B$ and $W_B > W_A$ systems as it is for $W_A = W_B$ systems. As MR is increased from values where A is in excess the trailing boundary or shoulder is depleted of excess A up to a point (equivalence) beyond

TABLE 3

Species Transport Coefficients and Positions for Systems
with $W_A=140Kd > W_B=60Kd$

Species	S_0 ($\times 10^{13}$ sec)	D ($\times 10^7$ cm ² /sec)	r_{max}^* (cm)	r_{min}^* (cm)
A	8.8161	5.6815	6.371	6.336
B	5.0114	7.5356	6.208	6.189
AB	11.183	5.0446	6.474	6.429
AB ₂	13.320	4.6222	6.569	6.515
AB ₃	15.298	4.3131	6.658	6.595
AB ₄	17.155	4.0729	6.742	6.671

$$\bar{v} = 0.73 \text{ cm}^3/\text{mg}$$

$$\rho = 1.0 \text{ g/cm}^3$$

$$\eta = 0.01 \text{ poise}$$

$$\begin{aligned} r_{max} &= r_0 \exp(S_0 \omega^2 \Delta t) \\ r_{min} &= r_0 \exp(S_0 \omega^2 \Delta t / (1 + k_{ave}(C_{AT} + C_{BT}))) \end{aligned}$$

where

$$\omega = 2000\pi \text{ radians/sec}$$

$$\Delta t = 1722.50 \text{ sec}$$

$$k_{ave} = 0.01 \text{ ml/mg}$$

$$C_{AT} = 7.0 \text{ mg/ml}$$

$$C_{BT} = 3.0 \text{ mg/ml}$$

TABLE 4

Species Transport Coefficients and Positions for Systems
with $W_B=140Kd > W_A=60Kd$

Species	S_0 ($\times 10^{13}$ sec)	D ($\times 10^7$ cm ² /sec)	r_{max}^* (cm)	r_{min}^* (cm)
A	5.0114	7.5356	6.208	6.189
B	8.8161	5.6815	6.371	6.336
AB	11.183	5.0446	6.474	6.429
AB ₂	15.929	4.2268	6.686	6.620
AB ₃	20.046	3.7678	6.876	6.792
AB ₄	23.775	3.4597	7.053	6.950

$$\bar{v} = 0.73 \text{ cm}^3/\text{mg}$$

$$\rho = 1.0 \text{ g/cm}^3$$

$$\eta = 0.01 \text{ poise}$$

$$* r_{max} = r_0 \exp(S_0 \omega^2 \Delta t)$$

$$r_{min} = r_0 \exp(S_0 \omega^2 \Delta t / (1 + k_{ave}(C_{AT} + C_{BT})))$$

where

$$\omega = 2000\pi \text{ radians/sec}$$

$$\Delta t = 1722.50 \text{ sec}$$

$$k_{ave} = 0.01 \text{ ml/mg}$$

$$C_{AT} = 3.0 \text{ mg/ml}$$

$$C_{BT} = 7.0 \text{ mg/ml}$$

Figure 24: Gradient Profiles of Uncooperative AB_2 Systems of Different Strengths with Non-Identical Monomers ($W_A > W_B$)

$$W_A = 140Kd$$

$$W_B = 60Kd$$

$$C_{AT} = 7.0 \text{ mg/ml}$$

$$[A] = 5.0 \times 10^{-5} \text{ M}$$

$$C_{BT} = 3.0 \text{ mg/ml}$$

$$[B] = 5.0 \times 10^{-5} \text{ M}$$

$$[B]/[A] = 1.0$$

Frictional ratios (f/f_0) for all species = 1.1

All self and cross hydrodynamic constants (k) = 0.01

Rotor speed = 60,000 rpm.

Initial sharp boundary position (r_0) = 6.0 cm.

$\Delta t = 1722.50 \text{ sec}$

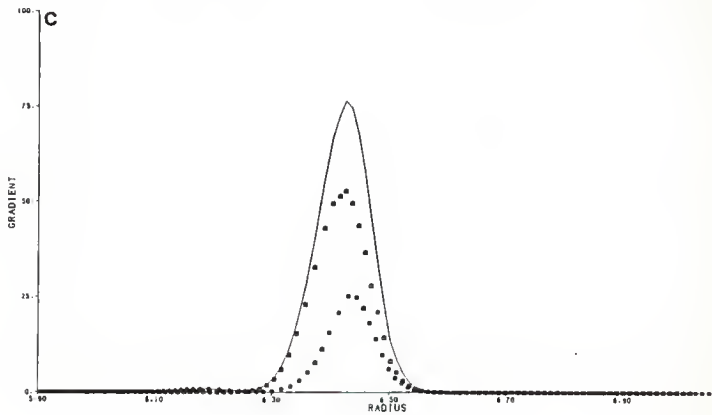
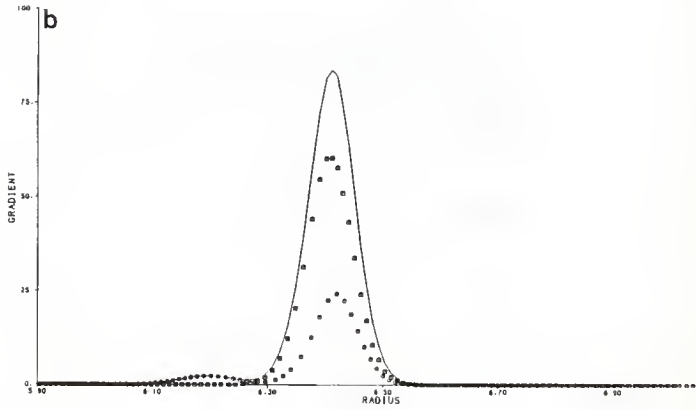
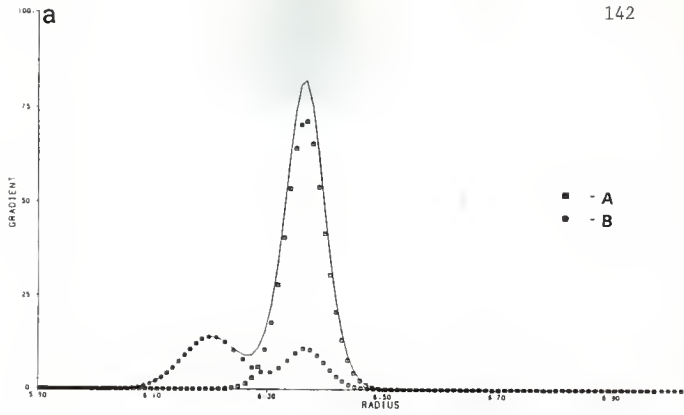
Species transport coefficients are given in table 3.

K
I

a. 5.0×10^3

b. 5.0×10^4

c. 1.0×10^5



which a trailing shoulder or boundary of B develops (see figs. 25 and 26). There are, however, some differences worth noting. First, the shape of the $W_A > W_B$ ($K_I = 10^5$) gradient, which has a trailing boundary of excess B at $MR = 1.0$, is not bimodal when the system is in excess A but is instead skewed to the left with the constituent A gradient (fig. 25). The absence of a trailing boundary for this system with A in excess is probably a result of the relatively small difference between the sedimentation coefficients of A and the aggregates ($S_{AB}/S_A = 1.268$). In the $W_A = W_B$ and $W_B > W_A$ systems (with $K_I = 10^5$), which have bimodal boundaries when A is in excess (as well as when B is in excess), the sedimentation coefficient of A is, by comparison with the $W_A > W_B$ system, smaller in relation to the sedimentation coefficients of the associated species (for $W_B > W_A$, $S_{AB}/S_A = 2.232$, for $W_A = W_B$, $S_{AB}/S_A = 1.587$). When constituent B is in excess both the $W_A > W_B$ and $W_B > W_A$ systems ($K_I = 10^5$) give bimodal profiles with trailing boundaries at positions corresponding approximately to the predicted positions of pure B, even though the difference between S_B and S_{AB} in the $W_B > W_A$ system is the same as between S_A and S_{AB} in the $W_A > W_B$ system, which does not have a distinct monomer boundary when A is in excess. The relatively greater difference in the $W_B > W_A$ system between S_B and S_{AB_2} ($S_{AB_2}/S_B = 1.81$) than between S_A and S_{AB_2} in the $W_A > W_B$ system ($S_{AB_2}/S_A = 1.51$) may be responsible for this difference.

Figure 25: Gradient Profiles of Uncooperative AB_2 Systems with $W_A > W_B$ at Different Constituent Mole Ratios

$$K_I = 1.0 \times 10^5$$

$$W_A = 140 \text{Kd}$$

$$W_B = 60 \text{Kd}$$

$$C_{AT} + C_{BT} = 10.0 \text{ mg/ml}$$

Frictional ratios (f/f_0) for all species = 1.1

All self and cross hydrodynamic constants (k) = 0.01

Rotor speed = 60,000 rpm.

Initial sharp boundary position (r_0) = 6.0 cm.

$$\Delta t = 1722.50 \text{ sec}$$

Species transport coefficients are given in table 3.

[B]/[A]

- a. 0.80
- b. 1.00
- c. 1.50

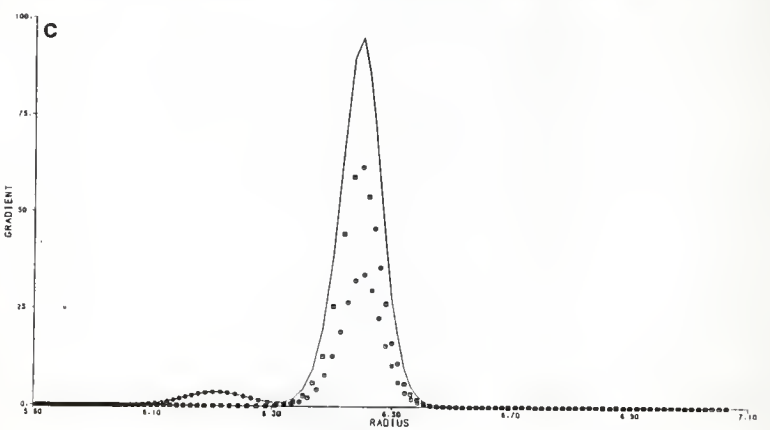
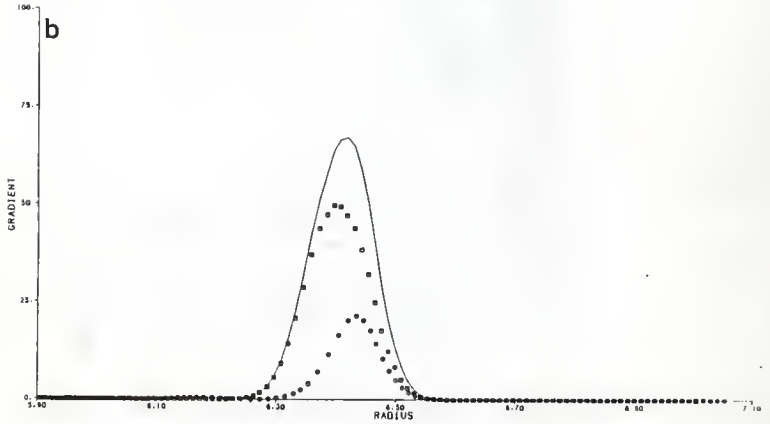
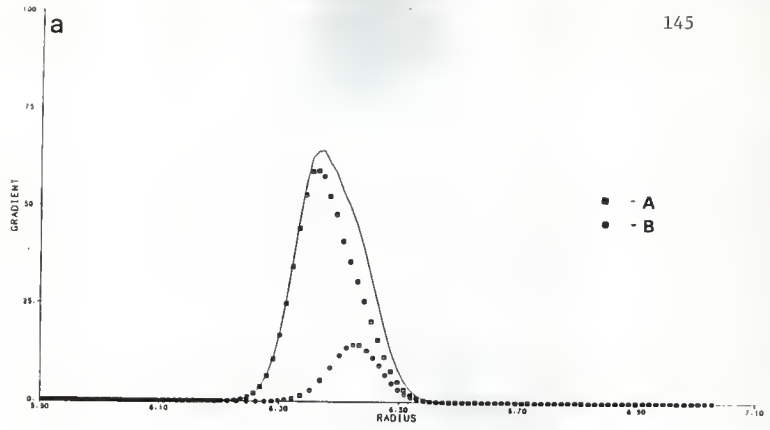


Figure 26: Gradient Profiles of Uncooperative AB_2 Systems with $W_B > W_A$ at Different Constituent Mole Ratios

$$K_I = 1.0 \times 10^5 \text{ M}$$

$$W_A = 60 \text{ Kd}$$

$$W_B = 140 \text{ Kd}$$

$$C_{AT} + C_{BT} = 10.0 \text{ mg/ml}$$

Frictional ratios (f/f_0) for all species = 1.1

All self and cross hydrodynamic constants (k) = 0.01

Rotor speed = 60,000 rpm.

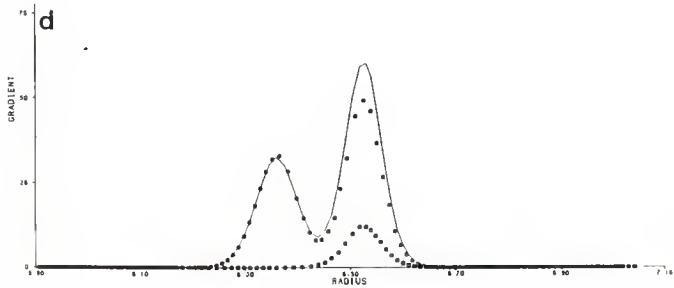
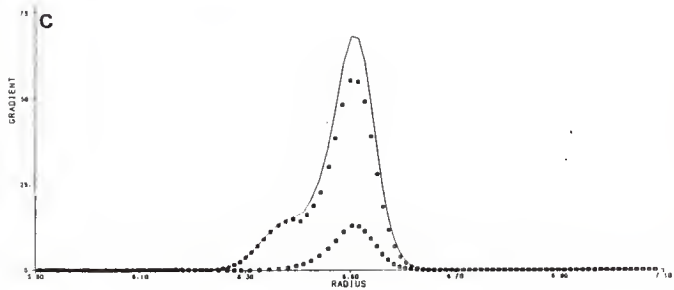
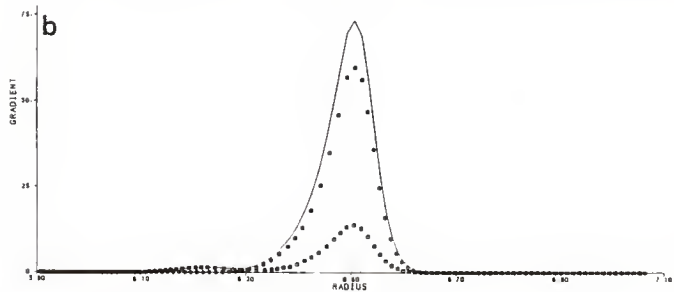
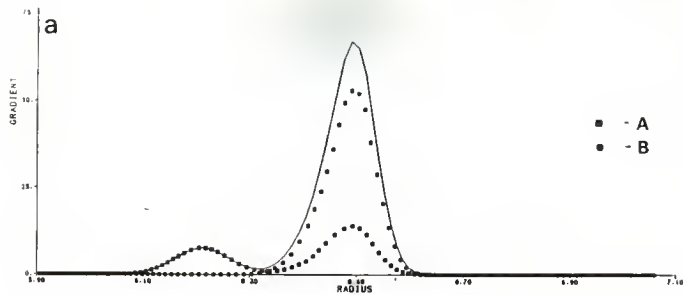
Initial sharp boundary position (r_0) = 6.0 cm.

$\Delta t = 1722.50 \text{ sec}$

Species transport coefficients are given in table 4.

[B]/[A]

- a. 1.00
- b. 1.50
- c. 2.20
- d. 3.00



Finally the equivalence mole ratios of the $W_A > W_B$ and $W_B > W_A$ systems (with $K_I = 10^5$) are much different than that of the system with identical monomers ($K_I = 10^5$): $MR_{eq} ([B]/[A])$ for the $W_A > W_B$ system (ca. 0.8) is smaller than that of the $W_A = W_B$ system (ca. 1.5) which is smaller than that of the $W_B > W_A$ system (ca. 2.1).

3.2 COMPLETELY COOPERATIVE SYSTEMS

So far we have considered only uncooperative AB_n systems where the step-wise association constants, K_1, K_2, \dots, K_n are described in terms of K_I in such a way that the intrinsic binding of a molecule of B to a vacant site on A is independent of the occupancy of other sites on A. We will now consider completely cooperative AB_n systems in which the formation of AB_n occurs in a single concerted step ($A + nB \rightleftharpoons AB_n$) without the formation of intermediate species. For these systems the mole-scale association constant, K_{nM} , is defined as follows

$$K_{nM} = \frac{[AB_n]}{[A][B]^n}$$

Simulated gradient profiles of cooperative AB_2 and AB_4 systems with various values of K_{nM} are shown in figures 27 and 28. As with noncooperative systems, the boundaries of cooperative systems are bimodal when association is strong enough and have shoulders or are skewed when the association

is weaker. Also similar to noncooperative systems are the position of the trailing boundary, which is nearly constant and about equal to the position predicted for pure monomer, and the direction of change in the leading boundary position with increasing strength of association. Unlike the leading boundaries of noncooperative AB_n systems, however, which move at average rates that are considerably slower than those of the pure AB_n species no matter how tight the association, the leading boundaries of cooperative AB_n systems migrate at rates that increase with K_{nM} to values that are only slightly slower than those of pure AB_n . R_L for cooperative AB_2 and AB_4 systems studied had maximum values of 6.71 cm. and 6.98 cm., respectively (see fig. 29-a), which are comparable to the theoretical positions of the pure AB_2 and AB_4 species (6.72 cm. and 7.03 cm.- see table 2). These large values for R_L , which occur in tightly associating systems, suggest that the leading boundaries of these systems consist largely of AB_n . This may also be inferred from the initial species concentrations and average constituent sedimentation coefficients (see figures 30 and 31). In AB_2 systems C_{AB_2} increases sigmoidally with $\log_{10} K_{2M}$ and, at large values of K_{2M} , is the dominant species in the mixture. Also at large values of K_{2M} the average sedimentation coefficient of constituent B is not much smaller than that of pure AB_2 . Thus, for instance, at $K_{2M}=10^{11}$:

$$S_{B,o} = 14.20 \times 10^{-13} \text{ sec.}, \text{ and}$$

$$S_{AB_2,o} = 14.65 \times 10^{-13} \text{ sec.}$$

$S_{A,0}$ in these systems is considerably smaller than $S_{AB_2,0}$, as it should be, since there is considerable excess A in the mixture. Similarly, in cooperative AB_4 systems, when association is tight the predominant species is AB_4 and $\bar{S}_{B,0}$ approaches $S_{AB_4,0}$. At $K_{4M}=10^{20}$:

$$\bar{S}_{B,0}=18.64 \times 10^{-13} \text{ sec. , and}$$

$$S_{AB_4,0}=20.60 \times 10^{-13} \text{ sec.}$$

There is a general difference between the series of cooperative profiles in figures 27 and 28 and the series of noncooperative profiles in figures 27-30 in the manner in which bimodality develops as the strength of association is increased. In the cooperative series this involves formation of a leading boundary from the leading edge of the original single boundary (which becomes the trailing boundary), whereas, in the uncooperative series, a trailing boundary develops at the trailing edge of the single boundary (which becomes the leading boundary). Another related difference is that in the cooperative series the height of the leading boundary increases with K_{nM} and the height of the trailing boundary decreases with K_{nM} , while, in the noncooperative series, the leading boundary height decreases with K_I and the trailing boundary height is constant.

Changes in R_L , H_L , and H_T with K_{nM} for cooperative AB_2 and AB_4 systems are illustrated in figure 29. Of these quantities, R_L , leading boundary position, appears to be the least ambiguous in discriminating between AB_2 and AB_4 (coop-

Figure 27: Gradient Profiles of Completely Cooperative AB_2 Systems of Different Strengths

$$W_A = 100\text{Kd}$$

$$W_B = 100\text{Kd}$$

$$C_{AT} = 5.0 \text{ mg/ml}$$

$$C_{BT} = 5.0 \text{ mg/ml}$$

$$[A] = 5 \times 10^{-5} \text{ M}$$

$$[B] = 5 \times 10^{-5} \text{ M}$$

$$[B]/[A] = 1.0$$

Frictional ratios (f/f_0) for all species = 1.1

All self and cross hydrodynamic constants (k) = 0.01

Species transport coefficients are given in table 2.

Rotor speed = 60,000 rpm.

Initial sharp boundary position (r_0) = 6.0 cm.

$\Delta t = 2155.51 \text{ sec}$

$K_{2M} \text{ (M}^{-2}\text{)}$

- a. 2.5×10^7
- b. 1.0×10^8
- c. 1.0×10^9
- d. 1.0×10^{11}

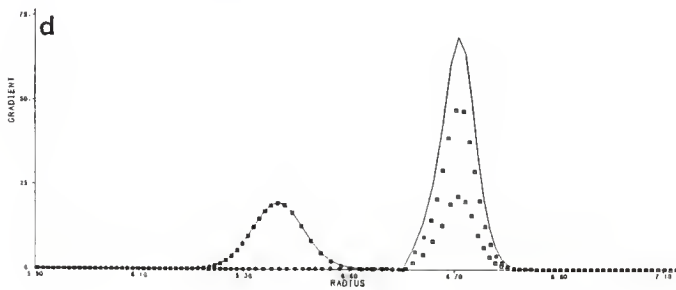
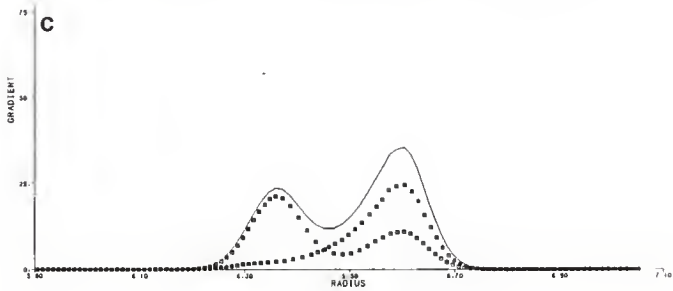
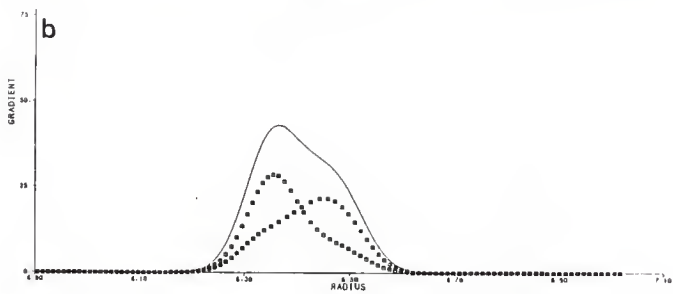
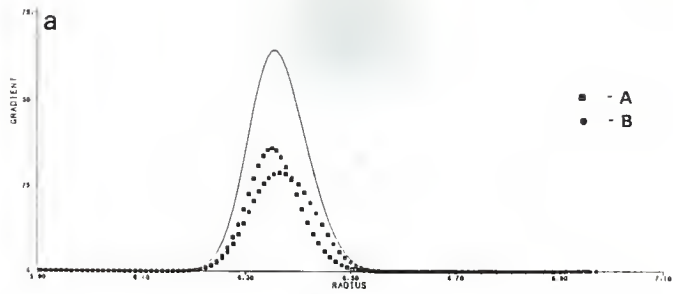


Figure 28: Gradient Profiles of Completely Cooperative AB_4 Systems of Different Strengths

$$W_A = 100Kd$$

$$W_B = 100Kd$$

$$C_{AT} = 5.0 \text{ mg/ml}$$

$$C_{BT} = 5.0 \text{ mg/ml}$$

$$[A] = 5 \times 10^{-5} \text{ M}$$

$$[B] = 5 \times 10^{-5} \text{ M}$$

$$[B]/[A] = 1.0$$

Frictional ratios (f/f_0) for all species = 1.1

All self and cross hydrodynamic constants (k) = 0.01

Species transport coefficients are given in table 2.

Rotor speed = 60,000 rpm.

Initial sharp boundary position (r_0) = 6.0 cm.

$\Delta t = 2155.51 \text{ sec}$

$$K_{4M} (M^{-4})$$

a. 1.0×10^{16}

b. 1.0×10^{17}

c. 1.0×10^{18}

d. 1.0×10^{19}

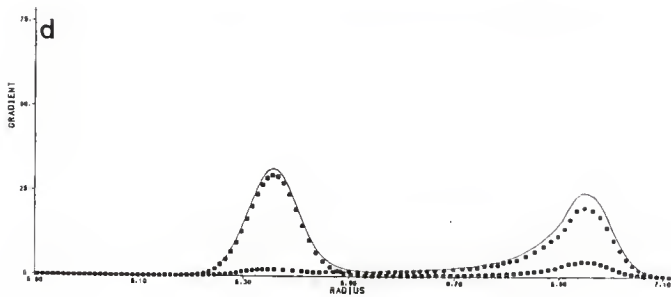
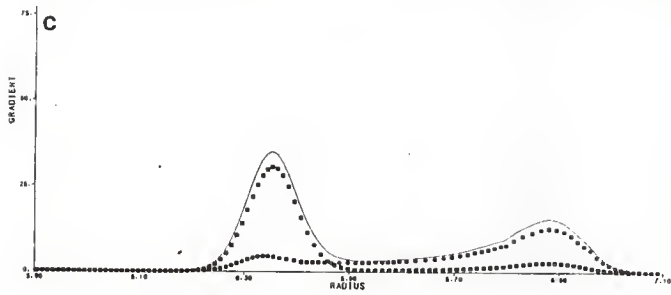
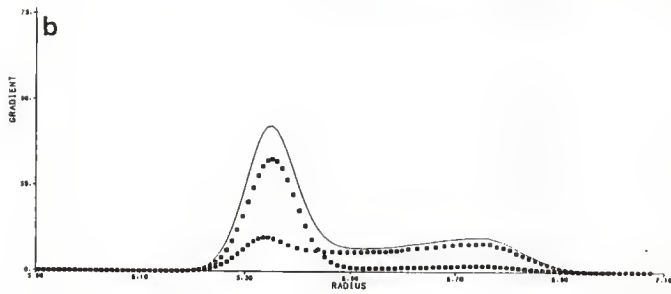
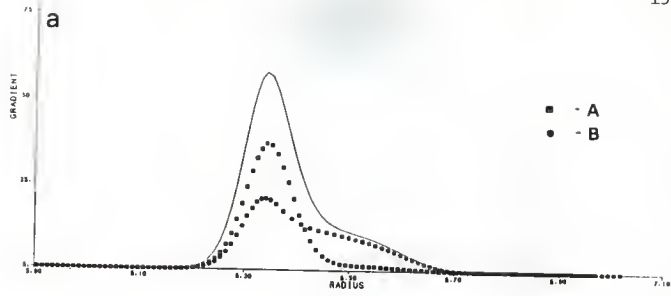


Figure 29: Boundary Heights (H_L and H_T) and Leading Boundary Positions (R_L) for Cooperative AB_n Gradient Profiles

$$W_A = 100Kd$$

$$W_B = 100Kd$$

$$C_{AT} = 5.0 \text{ mg/ml}$$

$$C_{BT} = 5.0 \text{ mg/ml}$$

$$[A] = 5 \times 10^{-5} \text{ M}$$

$$[B] = 5 \times 10^{-5} \text{ M}$$

$$[B]/[A] = 1.0$$

Frictional ratios (f/f_0) for all species = 1.1

All self and cross hydrodynamic constants (k) = 0.01

Species transport coefficients are given in table 2.

Rotor speed = 60,000 rpm.

Initial sharp boundary position (r_0) = 6.0 cm.

$\Delta t = 2155.51 \text{ sec}$

- a. H_L vs. $\log_{10} K_{nM}$ for completely cooperative AB_2 and AB_4 profiles.
- b. H_T vs. $\log_{10} K_{nM}$ for completely cooperative AB_2 and AB_4 profiles.
- c. R_L vs. $\log_{10} K_{nM}$ for completely cooperative AB_2 and AB_4 profiles.

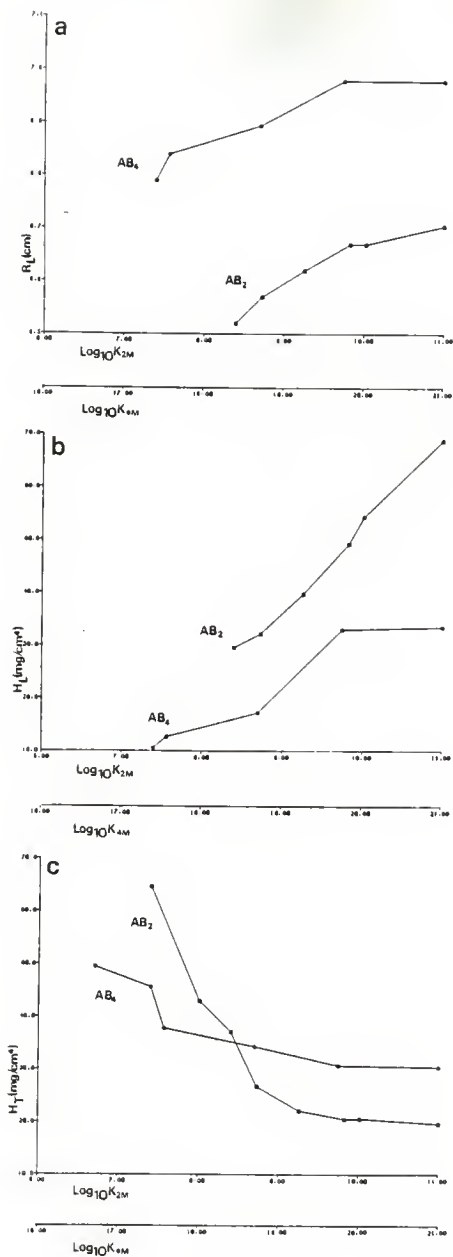


Figure 30: Species Concentrations and Average Sedimentation Coefficients for Completely Cooperative AB_2 Systems

$$W_A = 100\text{Kd}$$

$$W_B = 100\text{Kd}$$

$$C_{AT} = 5.0 \text{ mg/ml}$$

$$C_{BT} = 5.0 \text{ mg/ml}$$

$$[A] = 5 \times 10^{-5} \text{ M}$$

$$[B] = 5 \times 10^{-5} \text{ M}$$

$$[B]/[A] = 1.0$$

Frictional ratios (f/f_0) for all species = 1.1

Species transport coefficients are given in table 2.

- a. Species concentrations vs. $\log_{10} K_{2M}$ for completely cooperative AB_2 systems
- b. Average constituent sedimentation coefficients vs. $\log_{10} K_{2M}$ for completely cooperative AB_2 systems

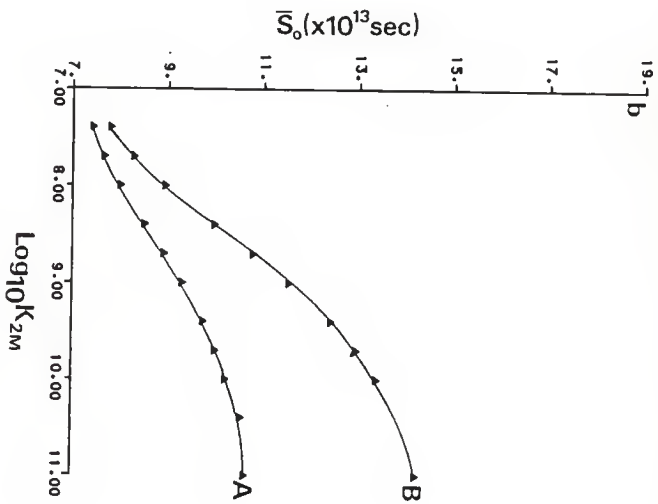
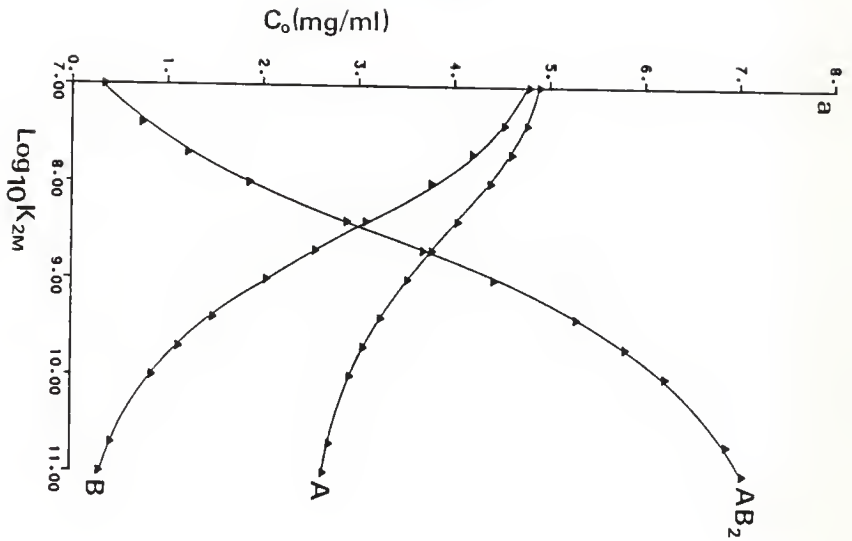


Figure 31: Species Concentrations and Average Sedimentation Coefficients for Completely Cooperative AB_4 Systems

$$W_A = 100\text{Kd}$$

$$W_B = 100\text{Kd}$$

$$C_{AT} = 5.0 \text{ mg/ml}$$

$$C_{BT} = 5.0 \text{ mg/ml}$$

$$[A] = 5 \times 10^{-5} \text{ M}$$

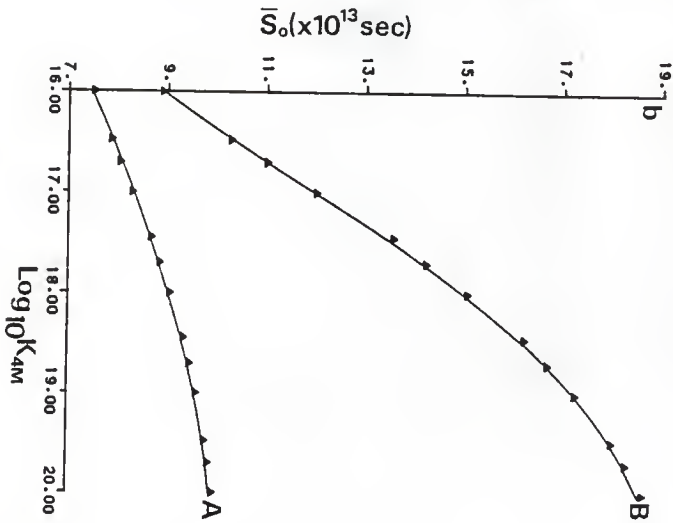
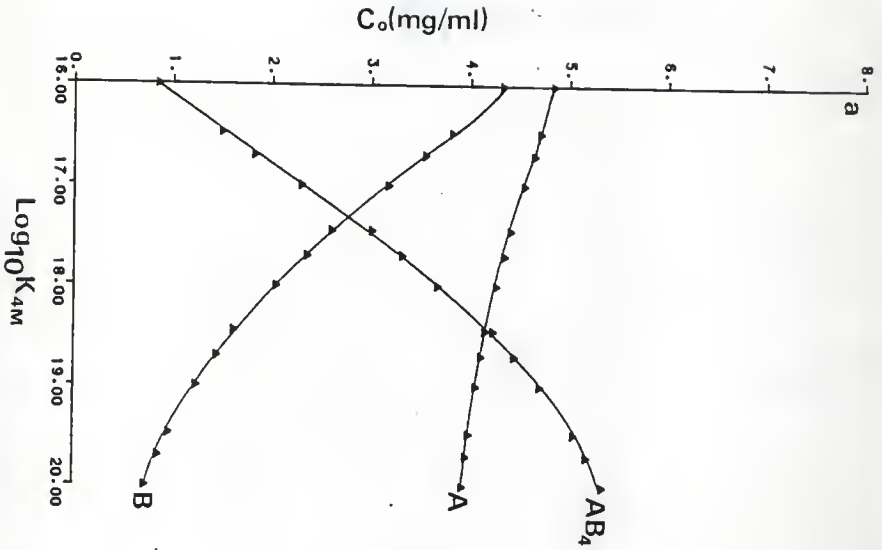
$$[B] = 5 \times 10^{-5} \text{ M}$$

$$[B]/[A] = 1.0$$

Frictional ratios (f/f_0) for all species = 1.1

Species transport coefficients are given in table 2.

- a. Species concentrations vs. $\log_{10} K_{4M}$ for completely cooperative AB_4 systems
- b. Average constituent sedimentation coefficients vs. $\log_{10} K_{4M}$ for completely cooperative AB_4 systems



erative) systems. At all values of K_{NM} where R_L could be measured, the leading boundaries of the AB_4 systems migrated more rapidly than the leading boundaries of any of the AB_2 systems. AB_3 systems, however, which were not included in this study, would most likely have values of R_L overlapping those of AB_2 and AB_4 systems.

Plots of H_L vs. R_L (figure 32-a) demonstrate a significant lack of similarity (with respect to H_L and R_L) between the shapes of all cooperative AB_2 and AB_4 profiles (for systems with leading boundaries) as well as between the shapes of cooperative and uncooperative systems. Some uncooperative AB_4 (U-4) and cooperative AB_2 (C-2) profiles have similar or identical leading boundary heights and positions ($H_L \sim 39 \text{ mg/cm}^4$ and $R_L = \text{ca. } 6.62 \text{ cm.}$). These U-4 and C-2 systems, however, have very different trailing boundary heights. The U-4 systems in this range ($K_{I-} \sim 4.0 \times 10^4$) give trailing boundaries with heights of ca. 14.2 mg/cm^4 while the trailing boundaries of the C-2 systems in this range ($K_{2M} = 1.5 \times 10^9$) have heights of ca. 22.0 mg/cm^4 (see figures 32-b and 33). Likewise, uncooperative AB_2 (U-2) and cooperative AB_2 (C-2) systems with similar leading boundary heights and positions ($H_L \sim 54 \text{ mg/cm}^4$ and $R_L \sim 6.66 \text{ cm.}$) have different trailing boundary heights (U-2: $H_T = 11.7 \text{ mg/cm}^4$, C-2: $H_T = 20.8 \text{ mg/cm}^4$)

Plots of H_T vs. H_L and H_T vs. R_L further demonstrate the dissimilarity between the boundary shapes of C-2 and C-4

Figure 32: Comparison of Boundary Dimensions for Uncooperative and Cooperative AB_n Systems

$$W_A = 100Kd$$

$$W_B = 100Kd$$

$$C_{AT} = 5.0 \text{ mg/ml}$$

$$C_{BT} = 5.0 \text{ mg/ml}$$

$$[A] = 5 \times 10^{-5} \text{ M}$$

$$[B] = 5 \times 10^{-5} \text{ M}$$

$$[B]/[A] = 1.0$$

Frictional ratios (f/f_0) for all species = 1.1

All self and cross hydrodynamic constants (k) = 0.01

Species transport coefficients are given in table 2.

Rotor speed = 60,000 rpm.

Initial sharp boundary position (r_0) = 6.0 cm.

$$\Delta t = 2155.51 \text{ sec}$$

Solid Lines: Cooperative Systems

Dashed Lines: Uncooperative Systems

- a. H_L vs. R_L for completely cooperative and uncooperative AB_2 and AB_4 profiles
- b. H_T vs. R_L for completely cooperative and uncooperative AB_2 and AB_4 profiles
- c. H_T vs. H_L for completely cooperative and uncooperative AB_2 and AB_4 profiles
- d. R_L vs. $\log_{10} K_{nM}$ for completely cooperative AB_2 and AB_4 profiles

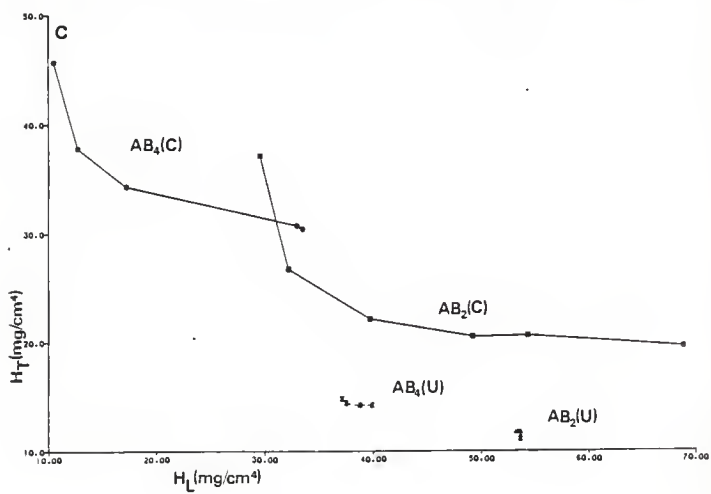
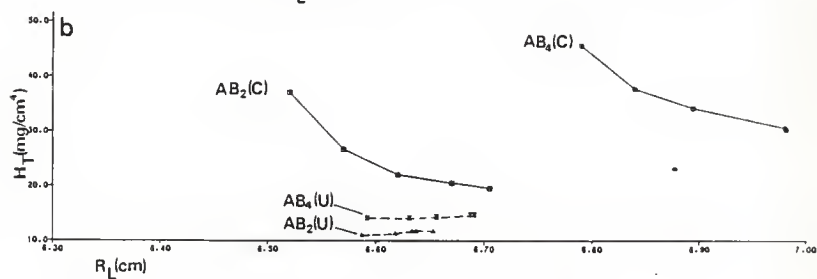
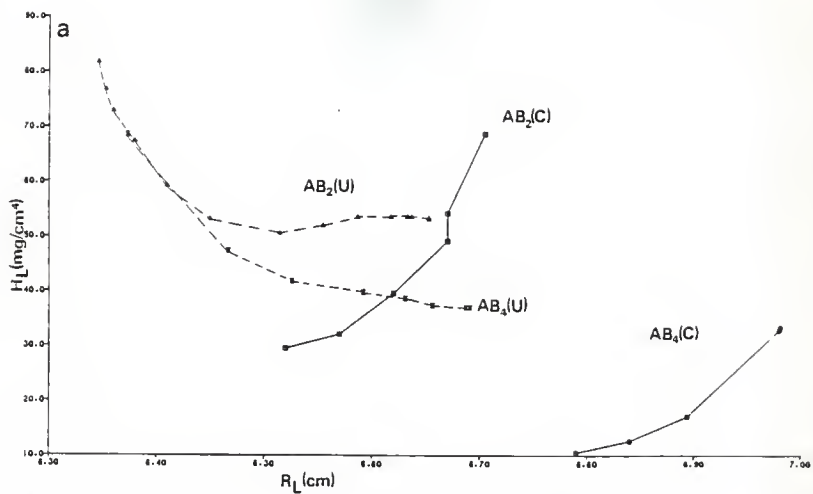


Figure 33: Gradient Profiles of an Uncooperative AB_4 and Completely Cooperative AB_2 System with Similar Leading Boundaries

$$W_A = 100Kd$$

$$W_B = 100Kd$$

$$C_{AT} = 5.0 \text{ mg/ml}$$

$$C_{BT} = 5.0 \text{ mg/ml}$$

$$[A] = 5 \times 10^{-5} \text{ M}$$

$$[B] = 5 \times 10^{-5} \text{ M}$$

$$[B]/[A] = 1.0$$

Frictional ratios (f/f_0) for all species = 1.1

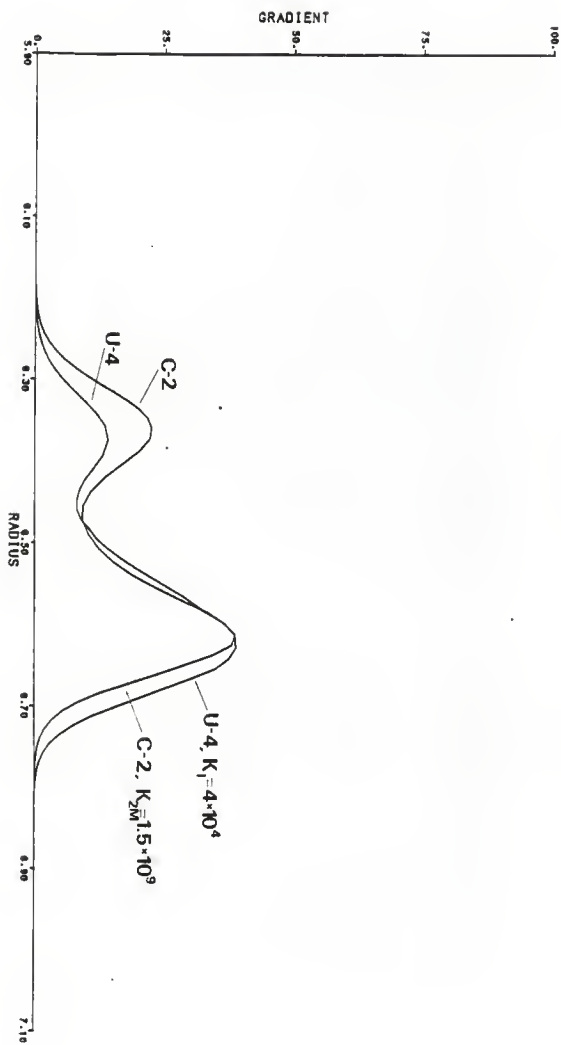
All self and cross hydrodynamic constants (k) = 0.01

Species transport coefficients are given in table 2.

Rotor speed = 60,000 rpm.

Initial sharp boundary position (r_0) = 6.0 cm.

$\Delta t = 2155.51 \text{ sec}$



systems as well as between cooperative and uncooperative systems (fig. 32-b and c).

Gradient profiles of C-2 and C-4 systems that are not very weak but that are not strong enough to give bimodal boundaries are also dissimilar as seen in figure 34 in which a series of C-4 gradient profiles is superimposed onto a series of C-2 profiles. The most obvious difference is that the C-2 boundaries have higher, shorter leading shoulders than C-4 boundaries.

Similar sets of superimposed boundaries for U-2 and C-2 systems (figure 35) demonstrate non-similarity between non-bimodal U-2 and C-2 boundaries. U-2 and C-2 boundaries that are skewed are skewed in opposite directions. U-2 systems are skewed to the right (downward or outward) and C-2 boundaries are skewed to the left (upward or inward). U-2 and C-2 boundaries that have shoulders have them on opposite sides of the main boundary. U-2 boundaries have trailing shoulders and C-2 boundaries have leading shoulders. U-4 and C-4 boundaries differ similarly (figure 36).

Figure 34: Comparison of Completely Cooperative AB_2 and AB_4 Gradient Profiles

$$W_A = 100\text{Kd}$$

$$W_B = 100\text{Kd}$$

$$C_{AT} = 5.0 \text{ mg/ml}$$

$$C_{BT} = 5.0 \text{ mg/ml}$$

$$[A] = 5 \times 10^{-5} \text{ M}$$

$$[B] = 5 \times 10^{-5} \text{ M}$$

$$[B]/[A] = 1.0$$

Frictional ratios (f/f_0) for all species = 1.1

All self and cross hydrodynamic constants (k) = 0.01

Species transport coefficients are given in table 2.

Rotor speed = 60,000 rpm.

Initial sharp boundary position (r_0) = 6.0 cm.

$\Delta t = 2155.51 \text{ sec}$

Solid Lines: AB_4 , K_{4M} from left to right =

$$1.0 \times 10^{16}$$

$$1.0 \times 10^{17}$$

$$1.0 \times 10^{18}$$

$$1.0 \times 10^{19}$$

Asterisks : AB_2 , K_{2M} from left to right =

$$2.5 \times 10^7$$

$$1.0 \times 10^8$$

$$1.0 \times 10^9$$

$$1.0 \times 10^{11}$$

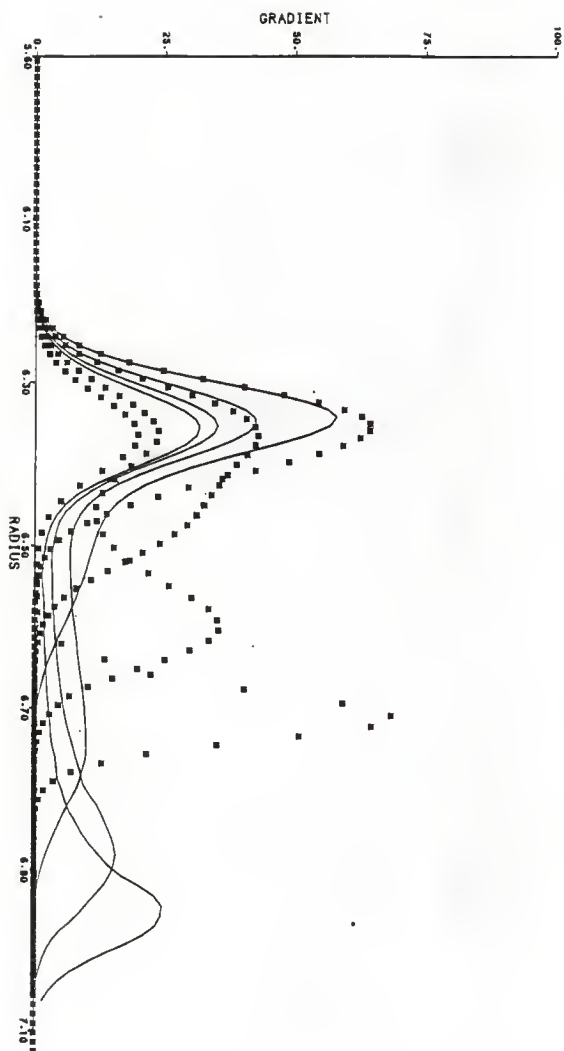


Figure 35: Comparison of Completely Cooperative and Uncooperative AB_2 Gradient Profiles

$$W_A = 100Kd$$

$$W_B = 100Kd$$

$$C_{AT} = 5.0 \text{ mg/ml}$$

$$C_{BT} = 5.0 \text{ mg/ml}$$

$$[A] = 5 \times 10^{-5} \text{ M}$$

$$[B] = 5 \times 10^{-5} \text{ M}$$

$$[B]/[A] = 1.0$$

Frictional ratios (f/f_0) for all species = 1.1

All self and cross hydrodynamic constants (k) = 0.01

Species transport coefficients are given in table 2.

Rotor speed = 60,000 rpm.

Initial sharp boundary position (r_0) = 6.0 cm.

$$\Delta t = 2155.51 \text{ sec}$$

Solid Lines: cooperative, K_{2M} from left to right =

$$2.5 \times 10^7$$

$$1.0 \times 10^8$$

$$1.0 \times 10^9$$

$$1.0 \times 10^{11}$$

Asterisks : uncooperative, K_I from left to right =

$$1.0 \times 10^3$$

$$1.0 \times 10^4$$

$$5.0 \times 10^4$$

$$1.0 \times 10^6$$

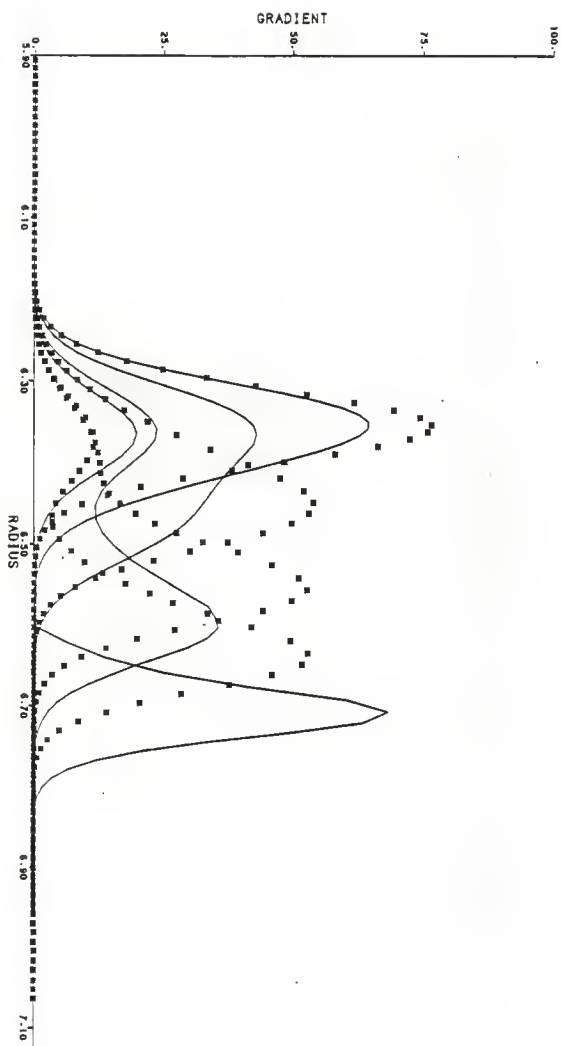


Figure 36: Comparison of Completely Cooperative and Uncooperative AB_4 Gradient Profiles

$$W_A = 100Kd$$

$$W_B = 100Kd$$

$$C_{AT} = 5.0 \text{ mg/ml}$$

$$C_{BT} = 5.0 \text{ mg/ml}$$

$$[A] = 5 \times 10^{-5} \text{ M}$$

$$[B] = 5 \times 10^{-5} \text{ M}$$

$$[B]/[A] = 1.0$$

Frictional ratios (f/f_0) for all species = 1.1

All self and cross hydrodynamic constants (k) = 0.01

Species transport coefficients are given in table 2.

Rotor speed = 60,000 rpm.

Initial sharp boundary position (r_0) = 6.0 cm.

$\Delta t = 2155.51 \text{ sec}$

Solid lines: cooperative, K_{4M} from left to right =

$$1.0 \times 10^{16}$$

$$1.0 \times 10^{17}$$

$$1.0 \times 10^{18}$$

$$1.0 \times 10^{19}$$

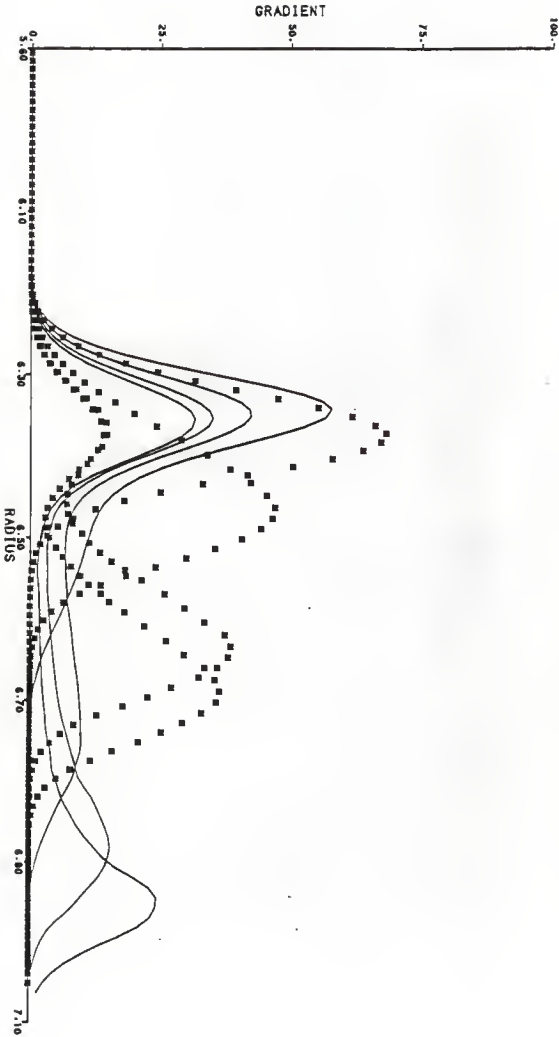
Asterisks : uncooperative, K_I from left to right =

$$1.0 \times 10^3$$

$$5.0 \times 10^3$$

$$5.0 \times 10^4$$

$$1.0 \times 10^6$$



3.2.1 Effect of Constituent Mole Ratio

For completely cooperative AB_n systems, the mole ratio at which the trailing boundary or shoulder is smallest, " MR_{eq} ", seems not to depend upon the strength of association (K_{nM}). Instead MR_{eq} appears to depend only on the stoichiometry of the cooperative system. Cooperative AB_2 and AB_4 systems with various values of K_{nM} (and identical monomers) had minimum trailing boundaries¹³ (or shoulders) at mole ratios of 2.0 and 4.0 respectively (figures 37 - 39). Thus, in general, a cooperative AB_n system (with identical monomers) would be expected to have an equivalence point at a mole ratio of equal to n .

Since uncooperative AB_n systems have equivalence mole ratios of less than n (except when K_i is very large - see figure 21) it should be possible, if the overall stoichiometry of an AB_n system is known (ie. if n is known), to determine whether the system is uncooperative or completely cooperative (if it is one or the other) from MR_{eq} alone. Also, whether or not n is known, if MR_{eq} is not a whole number greater than one, then one can probably be reasonably certain that the system in question is not completely coop-

¹³ For systems with bimodal boundaries at their equivalence points, MR_{eq} was taken as the mole ratio at which H_T was smallest. For weaker systems that were not bimodal at MR_{eq} , but instead had a trailing shoulder, MR_{eq} was taken as the mole ratio at which the trailing shoulder was smallest, approximated by superimposing and comparing profiles at different mole ratios.

Figure 37: Gradient Profiles of a Completely Cooperative AB_2 Systems at Different Constituent Mole Ratios

$$K_{2M} = 1.0 \times 10^9$$

$$W_A = 100Kd$$

$$W_B = 100Kd$$

$$C_{AT} + C_{BT} = 10.0 \text{ mg/ml}$$

$$[B]_T + [A]_T = 1.0 \times 10^{-4}$$

Frictional ratios (f/f_0) for all species = 1.1

All self and cross hydrodynamic constants (k) = 0.01

Species transport coefficients are given in table 2.

Rotor speed = 60,000 rpm.

Initial sharp boundary position (r_0) = 6.0 cm.

$\Delta t = 2155.51 \text{ sec}$

[B]/[A]

- a. 1.50
- b. 2.00
- c. 2.50

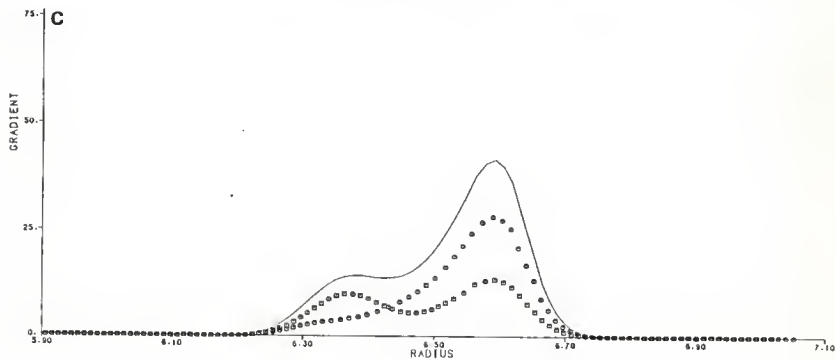
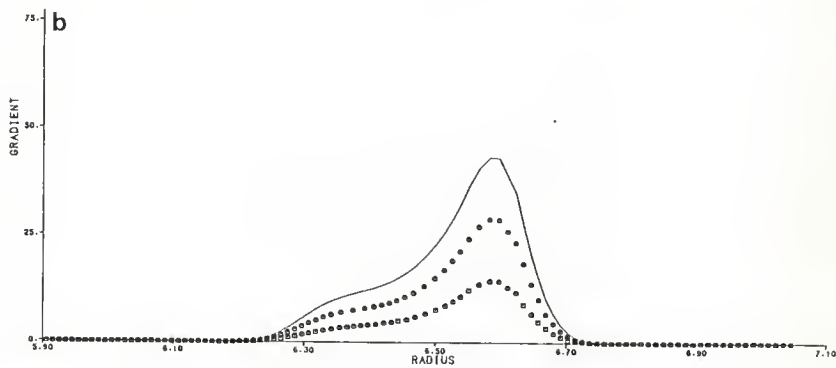
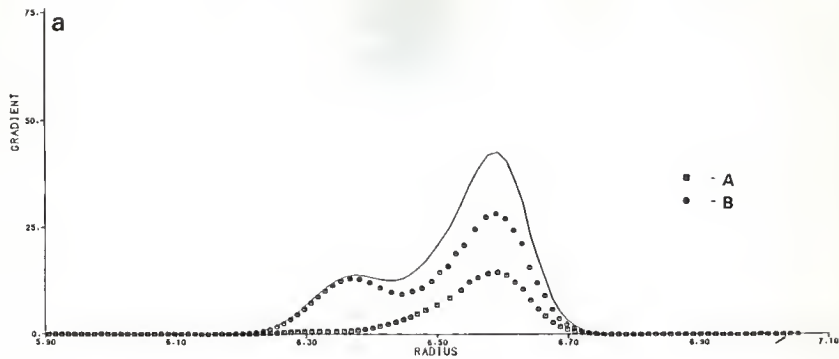


Figure 38: Gradient Profiles of a Weak Completely Cooperative AB_2 Systems at Different Constituent Mole Ratios

$$K_{2M} = 1.0 \times 10^8$$

$$W_A = 100Kd$$

$$W_B = 100Kd$$

$$C_{AT} + C_{BT} = 10.0 \text{ mg/ml}$$

$$[B]_T + [A]_T = 1.0 \times 10^{-4}$$

Frictional ratios (f/f_0) for all species = 1.1

All self and cross hydrodynamic constants (k) = 0.01

Species transport coefficients are given in table 2.

Rotor speed = 60,000 rpm.

Initial sharp boundary position (r_0) = 6.0 cm.

$\Delta t = 2155.51 \text{ sec}$

[B]/[A]

- a. 1.50
- b. 2.00
- c. 2.50

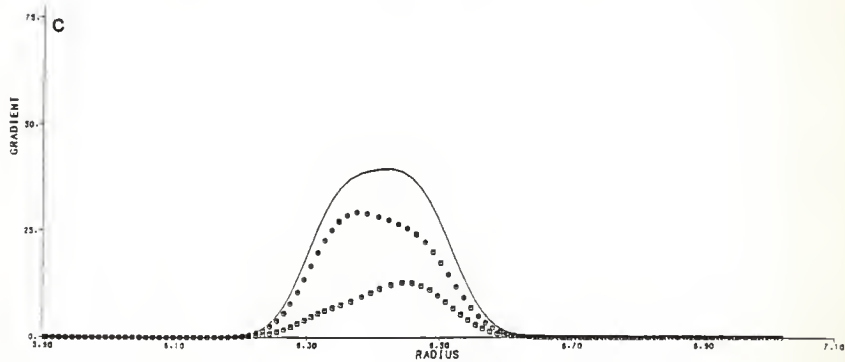
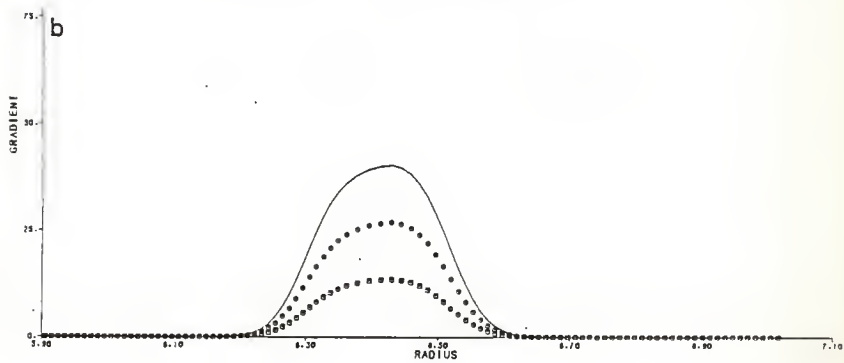
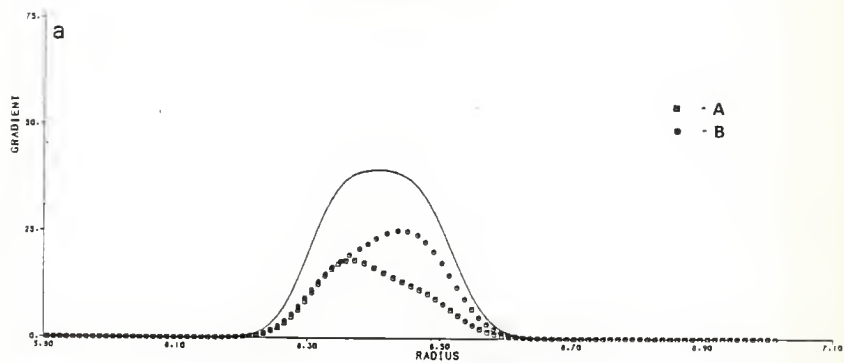


Figure 39: Gradient Profiles of Completely Cooperative AB_4 Systems at Different Constituent Mole Ratios

$$K_{4M} = 1.0 \times 10^{17}$$

$$W_A = 100Kd$$

$$W_B = 100Kd$$

$$C_{AT} + C_{BT} = 10.0 \text{ mg/ml}$$

$$[B]_T + [A]_T = 1.0 \times 10^{-4}$$

Frictional ratios (f/f_0) for all species = 1.1

All self and cross hydrodynamic constants (k) = 0.01

Species transport coefficients are given in table 2.

Rotor speed = 60,000 rpm.

Initial sharp boundary position (r_0) = 6.0 cm.

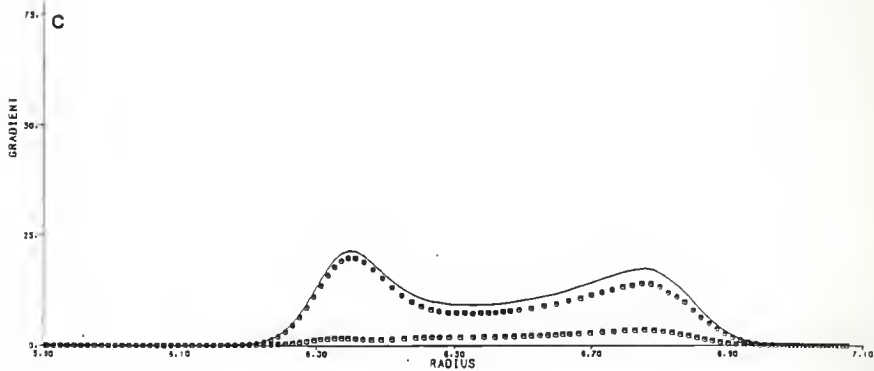
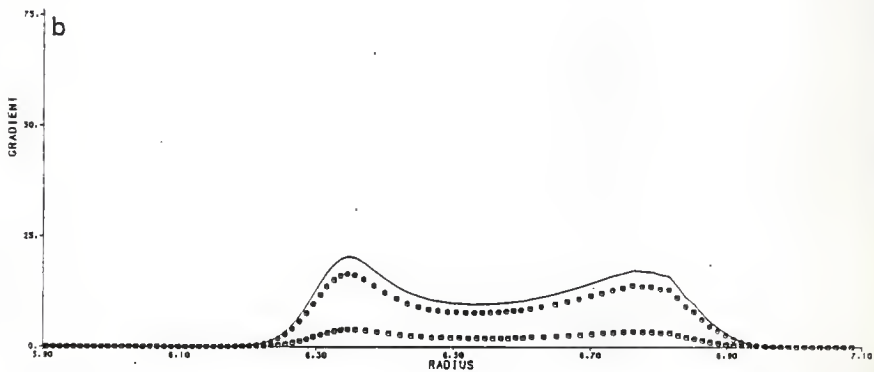
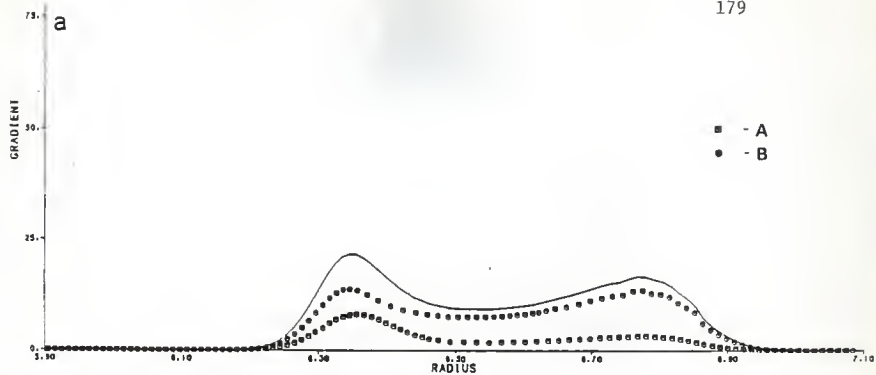
$\Delta t = 2155.51 \text{ sec}$

[B]/[A]

a. 3.00

b. 4.00

c. 5.00



erative. If n is not known, however, and MR_{eq} is an integer greater than one, then the system in question could be either a completely cooperative AB_n system or an uncooperative AB_m system (where $m > n$).

The changes in the profiles of cooperative systems with mole ratio and the general features of cooperative profiles at the equivalence point are distinctly different, qualitatively, than those of uncooperative systems. As the mole ratio is increased, in a cooperative system, from values at which there is an excess of constituent A (and most of the material in the trailing boundary or shoulder is constituent A) the constituent B gradient begins to increase its contribution to the trailing boundary (or shoulder) before all of the excess constituent A is eliminated (ie. before the contribution of constituent A to the trailing element of the boundary stops decreasing). As a result, the trailing boundary or shoulder of a cooperative system is not completely eliminated at any mole ratio as it is with uncooperative systems at MR_{eq} ¹⁴. Since the trailing boundary (or

¹⁴ The equivalence point occurs at the mole ratio where the increase in the contribution of constituent B to the trailing boundary (or shoulder) with an increase in MR is equal to the decrease in the contribution of constituent A to the trailing element with the same increase in MR. For systems with measurable trailing boundaries this might be expressed as:

$$\frac{dH_T(B)}{d(MR)} = - \frac{dH_T(A)}{d(MR)}$$

shoulder) does not disappear in cooperative profiles at the equivalence point as it does in noncooperative profiles it should be possible to determine whether a system is completely cooperative or noncooperative (if it is one or the other) simply by examining the experimental gradient profile (schlieren pattern) at the equivalence point. So, for instance, when MR_{eq} is an integer, n , greater than one and the stoichiometry is not known, it should be possible to determine from the profile at the equivalence point whether the system is completely cooperative (AB_n) or uncooperative with a higher stoichiometry (AB_m where $m > n$).

3.2.2 Cooperative Systems with Nonidentical Monomers

Simulated boundaries of C-4 systems with $W_A > W_B$ ($W_A = 140$ Kd, $W_B = 60$ Kd) and different association constants, all at $MR = 3.0$, are shown in figure 40. The obvious difference between these profiles and any others considered previously is

where $H_T(A)$ and $H_T(B)$ are the heights of the A and B constituent gradients at the peak of the trailing boundary. In cooperative systems this does not necessarily occur at the point where the trailing edges of the constituent gradients overlap. In fact for all cases studied the trailing edge of the constituent B gradient lies above the trailing edge of constituent A gradient at the equivalence mole ratio. With noncooperative systems essentially all of the excess A is eliminated from the trailing boundary (increasing MR) and the trailing edges of the constituent gradients meet before the constituent B boundary begins to change, and, increasing MR beyond this point has very little effect on the trailing edge of the constituent A boundary. Thus, for uncooperative systems, MR_{eq} occurs at the point where the trailing edges of the individual constituent profiles overlap the most (and the total boundary is least skewed).

that they are trimodal. Constituent gradients show that the slowest boundary contains constituent B only, the middle boundary contains mostly constituent A and the leading boundary contains both A and B as usual.

As the constituent mole ratio of one of these systems is increased (from 1.0) the fast monomer boundary (A) initially moving at about the rate of free A monomer (R_{TA} (position of trailing boundary containing A)=6.35 cm., R_{miuA} =6.34 cm.), shrinks and migrates at progressively faster rates until it becomes a shoulder on the trailing edge of the leading boundary (figure 41). Meanwhile, the slower B monomer boundary, which moves at a rate comparable to pure B (R_{TB} =6.20 cm.; R_{maxB} =6.21 cm.) at all mole ratios considered, steadily becomes larger.

The equivalence point for these systems cannot be determined accurately from either the total gradient or constituent gradient profiles because differences in the sizes of the total trailing element at mole ratios that seem to be near the equivalence point ($3.0 < MR < 5.0$ in figure 41) are ambiguous. Even though it may not be possible to determine the equivalence mole ratio of this type of system, a sampling of gradient profiles at various mole ratios should be helpful in distinguishing between completely cooperative and uncooperative systems. At MR_{eq} , uncooperative (AB_n) systems have no trailing boundary or shoulder, whereas cooperative systems have at least a trailing shoulder at all mole

Figure 40: Gradient Profiles of Completely Cooperative AB_4 Systems of Different Strengths with $W_A > W_B$

$$W_A = 140\text{Kd}$$

$$W_B = 60\text{Kd}$$

$$C_{AT} = 4.375 \text{ mg/ml}$$

$$[A] = 3.125 \times 10^{-5} \text{ M}$$

$$C_{BT} = 5.625 \text{ mg/ml}$$

$$[B] = 9.375 \times 10^{-5} \text{ M}$$

$$[B]/[A] = 3.0$$

Frictional ratios (f/f_0) for all species = 1.1

All self and cross hydrodynamic constants (k) = 0.01

Rotor speed = 60,000 rpm.

Initial sharp boundary position (r_0) = 6.0 cm.

$\Delta t = 1722.50 \text{ sec}$

Species transport coefficients are given in table 3.

$$K_{4M} \text{ (M}^{-4}\text{)}$$

a. 1.0×10^{16}

b. 1.0×10^{17}

c. 1.0×10^{18}

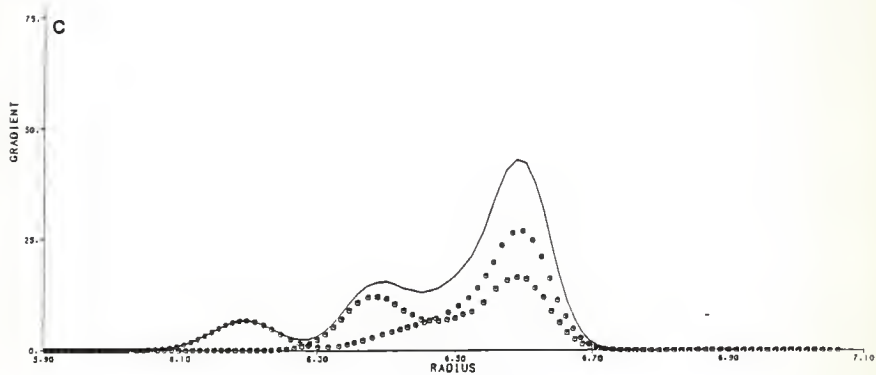
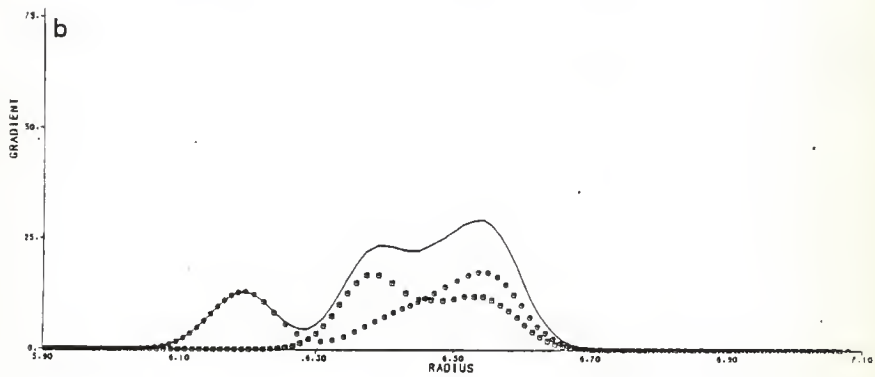
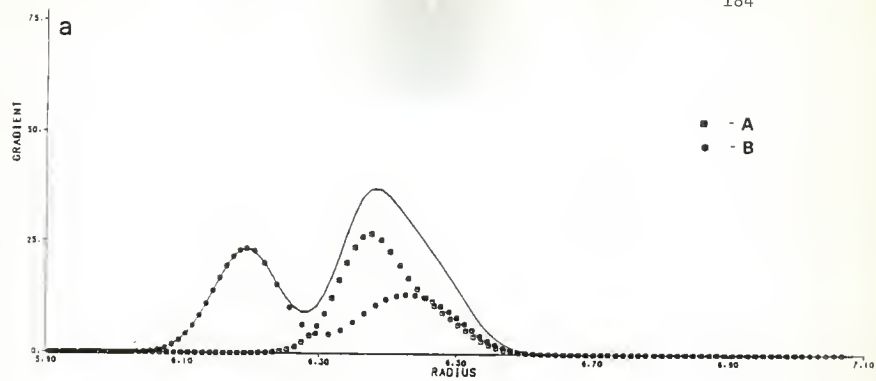


Figure 41: Gradient Profiles of Cooperative AB_4 Systems
with $W_A > W_B$ at Different Constituent Mole Ratios

$$K_{4M} = 1.0 \times 10^{17}$$

$$W_A = 140 \text{Kd}$$

$$W_B = 60 \text{Kd}$$

$$C_{AT} + C_{BT} = 10.0 \text{ mg/ml}$$

Frictional ratios (f/f_0) for all species = 1.1

All self and cross hydrodynamic constants (k) = 0.01

Rotor speed = 60,000 rpm.

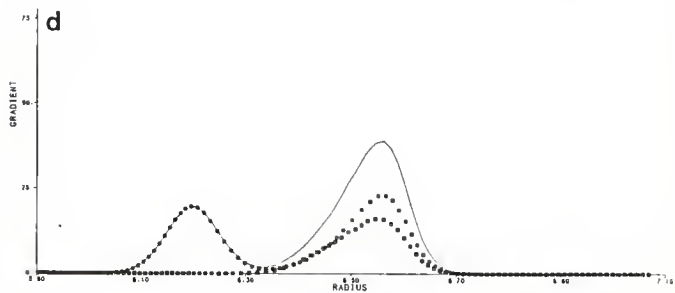
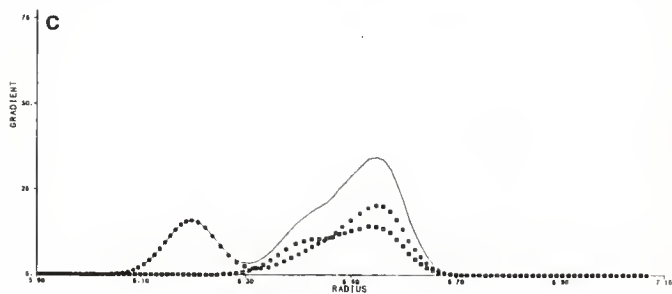
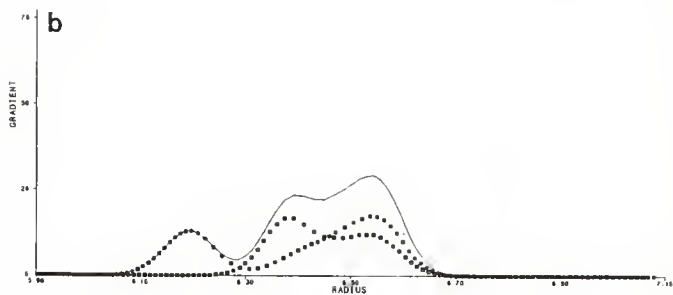
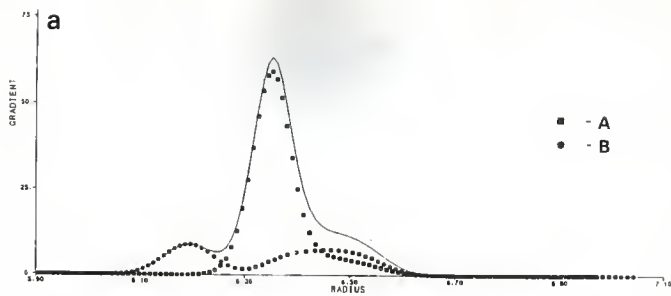
Initial sharp boundary position (r_0) = 6.0 cm.

$\Delta t = 1722.50 \text{ sec}$

Species transport coefficients are given in table 3.

[B]/[A]

- a. 1.00
- b. 3.00
- c. 4.00
- d. 5.00



ratios (except, of course, when K_{nM} is small to begin with), and at least some cooperative AB_n systems with monomers of significantly different sizes¹⁵ have trimodal boundaries at some mole ratios which noncooperative systems do not have at any mole ratio.

¹⁵ Trimodal boundaries have been observed for AB_4 systems with $W_A=140K$ and $W_B=60Kd$ (figure 42), as well as for systems with $W_A=60K$ and $W_B=140Kd$ (figure 42), but not for AB_4 systems with monomers that differed less in size ($W_A=80K$, $W_B=120K$).

Figure 42: Gradient Profile of a Completely Cooperative AB_4 System With $W_B > W_A$

$$W_A = 60\text{Kd}$$

$$W_B = 140\text{Kd}$$

$$C_{AT} = 5.0 \text{ mg/ml}$$

$$[A] = 8.333 \times 10^{-5} \text{ M}$$

$$C_{BT} = 5.0 \text{ mg/ml}$$

$$[B] = 3.571 \times 10^{-5} \text{ M}$$

$$[B]/[A] = 0.429$$

Frictional ratios (f/f_0) for all species = 1.1

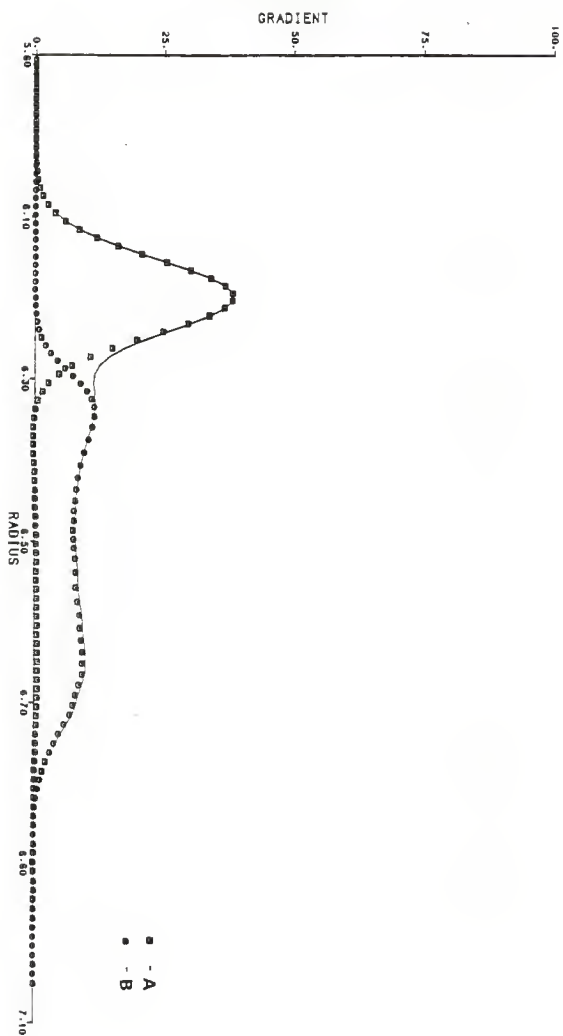
All self and cross hydrodynamic constants (k) = 0.01

Rotor speed = 60,000 rpm.

Initial sharp boundary position (r_0) = 6.0 cm.

$\Delta t = 1722.50 \text{ sec}$

Species transport coefficients are given in table 4.



3.3 GENERAL AB₂ SYSTEMS

It has previously been demonstrated that gradient profiles of uncooperative and cooperative AB₂ systems are generally not alike. Real biological AB₂ systems, of course, do not all necessarily belong to one of these two classes of systems. (In fact 'completely cooperative systems are probably very rare.) In the full range of possibilities, uncooperative systems are at the midpoint, and completely cooperative systems are at one extreme of a continuum with respect to cooperativity. At the other end of the continuum are anti-cooperative systems, the extreme of which would be an AB₂ system in which binding at one site completely prevents bonding at the second site. This case is indistinguishable from a simple AB₁ system.

Simulated gradient profiles for AB₂ systems with various degrees of cooperativity and anticooperativity were studied to see if boundary shapes differ among systems with different degrees of cooperativity as they do among completely cooperative and uncooperative systems. Plots of H_L vs. R_L (figure 43-a) for groups of systems with K_{1M}/K'_{2M} (an index of cooperativity¹⁶) constant and K_{1M} and K'_{2M} varied in the

¹⁶ For uncooperative AB₂ systems $K_{1M}/K'_{2M}=4.0$, for cooperative systems $K_{1M}/K'_{2M}<4.0$ and for anti-cooperative systems $K_{1M}/K'_{2M}>4.0$. where

$$K_{1M} = \frac{[AB]}{[A][B]}$$

appropriate proportions show that, at least when the associations are not very tight, the positions and heights of the leading boundaries are together unambiguously diagnostic for the type and degree of cooperativity (K_{1M}/K'_{2M}). For example the boundary of a cooperative system with $K_{1M}/K'_{2M}=2.5$ is generally different from that of a more cooperative system (eg. $K_{1M}/K'_{2M}=1.0$) or of a less cooperative system (eg. $K_{1M}/K'_{2M}=4.0$) as long as the association is not very strong. As the systems become tighter the curves in figure 43-a begin to run together. Plots of H_T vs. R_L (fig. 43-b) for the same groups of systems, however, show that, while tight systems with different degrees of cooperativity may have leading boundaries with the same heights and positions, they will probably not have identical trailing boundary heights. There may be some ambiguity in assigning a particular model to a real boundary on the basis of its trailing boundary height since the differences between H_T s of systems with different values of K_{1M}/K'_{2M} are not very large, but it should, at least, be possible to distinguish a strongly co-

$$K'_{2M} = \frac{[AB_2]}{[AB][B]}$$

and

$$K_{2M} = K_{1M} \times K'_{2M} = \frac{[AB_2]}{[A][B]^2}$$

operative system from an uncooperative or anti-cooperative system.

Since the values of K_{1M} and K'_{2M} are unique for a given degree of cooperativity (K_{1M}/K'_{2M}) and association strength (K_{1M}), if systems with different degrees of cooperativity and association strength have unique boundary shapes, then, so should systems with different values of K_{1M} and K'_{2M} . The independent effects of K_{1M} and K'_{2M} on boundary shape are illustrated in figure 44. As K_{1M} is increased, with K'_{2M} held constant, the most noticeable changes in boundary shape are an increase in H_L and a decrease in H_T . Increasing K'_{2M} , with K_{1M} constant, increases the leading boundary's sedimentation rate. The leading boundary height decreases as K'_{2M} is increased through low values of K'_{2M} , then passes through a minimum and increases as K'_{2M} is increased further. The effect of K'_{2M} on H_T depends on the magnitude of K_{1M} . At low values of K_{1M} , the trailing boundary becomes smaller as K'_{2M} is increased and at large values of K_{1M} it becomes larger as K'_{2M} is increased.

The changes in H_L , H_T , and R_L with K'_{2M} for several groups of systems with different values of K_{1M} (at a 1:1 constituent mole ratio) are illustrated in figure 45. Plots of H_L vs. R_L (K'_{2M} varied, K_{1M} constant) for the same groups of systems indicate that boundaries of systems with different values of K_{1M} are not alike at low and intermediate values of K'_{2M} , but are similar (with respect to H_L and

Figure 43: Comparison of Boundary Dimensions for AB_2 Systems with Different Degrees of Cooperativity

$$W_A = 100Kd$$

$$W_B = 100Kd$$

$$C_{AT} = 5.0 \text{ mg/ml}$$

$$C_{BT} = 5.0 \text{ mg/ml}$$

$$[A] = 5 \times 10^{-5} \text{ M}$$

$$[B] = 5 \times 10^{-5} \text{ M}$$

$$[B]/[A] = 1.0$$

Frictional ratios (f/f_0) for all species = 1.1

All self and cross hydrodynamic constants (k) = 0.01

Species transport coefficients are given in table 2.

Rotor speed = 60,000 rpm.

Initial sharp boundary position (r_0) = 6.0 cm.

$\Delta t = 2155.51 \text{ sec}$

- a. H_L vs. R_L for families of AB_2 systems
with K_{1M}/K'_{2M} constant
- b. H_T vs. R_L for families of AB_2 systems
with K_{1M}/K'_{2M} constant

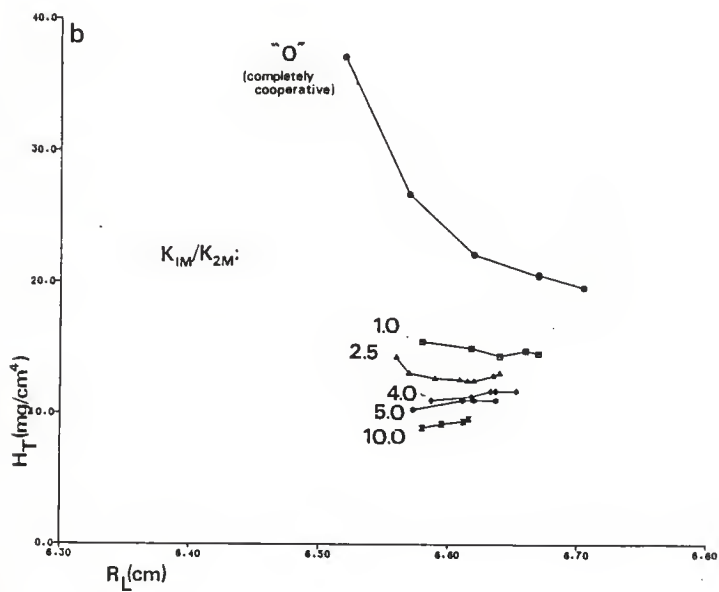
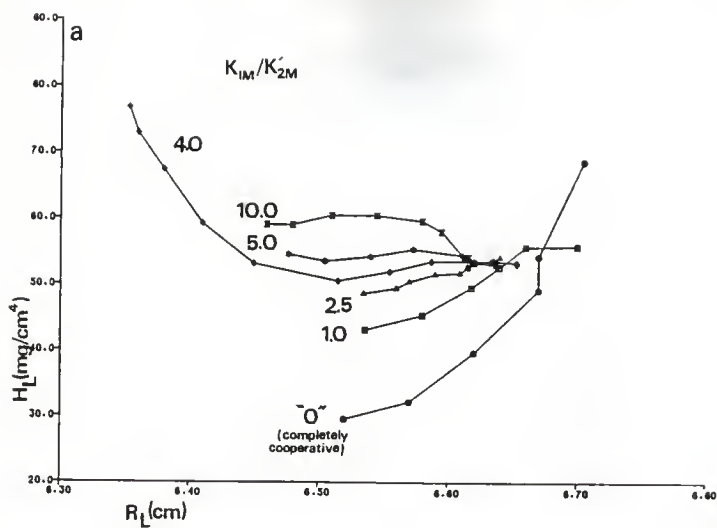


Figure 44: Gradient Profiles of AB_2 Systems with K_{1M} and K'_{2M} Varied Independently

$$W_A = 100Kd$$

$$W_B = 100Kd$$

$$C_{AT} = 5.0 \text{ mg/ml}$$

$$C_{BT} = 5.0 \text{ mg/ml}$$

$$[A] = 5 \times 10^{-5} \text{ M}$$

$$[B] = 5 \times 10^{-5} \text{ M}$$

$$[B]/[A] = 1.0$$

Frictional ratios (f/f_0) for all species = 1.1

All self and cross hydrodynamic constants (k) = 0.01

Species transport coefficients are given in table 2.

Rotor speed = 60,000 rpm.

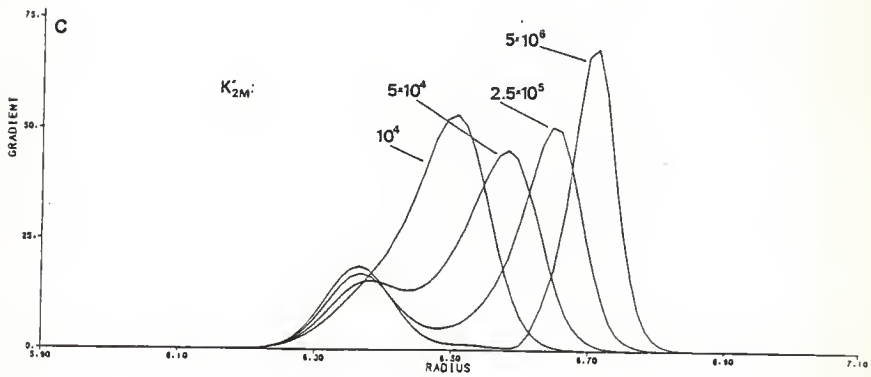
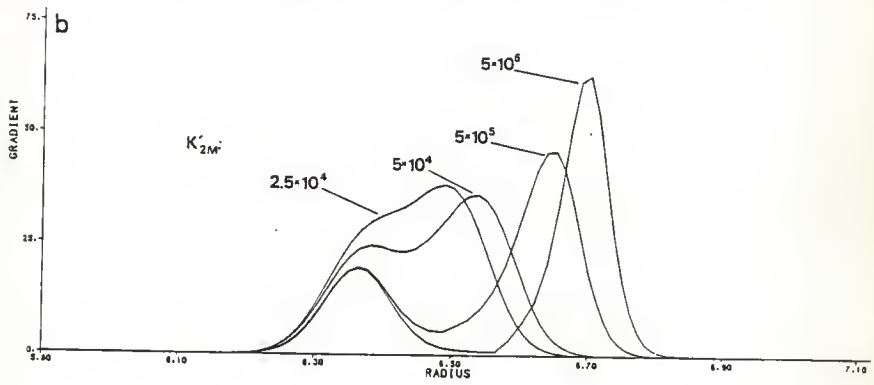
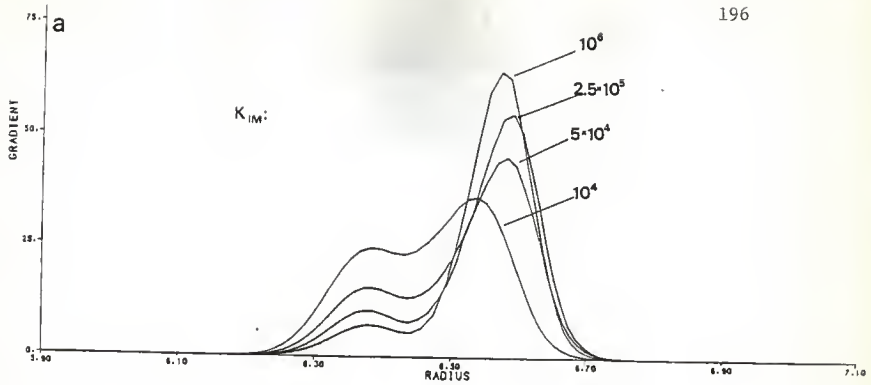
Initial sharp boundary position (r_0) = 6.0 cm.

$$\Delta t = 2155.51 \text{ sec}$$

a. K_{1M} varied, $K'_{2M} = 5.0 \times 10^4$

b. K_{1M} varied, $K'_{2M} = 1.0 \times 10^4$

c. K'_{2M} varied, $K_{1M} = 5.0 \times 10^4$



R_L) at higher values of K'_{2M} , where these curves converge (see figure 46-a). Plots of H_T vs. R_L (figure 46-b) demonstrate additional differences in boundary shape that seem to extend to somewhat tighter systems. These differences among the tighter systems are, however, fairly small and may not be practically useful.

Species concentration vs. $\log_{10} K'_{2M}$ curves (figure 47) show that at large values of K'_{2M} there is essentially no difference in the compositions of systems with different values of K_{1M} . Average constituent sedimentation coefficients are, therefore, also similar at large K'_{2M} s (figure 48). In view of these similarities it is not too surprising that the sedimenting boundary profiles of these systems are also alike.

In some cases, where systems with significantly different values of K_{1M} and K'_{2M} have very similar boundaries at a constituent mole ratio of 1:1, they may have more noticeably different boundaries at another ratio. For example, at a 1:1 mole ratio the boundary of the system with $K_{1M}=2 \times 10^5$ and $K'_{2M}=2.5 \times 10^5$ is nearly identical to that of the system with $K_{1M}=5 \times 10^5$ and $K'_{2M}=3 \times 10^5$ (see figure 49-a), but, at a constituent ratio, [B]:[A], of 2:1 the same two systems produce obviously different boundaries (fig. 49-b).

At a 2:1 constituent ratio the effects, on boundary shape, of changes in K'_{2M} (K_{1M} constant) are qualitatively different than those at a 1:1 mole ratio (see figure 50).

Figure 45: Changes in Boundary Dimensions with K'_{2M} for AB_2 Systems with K_{1M} Constant

$$W_A = 100Kd$$

$$W_B = 100Kd$$

$$C_{AT} = 5.0 \text{ mg/ml}$$

$$C_{BT} = 5.0 \text{ mg/ml}$$

$$[A] = 5 \times 10^{-5} \text{ M}$$

$$[B] = 5 \times 10^{-5} \text{ M}$$

$$[B]/[A] = 1.0$$

Frictional ratios (f/f_0) for all species = 1.1

All self and cross hydrodynamic constants (k) = 0.01

Species transport coefficients are given in table 2.

Rotor speed = 60,000 rpm.

Initial sharp boundary position (r_0) = 6.0 cm.

$$\Delta t = 2155.51 \text{ sec}$$

- a. H_L vs. $\log_{10} K'_{2M}$ for families of systems with K_{1M} constant
- b. H_T vs. $\log_{10} K'_{2M}$ for families of systems with K_{1M} constant
- c. R_L vs. $\log_{10} K'_{2M}$ for families of systems with K_{1M} constant

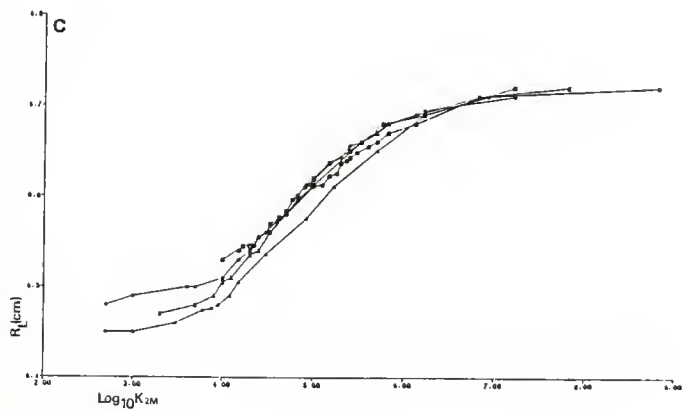
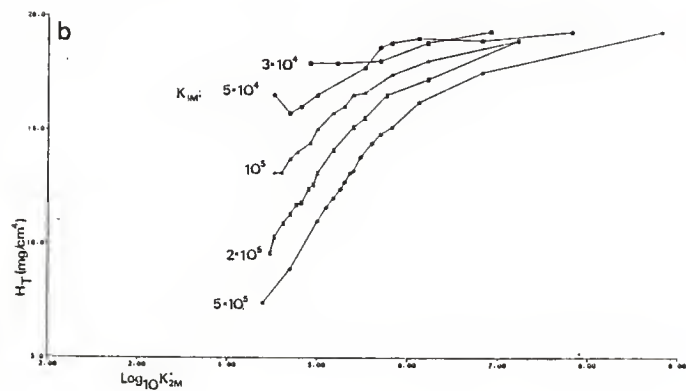
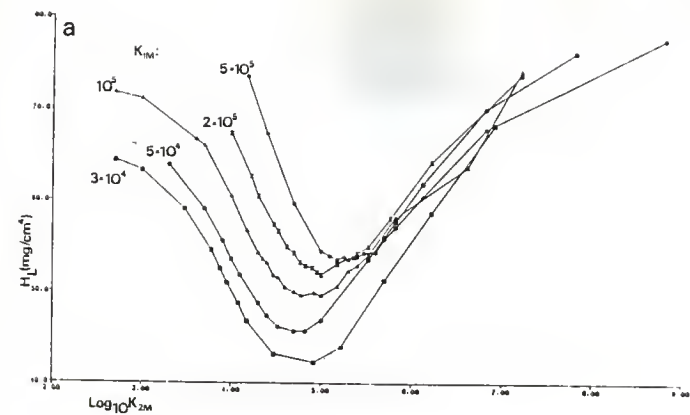


Figure 46: Comparison of Boundary Dimensions for AB_2 Systems with Different values of K'_{2M}

$$W_A = 100Kd$$

$$W_B = 100Kd$$

$$C_{AT} = 5.0 \text{ mg/ml}$$

$$C_{BT} = 5.0 \text{ mg/ml}$$

$$[A] = 5 \times 10^{-5} \text{ M}$$

$$[B] = 5 \times 10^{-5} \text{ M}$$

$$[B]/[A] = 1.0$$

Frictional ratios (f/f_0) for all species = 1.1

All self and cross hydrodynamic constants (k) = 0.01

Species transport coefficients are given in table 2.

Rotor speed = 60,000 rpm.

Initial sharp boundary position. (r_0) = 6.0 cm.

$$\Delta t = 2155.51 \text{ sec}$$

a. H_L vs. R_L for families of AB_2 systems with K'_{2M} constant

b. H_T vs. R_L for families of AB_2 systems with K'_{2M} constant

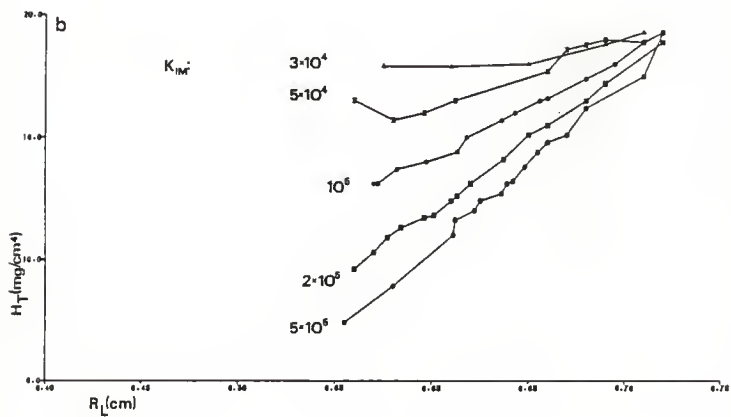
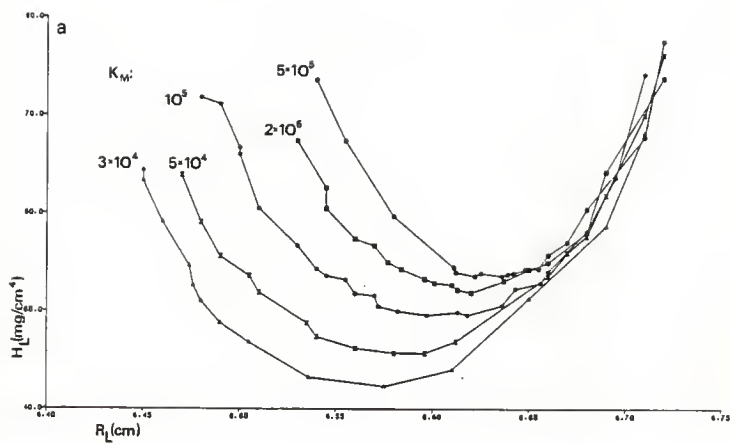


Figure 47: Species Concentrations for AB₂ Systems

$$W_A = 100\text{Kd}$$

$$W_B = 100\text{Kd}$$

$$C_{AT} = 5.0 \text{ mg/ml}$$

$$C_{BT} = 5.0 \text{ mg/ml}$$

$$[A] = 5 \times 10^{-5} \text{ M}$$

$$[B] = 5 \times 10^{-5} \text{ M}$$

$$[B]/[A] = 1.0$$

- a. Species concentrations vs. $\log_{10} K'_{2M}$ for systems with $K_{1M} = 5.0 \times 10^4$
- b. Species concentrations vs. $\log_{10} K'_{2M}$ for systems with $K_{1M} = 2.0 \times 10^5$
- c. Species concentrations vs. $\log_{10} K'_{2M}$ for systems with $K_{1M} = 5.0 \times 10^5$

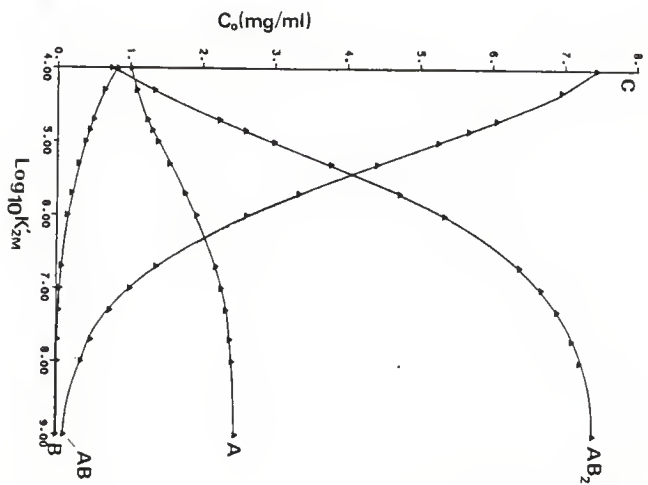
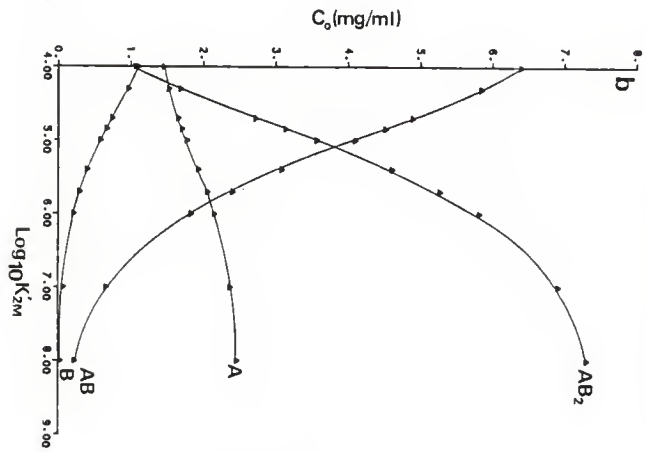
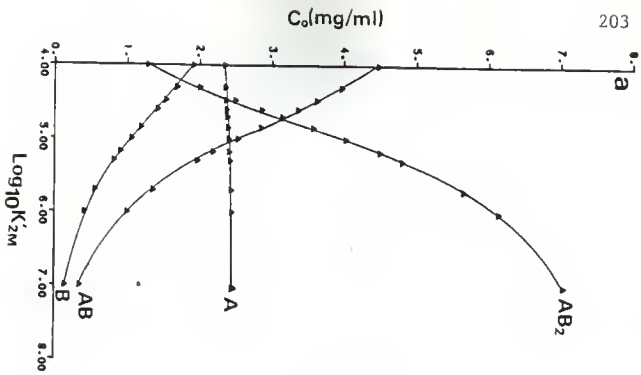


Figure 48: Average Constituent Sedimentation Coefficients
for AB_2 Systems

$$W_A = 100\text{Kd}$$

$$W_B = 100\text{Kd}$$

$$C_{AT} = 5.0 \text{ mg/ml}$$

$$C_{BT} = 5.0 \text{ mg/ml}$$

$$[A] = 5 \times 10^{-5}$$

$$[B] = 5 \times 10^{-5}$$

$$[B]/[A] = 1.0$$

Frictional ratios (f/f_0) for all species = 1.1

Species transport coefficients are given in table 2.

- a. $S\bar{s}_A$ vs. K'_{2M} for systems with
different values of K_{1M}
- b. $S\bar{s}_B$ vs. K'_{2M} for systems with
different values of K_{1M}

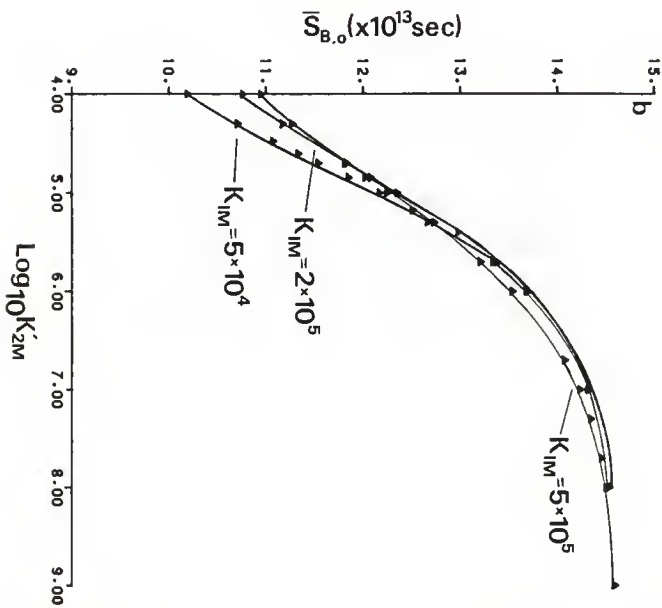
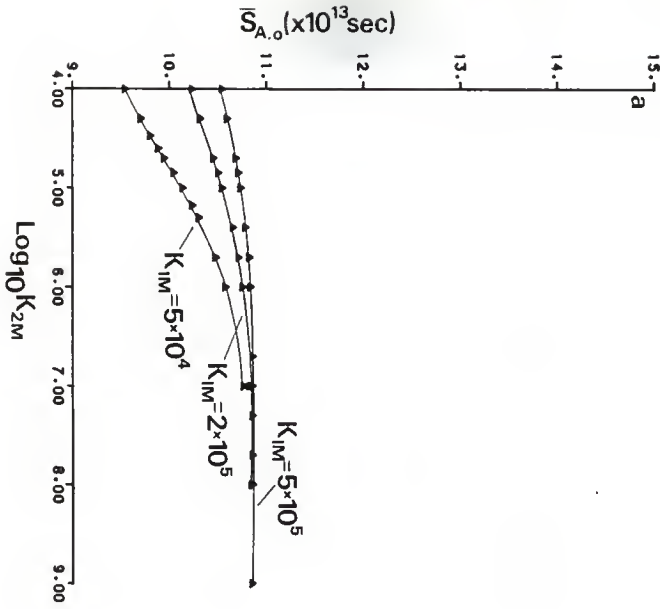


Figure 49: Gradient Profiles of Two AB_2 Systems at Two Different Constituent Ratios

$$W_A = 100Kd$$

$$W_B = 100Kd$$

Frictional ratios (f/f_0) for all species = 1.1

All self and cross hydrodynamic constants (k) = 0.01

Species transport coefficients are given in table 2.

Rotor speed = 60,000 rpm.

Initial sharp boundary position (r_0) = 6.0 cm.

$$\Delta t = 2155.51 \text{ sec}$$

a. $C_{AT} = 5.0 \text{ mg/ml}$

$$C_{BT} = 5.0 \text{ mg/ml}$$

$$[A] = 5 \times 10^{-5}$$

$$[B] = 5 \times 10^{-5}$$

$$[B]/[A] = 1.0$$

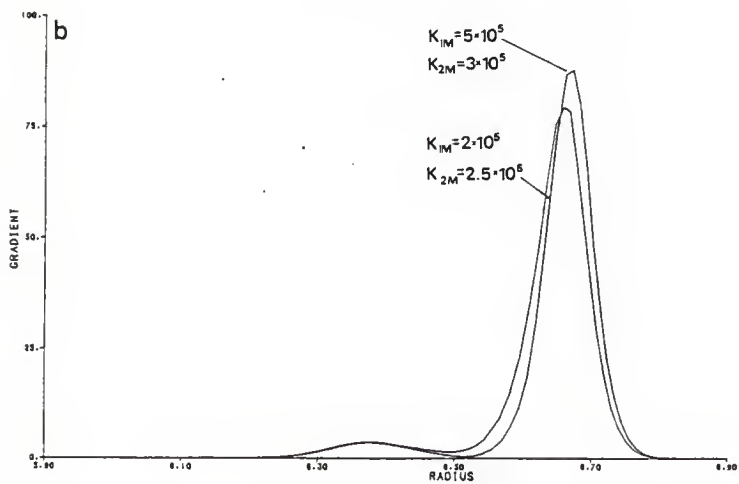
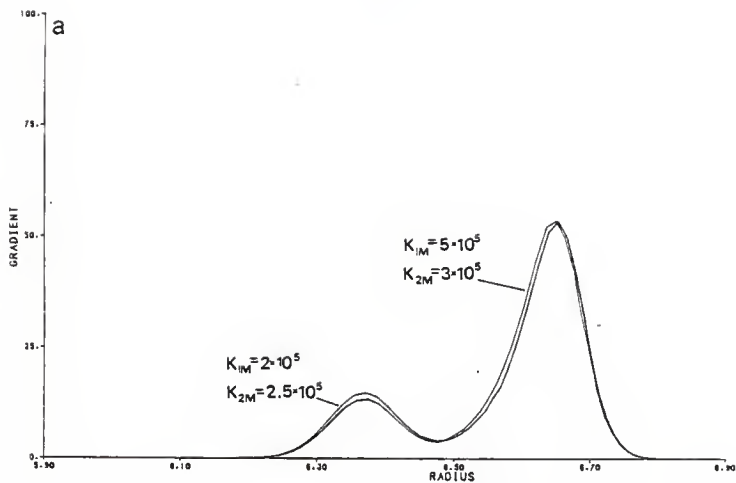
b. $C_{AT} = 3.33 \text{ mg/ml}$

$$C_{BT} = 6.67 \text{ mg/ml}$$

$$[A] = 3.33 \times 10^{-5}$$

$$[B] = 6.67 \times 10^{-5}$$

$$[B]/[A] = 2.0$$



At a 2:1 mole ratio H_L increases steadily as K'_{2M} is increased, rather than passing through a minimum as it does at a 1:1 ratio, and H_T decreases with increasing K'_{2M} at a 2:1 constituent ratio whereas, at a constituent ratio of 1:1, it decreases if K_{1M} is small ($< \text{ca. } 3 \times 10^4$) but increases if K_{1M} is larger.

Plots of H_L vs. R_L and H_T vs. R_L for AB_2 systems at a 2:1 constituent ratio (K'_{2M} varied, K_{1M} constant; figure 51) suggest that, in general, boundaries of AB_2 systems with different association constants may be more readily distinguishable, when K'_{2M} is large, at a 2:1 ratio than at a 1:1 ratio.

Figure 50: Changes in Boundary Dimensions With K'_{2M} for AB_2 Systems with K_{1M} Constant

$$W_A = 100Kd$$

$$W_B = 100Kd$$

$$C_{AT} = 3.33 \text{ mg/ml}$$

$$C_{BT} = 6.67 \text{ mg/ml}$$

$$[A] = 3.33 \times 10^{-5} \text{ M}$$

$$[B] = 6.67 \times 10^{-5} \text{ M}$$

$$[B]/[A] = 2.0$$

Frictional ratios (f/f_0) for all species = 1.1

All self and cross hydrodynamic constants (k) = 0.01

Species transport coefficients are given in table 2.

Rotor speed = 60,000 rpm.

Initial sharp boundary position (r_0) = 6.0 cm.

$$\Delta t = 2155.51 \text{ sec}$$

- a. H_L vs. $\log_{10} K'_{2M}$ for families of systems with K_{1M} constant at $[B]/[A] = 2.0$
- b. H_T vs. $\log_{10} K'_{2M}$ for families of systems with K_{1M} constant at $[B]/[A] = 2.0$
- c. R_L vs. $\log_{10} K'_{2M}$ for families of systems with K_{1M} constant at $[B]/[A] = 2.0$

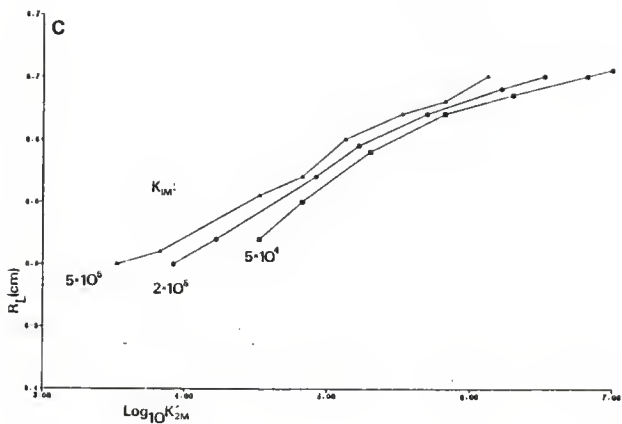
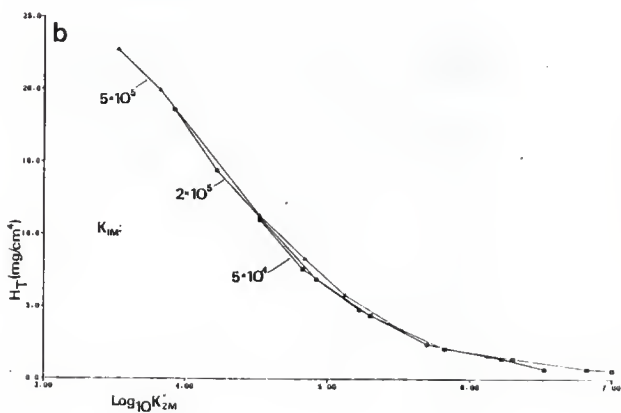
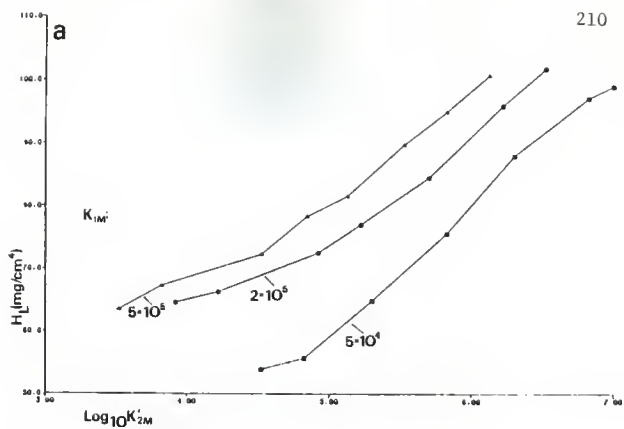


Figure 51: Comparison of Boundary Dimensions for AB_2 Systems with Different Values of K'_{2M} at a 2:1 Constituent Mole Ratio

$$W_A = 100\text{Kd}$$

$$W_B = 100\text{Kd}$$

$$C_{AT} = 3.33 \text{ mg/ml}$$

$$C_{BT} = 6.67 \text{ mg/ml}$$

$$[A] = 3.33 \times 10^{-5} \text{ M}$$

$$[B] = 6.67 \times 10^{-5} \text{ M}$$

$$[B]/[A] = 2.0$$

Frictional ratios (f/f_0) for all species = 1.1

All self and cross hydrodynamic constants (k) = 0.01

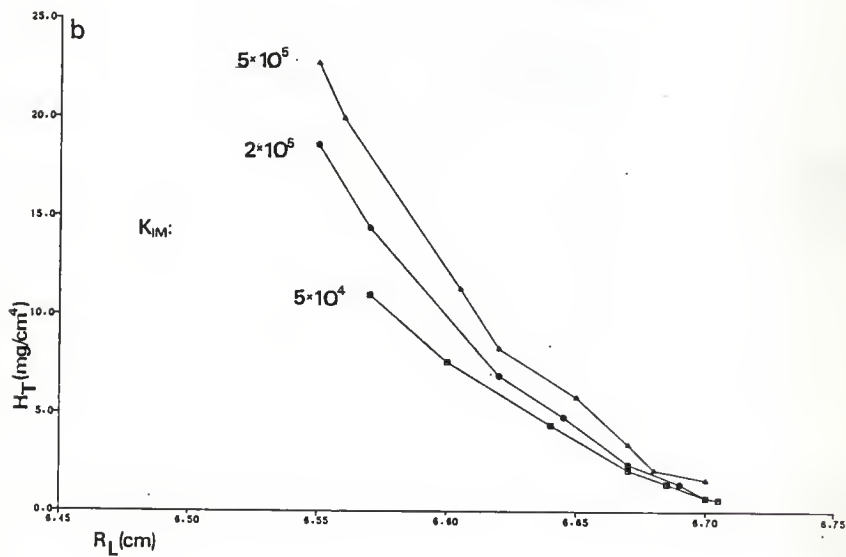
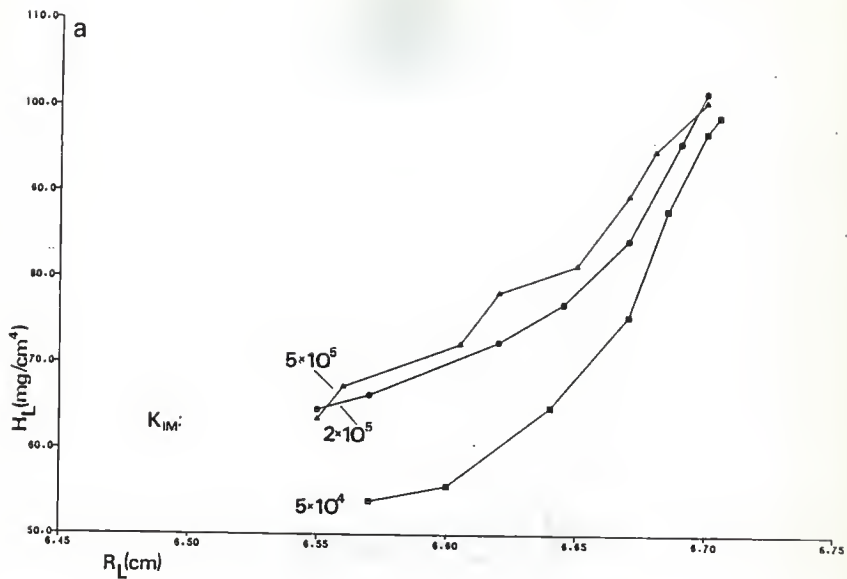
Species transport coefficients are given in table 2.

Rotor speed = 60,000 rpm.

Initial sharp boundary position (r_0) = 6.0 cm.

$$\Delta t = 2155.51 \text{ sec}$$

- a. H_L vs. R_L for families of AB_2 systems with K'_{2M} constant at $[B]/[A] = 2.0$
- b. H_T vs. R_L for families of AB_2 systems with K'_{2M} constant at $[B]/[A] = 2.0$



3.4 EFFECT OF AGGREGATE FRICTIONAL RATIOS

Since the sedimentation and diffusion coefficients of each species ij in a mixed associating system (with monomers of a given volume $(M\bar{v}/N)$) depend on the molecules frictional ratio¹⁷ $(f/f_0)_{ij}$, so does the shape of the boundary produced by the system in a velocity sedimentation experiment.

The frictional ratio of each monomer, A and B, can be computed from its diffusion coefficient and the minimum frictional coefficient.

$$\frac{RT}{DNf_0} = \frac{f}{f_0}$$

or from the Stokes radius ($R_s = f/6\pi\eta$) obtained from gel permeation and R_0 ($R_0 = (3M\bar{v}/4\pi N)^{1/3}$).

¹⁷ The sedimentation and diffusion coefficients of a molecule are related to its frictional ratio as follows:

$$S = \frac{M(1 - \bar{v}\rho)}{Nf_0(f/f_0)} \quad D = \frac{RT}{Nf_0(f/f_0)}$$

where f/f_0 is the ratio of the frictional coefficient of the molecule itself to that of an unhydrated spherical particle of equal volume (with radius R_0).

$$f_0 = 6\pi\eta R_0$$

where

$$R_0 = (3M\bar{v}/4\pi N)^{1/3}$$

$$\frac{R_s}{R_o} = \frac{f/6\pi\eta}{f_o/6\pi\eta} = \frac{f}{f_o}$$

The frictional ratios of the aggregates, however, cannot be obtained by these methods since the individual aggregates cannot be isolated from other species in a mixed associating system. It may, therefore, be necessary, when modeling velocity sedimentation of mixed associating systems, to consider systems with a variety of plausible combinations of aggregate frictional ratios.

Simulated boundaries for noncooperative AB_2 systems ($K_I=10^5$) in which the frictional ratios of AB and AB_2 ($(f/f_o)_{AB}$ and $(f/f_o)_{AB_2}$, are varied, but kept equal to one another, are shown in figure 52. As one would expect, increasing the aggregate frictional ratios sharply decreases the average sedimentation rate of the reaction boundary, but does not affect the sedimentation rate of the trailing monomer boundary. The heights of both the leading and trailing boundaries are also increased slightly. If $(f/f_o)_{AB}$ and $(f/f_o)_{AB_2}$ are made large enough, the boundary becomes unimodal, with a trailing shoulder that becomes less prominent as the frictional ratios are increased further. Thus systems in which the aggregates are highly asymmetrical and/or hydrated (ie. large f/f_o) are likely not to generate bimodal boundaries unless the association is relatively tight.

Figure 52: Gradient Profiles of Uncooperative AB_2 Systems with Different Aggregate Frictional Ratios

$$W_A = 100 \text{ Kd}$$

$$W_B = 100 \text{ Kd}$$

$$C_{AT} = 5.0 \text{ mg/ml}$$

$$C_{BT} = 5.0 \text{ mg/ml}$$

$$[A] = 5 \times 10^{-5} \text{ M}$$

$$[B] = 5 \times 10^{-5} \text{ M}$$

$$[B]/[A] = 1.0$$

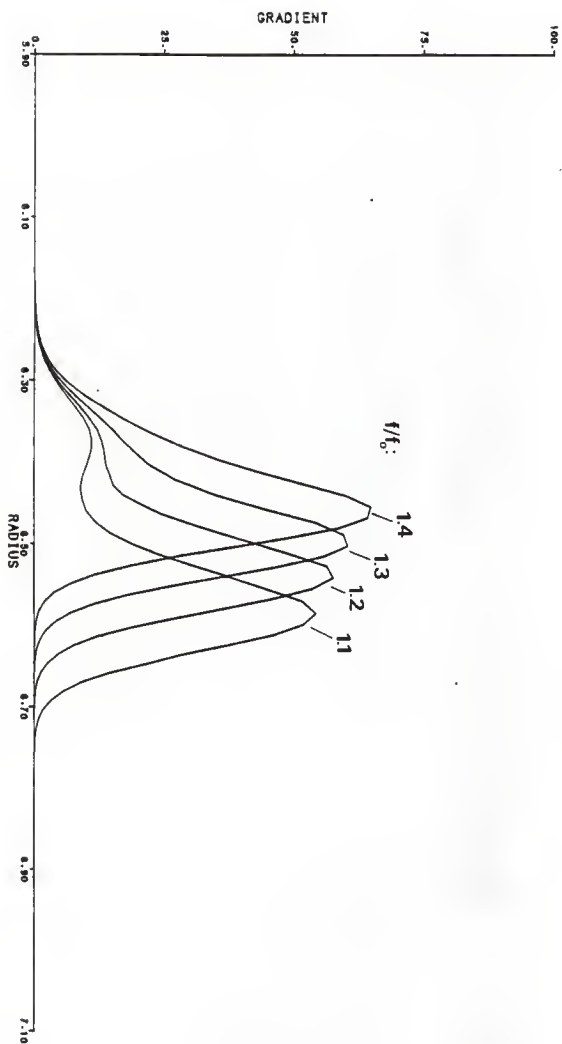
All self and cross hydrodynamic constants (k) = 0.01 ml/mg

Species transport coefficients are given in table 2.

Rotor speed = 60,000 rpm.

Initial sharp boundary position (r_0) = 6.0 cm.

$\Delta t = 2155.51 \text{ sec}$



While it may be that, among AB_2 systems with the same aggregate frictional ratios, systems with different values of K_{1M} and K'_{2M} generally generate boundaries of different dimensions or shapes (unless the association is very tight - see p. 192), it does not seem unlikely that systems with different aggregate frictional ratios, as well as different association constants, would, in some cases, generate identical or very similar boundaries. Thus, when fitting model system boundaries to the observed boundaries of real systems, satisfactory fits might be obtained with two or more different systems (ie. systems with different combinations of frictional ratios and association constants). Different systems that have similar boundaries at one constituent mole ratio, however, might not have such similar boundary shapes at another mole ratio. Some incorrect models might, therefore, be eliminated by modeling at different mole ratios.

3.5 EFFECT OF HYDRODYNAMIC DEPENDENCE

Hydrodynamic concentration dependence for sedimentation coefficients is described in the simulation model by the following expressions.

$$\bar{S}_A = \bar{S}_{A,0} / (1 + k_{AA}C_{AT} + k_{AB}C_{BT})$$

$$\bar{S}_B = \bar{S}_{B,0} / (1 + k_{BB}C_{BT} + k_{BA}C_{AT})$$

where $\bar{S}_{A,0}$ and $\bar{S}_{B,0}$ are the ideal local average constituent sedimentation coefficients, C_{AT} and C_{BT} are the local constituent concentrations, k_{AA} and k_{BB} are the self hydrodynamic constants and k_{AB} and k_{BA} are the cross hydrodynamic constants.

In all of the simulated experiments discussed so far all four of the hydrodynamic constants had values of .01 (.01 is about average for real systems in which actual values may vary from a low of about .005 to an upper limit of about .020). The effects of hydrodynamic dependence on boundary shapes of AB_2 systems were studied by varying hydrodynamic constants in three different ways.

- I) The effect of general hydrodynamic dependence was investigated by varying all of the constants together (ie. keeping all the hydrodynamic constants equal).
- II) The effect of general cross hydrodynamic dependence was studied by varying k_{AB} and k_{BA} together (ie. $k_{AB}=k_{BA}$) with k_{AA} and k_{BB} constant at .01.
- III) The specific effects of each of the four dependencies were studied by varying k_{AA} , k_{BB} , k_{AB} and k_{BA} one at a time while keeping the other three constant at .01.

Simulated profiles of uncooperative AB_2 systems ($K_I=10^5$, $W_A=W_B=100Kd$, $C_{AT}=C_{BT}=5.0$ mg/ml) with various degrees of hydrodynamic dependence (all k 's equal) are shown in figure

53-a. As one might expect, an increase in overall hydrodynamic dependence results in a sharpening of both the leading and trailing boundaries as well as a decrease in their average sedimentation rates. Because the leading boundaries' sedimentation rate is more strongly affected than that of the trailing boundary, increasing overall hydrodynamic dependence brings the leading and trailing boundaries closer together. For weaker systems this means that the distinguishing bimodal characteristics of the sedimenting boundary may be obscured by large hydrodynamic effects (Figure 53-a, $K_T=10^4$). However, if velocity sedimentation is allowed to continue for a longer time, bimodality, or related characteristics, that are obscured by hydrodynamic dependence, might eventually appear.

In general, if a boundary is leaning toward being bimodal (ie. if it has four curvature inflections), then it is capable of becoming bimodal at a later time, once it has sedimented through a distance large enough to separate the two components. However, in a real situation, if bimodality is to be observed then it must develop before the boundary becomes worthlessly distorted by end-of-cell effects.

Hydrodynamic dependence seems to obscure bimodality, as already noted, because it causes the two components of the boundary to separate more slowly. However, if there is a large hydrodynamic effect, the leading and trailing boundaries, or their rudiments, will be relatively sharp, and

Figure 53: Effect of Overall Hydrodynamic Dependence on Boundaries of Uncooperative AB_2 Systems

$$W_A = 100Kd$$

$$W_B = 100Kd$$

$$C_{AT} = 5.0 \text{ mg/ml}$$

$$C_{BT} = 5.0 \text{ mg/ml}$$

$$[A] = 5 \times 10^{-5} \text{ M}$$

$$[B] = 5 \times 10^{-5} \text{ M}$$

$$[B]/[A] = 1.0$$

Frictional ratios (f/f_0) for all species = 1.1

Species transport coefficients are given in table 2.

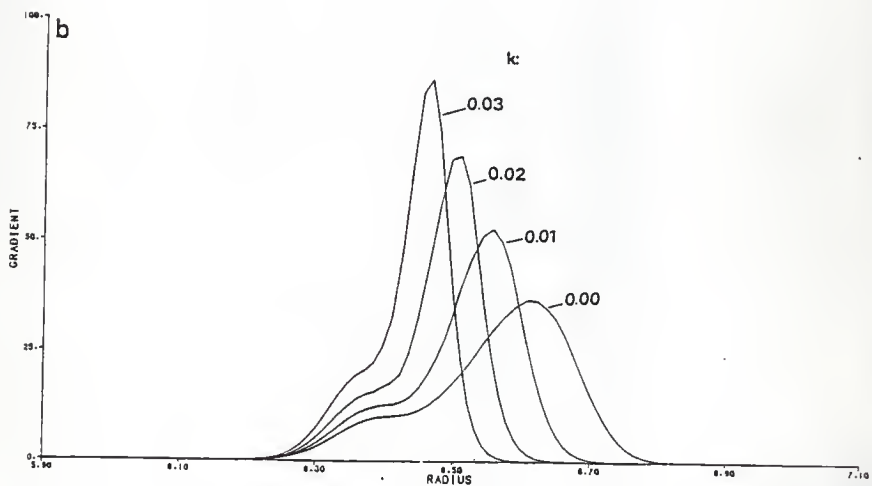
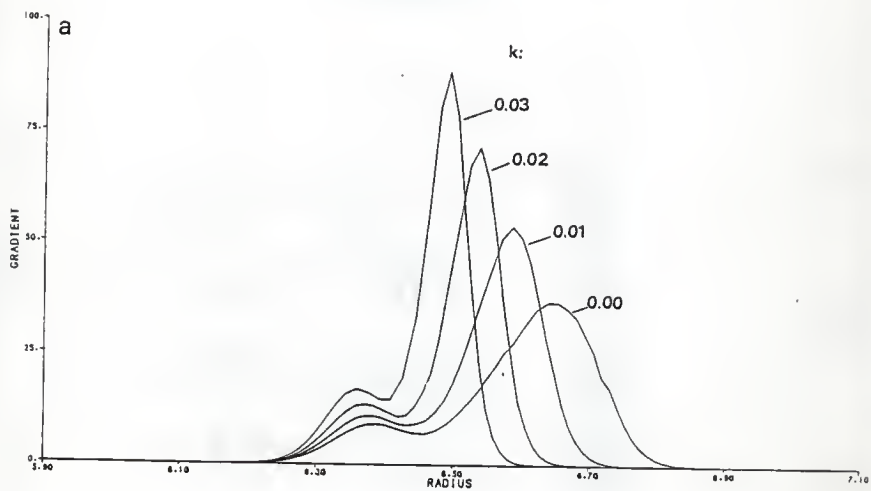
Rotor speed = 60,000 rpm.

Initial sharp boundary position (r_0) = 6.0 cm.

$\Delta t = 2155.51 \text{ sec}$

$$\text{a. } K_I = 1.0 \times 10^5 \text{ M}^{-1}$$

$$\text{b. } K_I = 5.0 \times 10^4 \text{ M}^{-1}$$



should, therefore, become resolved at relatively small separations. Comparisons of boundaries of otherwise identical systems with different k 's, which were allowed to sediment until their leading boundaries had migrated through equal distances (ie. longer times for higher values of k) demonstrate that reasonable and even unreasonable hydrodynamic effects do not obscure bimodality. In fact, in some instances (figure 54), systems with higher dependencies are more likely to have developed a bimodal boundary by the time their leading boundaries have reached a given position than are systems with lower dependency. Thus, in at least some cases, hydrodynamic effects (boundary sharpening) can actually help to bring out bimodal tendencies in a boundary.

Cross hydrodynamic dependence (figure 55) has the same effect, qualitatively, on the leading boundary, as general dependence (ie. the leading boundary becomes sharper and moves at a slower rate). The effect on the leading boundary of changing k_{AB} and k_{BA} from, for instance, .010 to .015, while being the same qualitatively, is, of course, considerably less drastic than the effect of increasing all of the hydrodynamic constants by the same amount. Increasing cross hydrodynamic dependence also increases the trailing boundary's height (as does general hydrodynamic dependence) but has very little if any effect on either its migration rate or sharpness. That there is no effect on the trailing boundary's migration rate or width is, of course, not sur-

Figure 54: Effect of Overall Hydrodynamic Dependence on Bimodality of Uncooperative AB_2 Profiles

boundaries of systems with different hydrodynamic dependences after migrating through equal distances.

$$K_I = 3.5 \times 10^4$$

$$W_A = 100 \text{Kd}$$

$$W_B = 100 \text{Kd}$$

$$C_{AT} = 5.0 \text{ mg/ml}$$

$$C_{BT} = 5.0 \text{ mg/ml}$$

$$[A] = 5 \times 10^{-5} \text{ M}$$

$$[B] = 5 \times 10^{-5} \text{ M}$$

$$[B]/[A] = 1.0$$

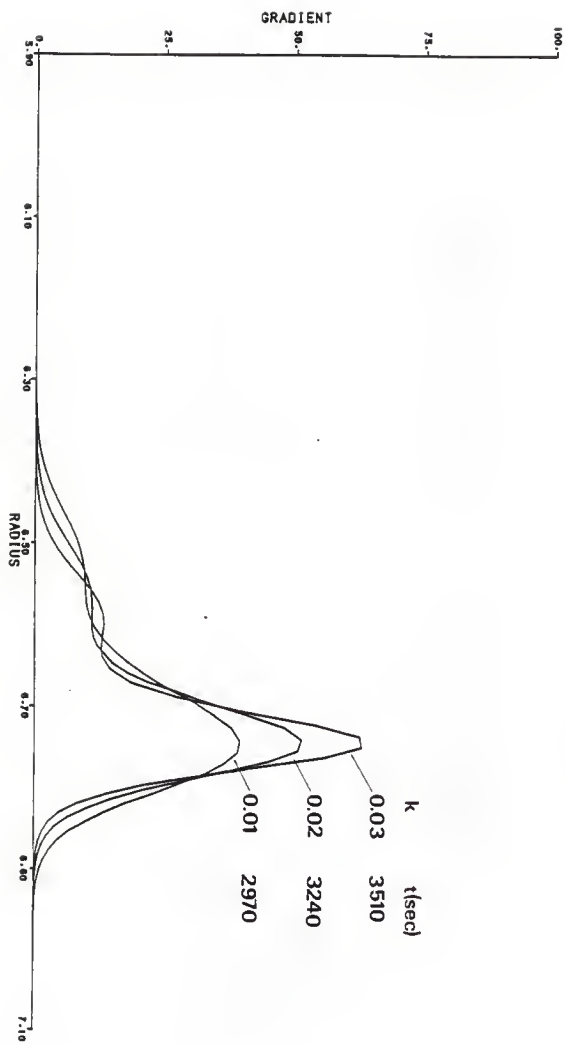
Frictional ratios (f/f_0) for all species = 1.1

Species transport coefficients are given in table 2.

Rotor speed = 60,000 rpm.

Initial sharp boundary position (r_0) = 6.0 cm.

$\Delta t = 2155.51 \text{ sec}$



prising, since the trailing boundary consists of only one constituent (A) and cross hydrodynamic effects should therefore be absent there.

Since leading boundaries of systems with large cross hydrodynamic effects move more slowly, in relation to their trailing elements, than do those of systems with smaller cross effects, bimodal behavior might be obscured in relatively weak systems by cross hydrodynamic dependence alone, particularly since it does not sharpen the trailing boundary.

The independent effects of each of the two self and two cross hydrodynamic constants (k_{AA} and k_{BB} , and k_{AB} and k_{BA}) are illustrated in figures 56 and 57.

The effects of the four types of hydrodynamic dependence on boundary shape are not each distinct. In general the effects of cross or self hydrodynamic dependence on \bar{S}_A (ie. the effects related to k_{AA} and k_{AB}) are very similar as are the effects of cross and self hydrodynamic dependence on \bar{S}_B (ie. the effects related to k_{BB} and k_{BA}) Both self and cross dependence of \bar{S}_A are associated with higher trailing boundaries and lower, narrower leading boundaries, while cross and self dependence of \bar{S}_B are associated with lower, broader trailing boundaries and taller, sharper leading boundaries as well as slower leading boundary migration rates. Self dependence of \bar{S}_A (k_{AA}) also slows down and sharpens the trailing boundary. None of the other three dependences af-

Figure 55: Effects of Cross Hydrodynamic dependence on Boundaries of Uncooperative AB_2 Systems

$$K_I = 1.0 \times 10^5 \text{ M}^{-1}$$

$$W_A = 100 \text{ Kd}$$

$$W_B = 100 \text{ Kd}$$

$$C_{AT} = 5.0 \text{ mg/ml}$$

$$C_{BT} = 5.0 \text{ mg/ml}$$

$$[A] = 5 \times 10^{-5} \text{ M}$$

$$[B] = 5 \times 10^{-5} \text{ M}$$

$$[B]/[A] = 1.0$$

Frictional ratios (f/f_0) for all species = 1.1

Species transport coefficients are given in table 2.

Rotor speed = 60,000 rpm.

Initial sharp boundary position (r_0) = 6.0 cm.

$\Delta t = 2155.51 \text{ sec}$

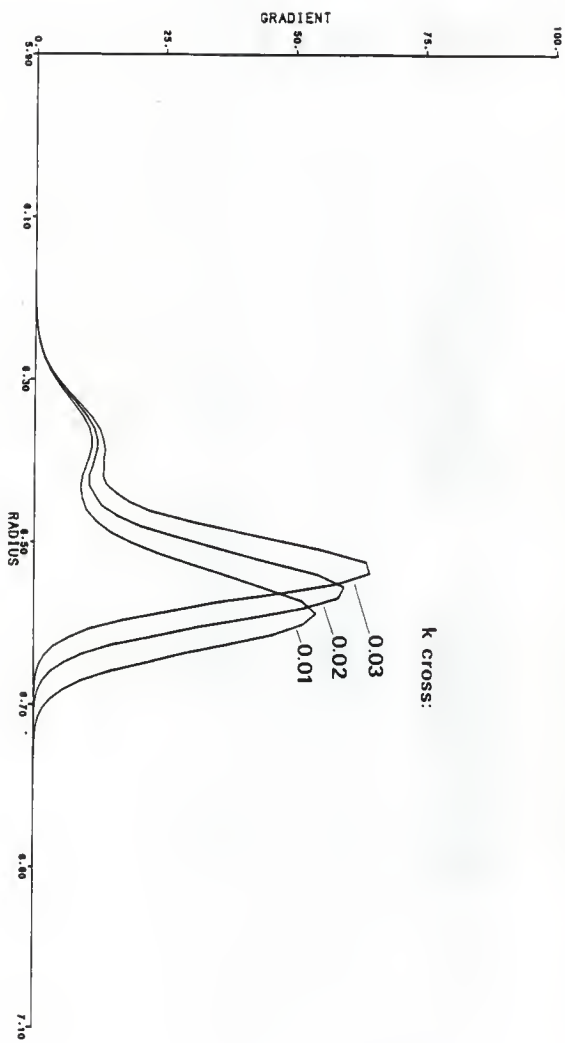


Figure 56: Effects of Individual Self Hydrodynamic Dependences on Boundaries of Uncooperative AB_2 Systems

$$K_I = 1.0 \times 10^5 \text{ M}^{-1}$$

$$W_A = 100 \text{ Kd}$$

$$W_B = 100 \text{ Kd}$$

$$C_{AT} = 5.0 \text{ mg/ml}$$

$$C_{BT} = 5.0 \text{ mg/ml}$$

$$[A] = 5 \times 10^{-5} \text{ M}$$

$$[B] = 5 \times 10^{-5} \text{ M}$$

$$[B]/[A] = 1.0$$

Frictional ratios (f/f_0) for all species = 1.1

Species transport coefficients are given in table 2.

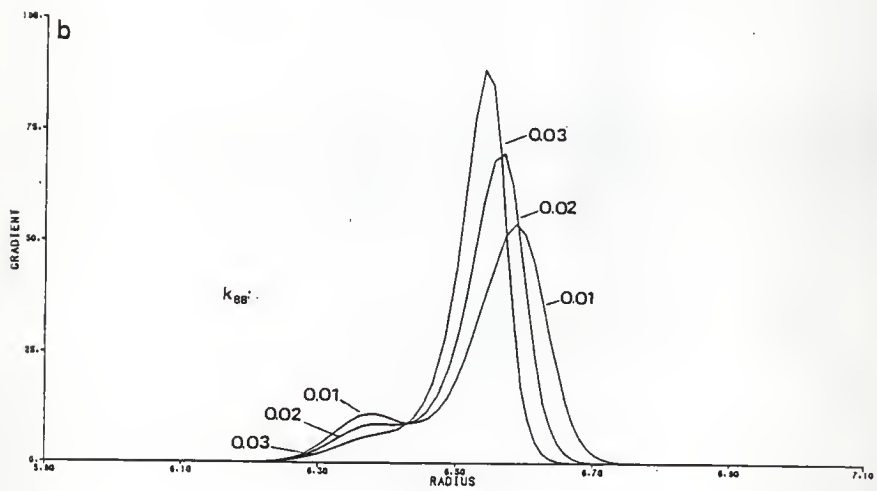
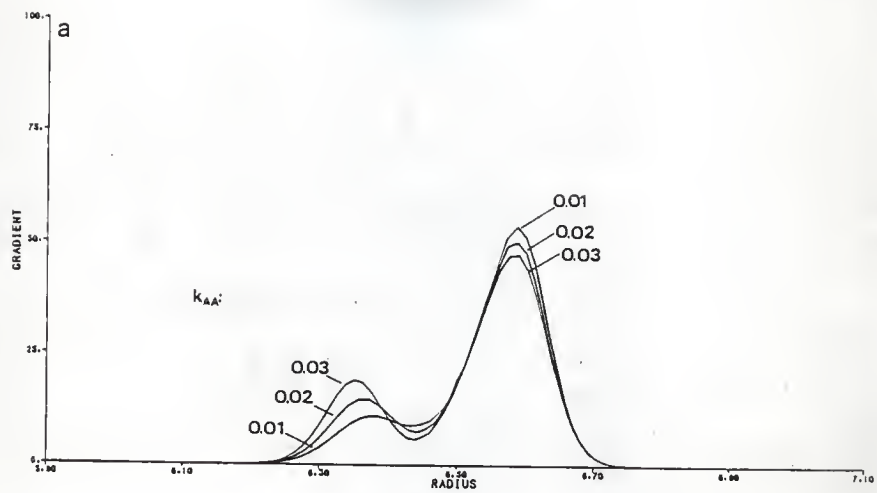
Rotor speed = 60,000 rpm.

Initial sharp boundary position (r_0) = 6.0 cm.

$$\Delta t = 2155.51 \text{ sec}$$

a. k_{AA} varied, all other $k_s = .01$

b. k_{BB} varied, all other $k_s = .01$



fect either the trailing boundary's migration rate or its width, nor should they, since the trailing boundary contains constituent A only.

Since hydrodynamic dependence affects the position and height of the leading boundary it is possible that some systems with different combinations of association constants that also have different combinations of self and cross hydrodynamic constants would give rise to identical boundaries. However, whereas changes in association constants that slow down the leading boundary generally either widen the leading boundary or do not affect its width at all, hydrodynamic dependence, in addition to slowing down the leading boundary, also decreases its width. It might therefore be possible in modeling real mixed systems to separate, somewhat, the effects of hydrodynamic dependence and association¹⁸. The situation is likely to be complicated, however, by a lack of knowledge about the frictional ratios of the aggregates, since these may also affect the width of the leading boundary.

¹⁸ The self hydrodynamic constants k_{AA} and k_{BB} would usually be obtained more easily from modeling studies with the individual constituents.

Figure 57: Effects of Individual Cross Hydrodynamic Dependences on Boundaries of Uncooperative AB_2 Systems

$$K_I = 1.0 \times 10^5$$

$$W_A = 100 \text{Kd}$$

$$W_B = 100 \text{Kd}$$

$$C_{AT} = 5.0 \text{ mg/ml}$$

$$C_{BT} = 5.0 \text{ mg/ml}$$

$$[A] = 5 \times 10^{-5} \text{ M}$$

$$[B] = 5 \times 10^{-5} \text{ M}$$

$$[B]/[A] = 1.0$$

Frictional ratios (f/f_0) for all species = 1.1

Species transport coefficients are given in table 2.

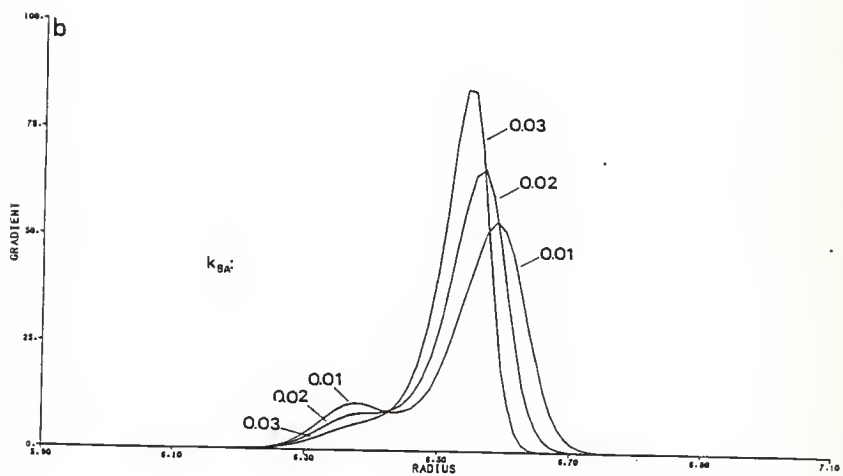
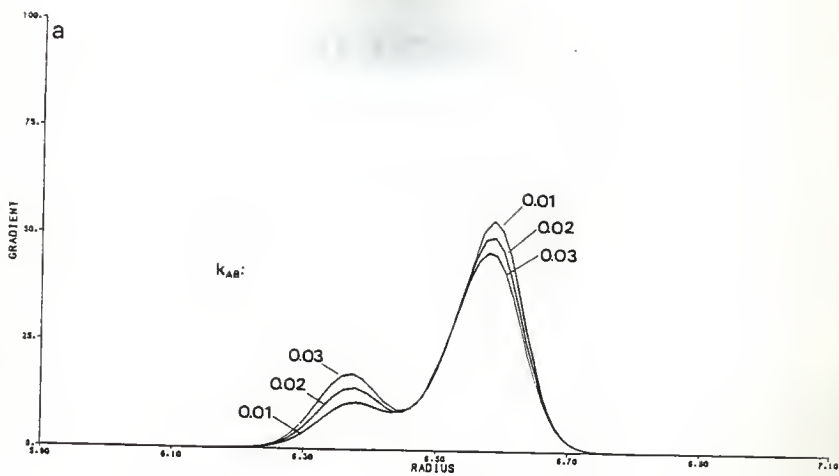
Rotor speed = 60,000 rpm.

Initial sharp boundary position (r_0) = 6.0 cm.

$\Delta t = 2155.51 \text{ sec}$

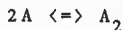
a. k_{AB} varied, all other $k_s = .01$

b. k_{BA} varied, all other $k_s = .01$



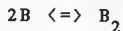
3.6 EFFECT OF SELF ASSOCIATION

Occasionally one or both of the constituents of a mixed associating system will self associate. The effects of self association of A and B to dimer,



$$K_{A_2M} = \frac{[A_2]}{[A]^2}$$

and



$$K_{B_2M} = \frac{[B_2]}{[B]^2}$$

on the sedimentation of profiles of AB_2 systems were studied using the COXMIX distorted grid simulation program for mixed associating systems and a modification of the SBABN table assembly program accommodating self association of either or both monomers to the dimer.

Simulated profiles of uncooperative AB_2 systems ($K_1=10^5$), at a constituent ratio of 1:1, with various values of K_{A_2} and K_{B_2} are shown in figures 58 and 59.

Increasing K_{A_2} , in these systems, at this mole ratio, has a strong effect on the shape of the trailing boundary. Even

at relatively small values of K_{A_2} (5×10^3), the trailing boundary is considerably lower and broader than it is in the absence of self association, probably due to spreading of the constituent A boundary. Also, as K_{A_2} is increased, the average sedimentation rate of the trailing boundary increases, probably because of the contribution of a dimer gradient to the trailing boundary. The leading boundary's height and position are not affected. Apparently only the excess A in the trailing boundary is significantly involved in self association.

As K_{A_2} is increased and the difference between the average migration rates of the leading and trailing boundaries becomes smaller, the bimodal appearance of the boundary is lost. Hence, self association may obscure the distinctive features of an AB_n boundary, particularly if the mixed association is weak.

Introducing self association of B to the system, at the same constituent concentrations, has relatively little effect on boundary shape, except at large values of K_{B_2} (5×10^4), where the size of the trailing boundary is increased and the average sedimentation rate and size of the trailing are decreased (figure 59). Apparently, because there is no B in the trailing boundary, self association of B cannot affect the boundary shape unless it is strong enough to significantly alter the availability of B monomer for the mixed association.

Figure 58: Effect of Self Association of A on the Boundary of an Uncooperative AB_2 System at a 1:1 Constituent Ratio

$$K_I = 1.0 \times 10^5 \text{ M}^{-1}$$

$$W_A = 100 \text{ Kd}$$

$$W_B = 100 \text{ Kd}$$

$$C_{AT} = 5.0 \text{ mg/ml}$$

$$C_{BT} = 5.0 \text{ mg/ml}$$

$$[A] = 5 \times 10^{-5} \text{ M}$$

$$[B] = 5 \times 10^{-5} \text{ M}$$

$$[B]/[A] = 1.0$$

Frictional ratios (f/f_0) for all species = 1.1

All self and cross hydrodynamic constants (k) = 0.01

Species transport coefficients are given in table 2.

Rotor speed = 60,000 rpm.

Initial sharp boundary position (r_0) = 6.0 cm.

$\Delta t = 2155.51 \text{ sec}$

a. no self association

$$\text{b. } K_{A_2} = 5.0 \times 10^3 \text{ M}^{-1}$$

$$\text{c. } K_{A_2} = 2.5 \times 10^4 \text{ M}^{-1}$$

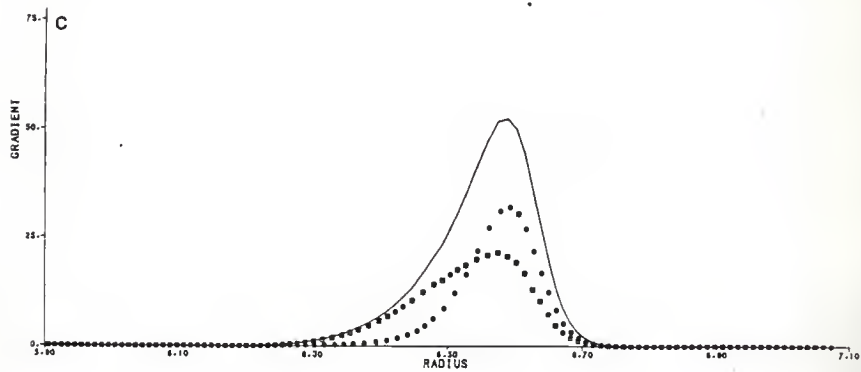
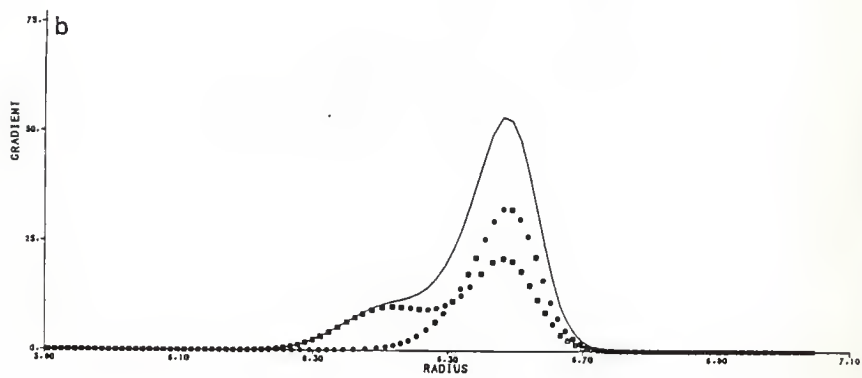
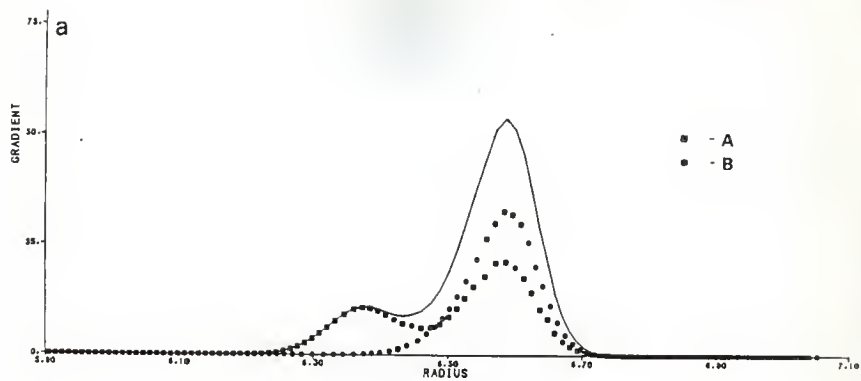


Figure 59: Effect of Self Association of B on the Boundary of an Uncooperative AB_2 System at a 1:1 Constituent Ratio

$$K_I = 1.0 \times 10^5 \text{ M}^{-1}$$

$$W_A = 100 \text{ Kd}$$

$$W_B = 100 \text{ Kd}$$

$$C_{AT} = 5.0 \text{ mg/ml}$$

$$C_{BT} = 5.0 \text{ mg/ml}$$

$$[A] = 5 \times 10^{-5} \text{ M}$$

$$[B] = 5 \times 10^{-5} \text{ M}$$

$$[B]/[A] = 1.0$$

Frictional ratios (f/f_0) for all species = 1.1

All self and cross hydrodynamic constants (k) = 0.01

Species transport coefficients are given in table 2.

Rotor speed = 60,000 rpm.

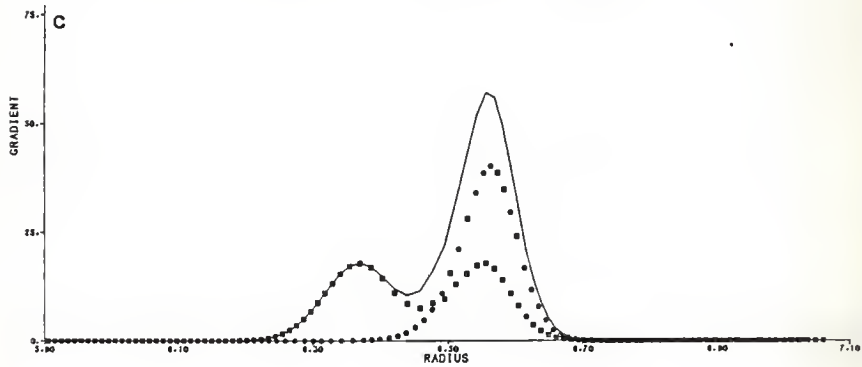
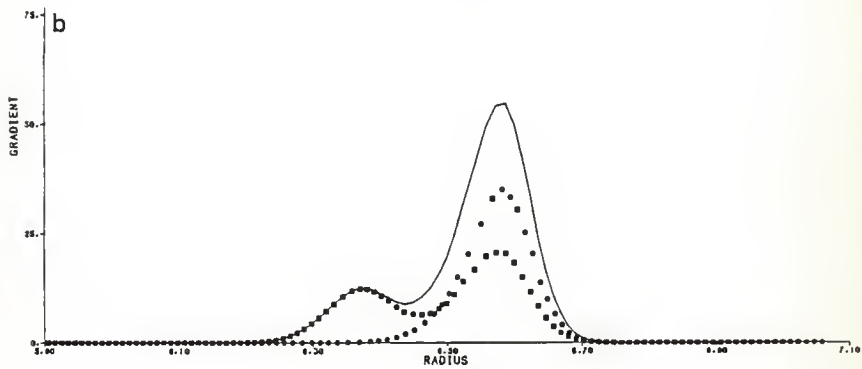
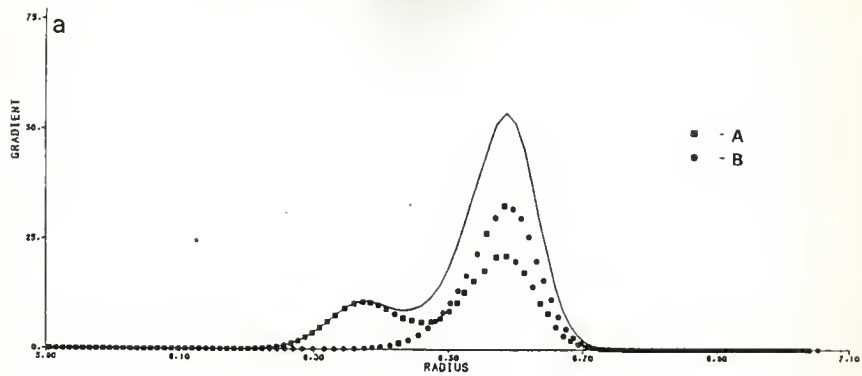
Initial sharp boundary position (r_0) = 6.0 cm.

$\Delta t = 2155.51 \text{ sec}$

a. no self association

b. $K_{B_2} = 5.0 \times 10^4 \text{ M}^{-1}$

c. $K_{B_2} = 5.0 \times 10^5 \text{ M}^{-1}$



If the constituent concentrations are changed, making B the constituent in excess, the effect of self association of B is much more obvious at low values of K_{B_2} (5×10^3). With B in excess the effects, on the boundary, of an increase in K_{B_2} are about the same as the effects of increasing K_{A_2} when A is in excess (ie. the trailing boundary becomes shorter and broader and moves at a faster rate so that it merges with the leading boundary -see figure 61) At these constituent concentrations increasing K_{A_2} has no noticeable effect on the boundary shape with values of K_{A_2} as large as 5×10^5 ; ie. The effect is the same as increasing K_{B_2} when A is in excess (figure 60).

Since, when one or the other of the constituents is in excess, the average migration rate of the trailing boundary is affected only by self association of the constituent in excess, and, since the average migration rate of trailing boundary is usually constant (among otherwise identical systems with different mixed-association constants and aggregate frictional ratios), when one of the constituents is in excess the trailing boundary position or its average migration rate might be useful in modeling studies to assess self association. Usually, however, the self association constants for A and B can be obtained from studies with the individual constituents.

Figure 60: Effect of Self Association of A on the Boundary of an Uncooperative AB_2 System at a 2:1 Constituent Ratio

$$K_I = 1.0 \times 10^5 \text{ M}^{-1}$$

$$W_A = 100 \text{ Kd}$$

$$W_B = 100 \text{ Kd}$$

$$C_{AT} = 3.333 \text{ mg/ml}$$

$$C_{BT} = 6.667 \text{ mg/ml}$$

$$[A] = 3.333 \times 10^{-5} \text{ M}$$

$$[B] = 6.667 \times 10^{-5} \text{ M}$$

$$[B]/[A] = 2.0$$

Frictional ratios (f/f_0) for all species = 1.1

All self and cross hydrodynamic constants (k) = 0.01

Species transport coefficients are given in table 2.

Rotor speed = 60,000 rpm.

Initial sharp boundary position (r_0) = 6.0 cm.

$\Delta t = 2155.51 \text{ sec}$

a. no self association

b. $K_{A_2} = 5.0 \times 10^4 \text{ M}^{-1}$

c. $K_{A_2} = 5.0 \times 10^5 \text{ M}^{-1}$

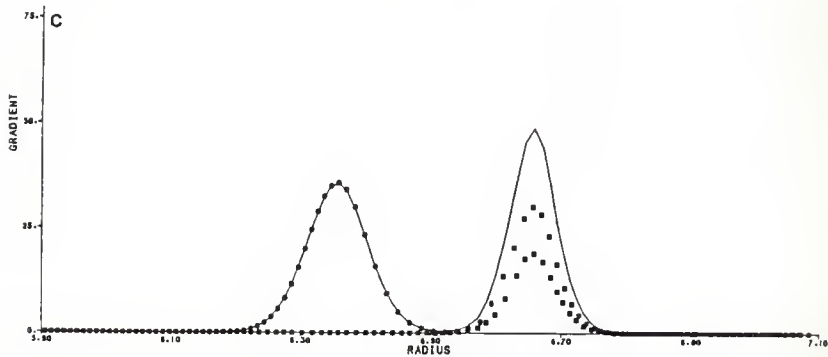
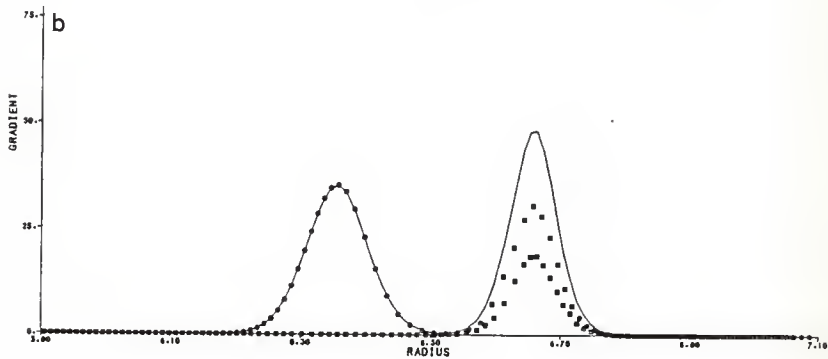
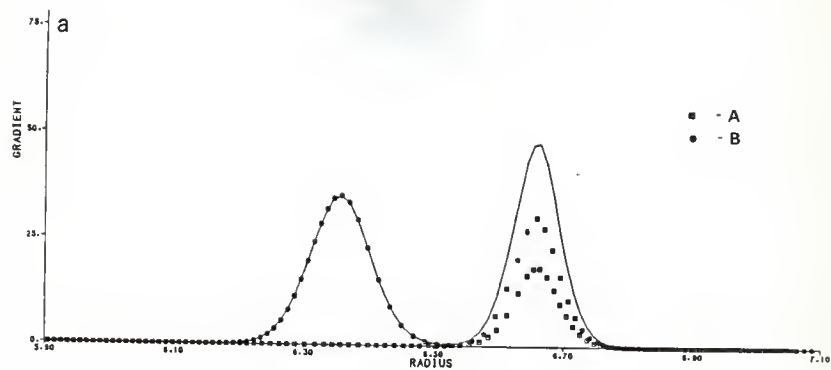


Figure 61: Effect of Self Association of B on the Boundary of an Uncooperative AB_2 System at a 2:1 Constituent Ratio

$$K_I = 1.0 \times 10^5 \text{ M}^{-1}$$

$$W_A = 100 \text{ Kd}$$

$$W_B = 100 \text{ Kd}$$

$$C_{AT} = 3.333 \text{ mg/ml}$$

$$C_{BT} = 6.667 \text{ mg/ml}$$

$$[A] = 3.333 \times 10^{-5} \text{ M}$$

$$[B] = 6.667 \times 10^{-5} \text{ M}$$

$$[B]/[A] = 2.0$$

Frictional ratios (f/f_0) for all species = 1.1

All self and cross hydrodynamic constants (k) = 0.01

Species transport coefficients are given in table 2.

Rotor speed = 60,000 rpm.

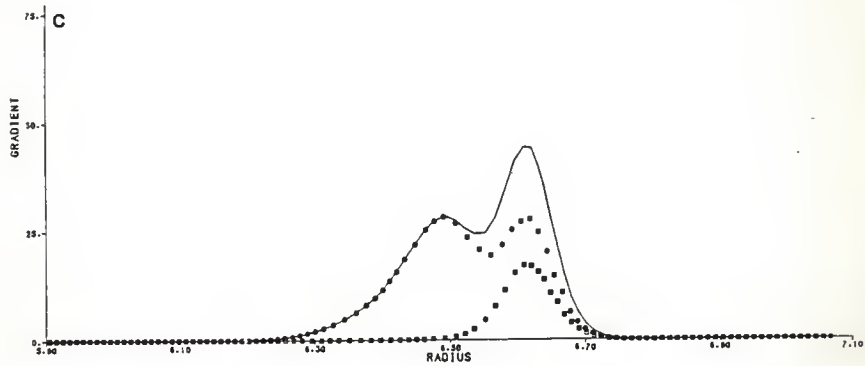
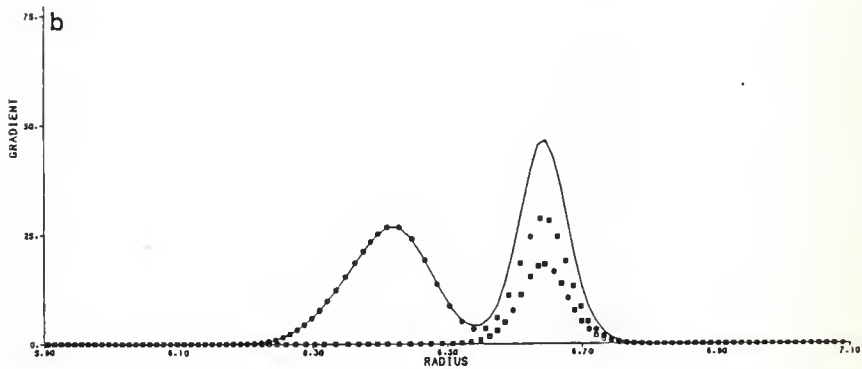
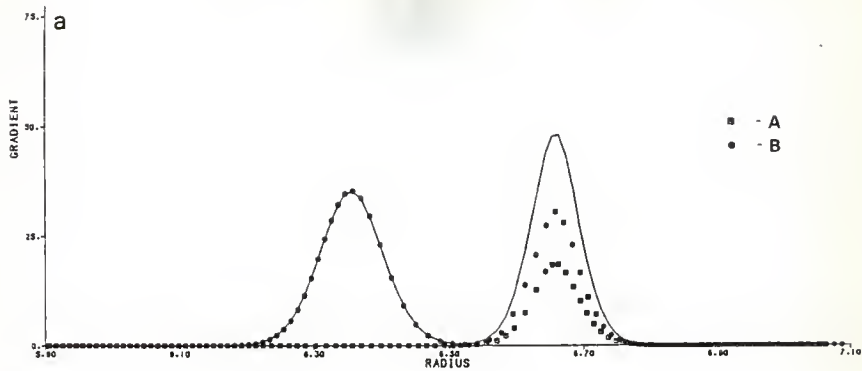
Initial sharp boundary position (r_0) = 6.0 cm.

$$\Delta t = 2155.51 \text{ sec}$$

a. no self association

b. $K_{B_2} = 5.0 \times 10^3 \text{ M}^{-1}$

c. $K_{B_2} = 2.5 \times 10^4 \text{ M}^{-1}$



3.7 EFFECT OF NON-INTERACTING CONTAMINANTS

Occasionally one or both of the constituent solute samples used to prepare a mixture for the ultracentrifuge cell may be contaminated with inactive monomer and/or fixed dimer. Inactive (crippled) monomer may be generated during extraction by procedures that can alter the conformation or chemical specificity of the protein's binding site(s). Fixed dimer and other fixed self aggregates usually result from formation of disulfide bonds.

Since the presence of non-interacting species, in a sample consisting of given total amounts of A and B, lowers the concentration of reactive constituents in the mixture (ie. the effective constituent concentrations), it follows that the initial distribution of reactive constituents among the monomer and aggregate species would be different for preparations with different proportions of inactive species. It should not be surprising, therefore, that the presence of either fixed dimer or crippled monomer have noticeable effects on the shape of a system's gradient profile.

Gradient profiles of AB_2 systems with various amounts of non-interacting species (monomer or dimer) were studied using the distorted grid simulation program for mixed associating systems modified to include a third channel of non-interacting contaminant. The modified program accounts for cross hydrodynamic dependences between the contaminant and the reactive constituents as well as self hydrodynamic dependence for the contaminant.

3.7.1 Fixed Dimer

Simulated profiles for preparations of an uncooperative AB_2 system with different amounts of fixed dimer in the constituent A component and the constituent B component of the mixture are shown in figures 62 and 63.

With the transfer of part of the total constituent A concentration to fixed A_2 (fig. 62), the trailing boundary, which consists of free A, becomes smaller as excess reactive A is depleted.

Transferring part of constituent B to fixed dimer (fig. 63), on the other hand, increases the trailing boundary's size - probably by freeing more of constituent A.

The height of the leading boundary is also changed in opposite directions by the presence of fixed A_2 and fixed B_2 . As the fraction of fixed A_2 is increased the resulting increase in the size of the non-interacting dimer boundary, which sediments just inside or below the trailing edge of the leading reactive constituent boundary, increases the height of the total leading boundary. When the fraction of fixed B_2 is increased the gain in the leading boundary height due to the dimer boundary is outweighed by a reduction in size due to a "transfer" of constituent A from the reaction boundary to the trailing boundary. Depleting reactive B increases excess reactive A, and the net effect is a slight decrease in leading boundary height.

Figure 62: Effect of Fixed A_2 on the Boundary of an Uncooperative AB_2 System.

$$K_I = 1.0 \times 10^5 \text{ M}^{-1}$$

$$W_A = 100 \text{ Kd}$$

$$W_B = 100 \text{ Kd}$$

$$C_{AT} = 5.0 \text{ mg/ml}$$

$$C_{BT} = 5.0 \text{ mg/ml}$$

$$[A] = 5 \times 10^{-5} \text{ M}$$

$$[B] = 5 \times 10^{-5} \text{ M}$$

$$[B]/[A] = 1.0$$

Frictional ratios (f/f_0) for all species = 1.1

All self and cross hydrodynamic constants (k) = 0.01

Species transport coefficients are given in table 2

Dimer transport coefficients are the same as for AB

Rotor speed = 60,000 rpm.

Initial sharp boundary position (r_0) = 6.0 cm.

$$\Delta t = 1357.91 \text{ sec}$$

- a. no fixed A_2
- b. 0.5 mg/ml (of total C_{AT}) present as fixed A_2
- c. 1.0 mg/ml (of total C_{AT}) present as fixed A_2

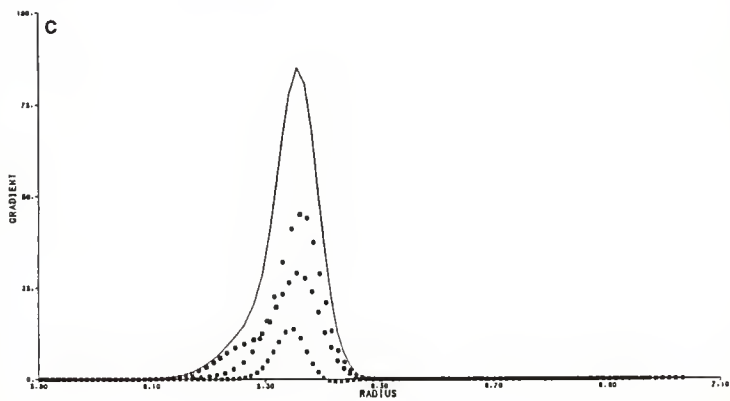
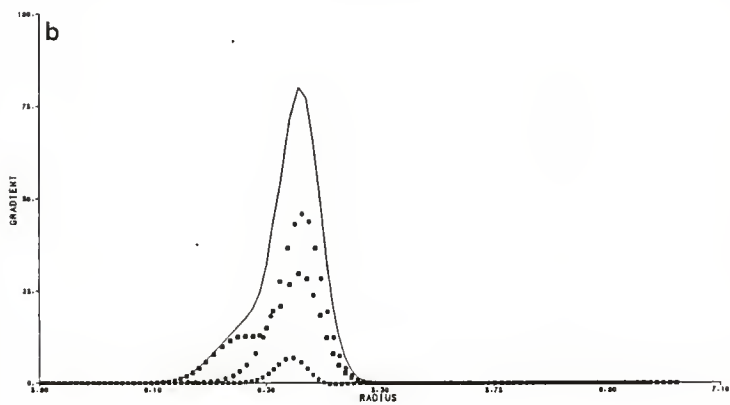
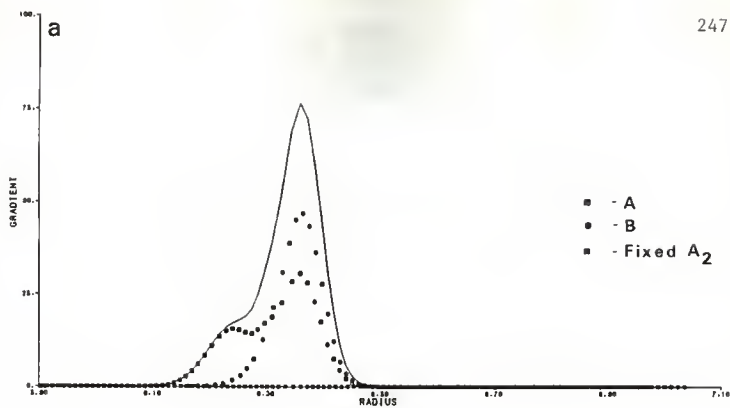


Figure 63: Effect of Fixed B_2 on the Boundary of an Uncooperative AB_2 System.

$$K_I = 1.0 \times 10^5 \text{ M}^{-1}$$

$$W_A = 100 \text{ Kd}$$

$$W_B = 100 \text{ Kd}$$

$$C_{AT} = 5.0 \text{ mg/ml}$$

$$C_{BT} = 5.0 \text{ mg/ml}$$

$$[A] = 5 \times 10^{-5} \text{ M}$$

$$[B] = 5 \times 10^{-5} \text{ M}$$

$$[B]/[A] = 1.0$$

Frictional ratios (f/f_0) for all species = 1.1

All self and cross hydrodynamic constants (k) = 0.01

Species transport coefficients are given in table 2

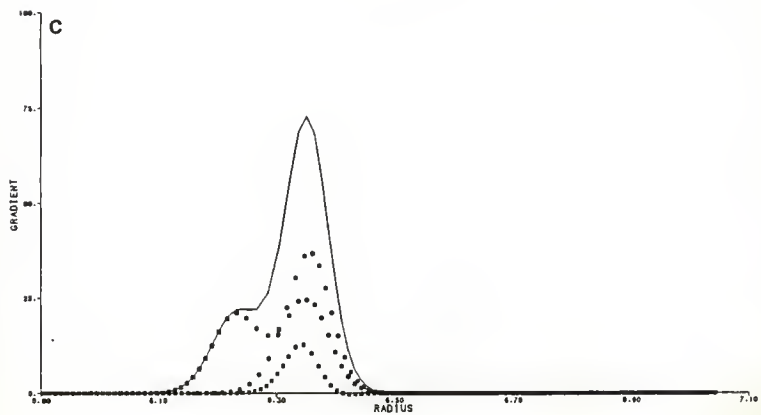
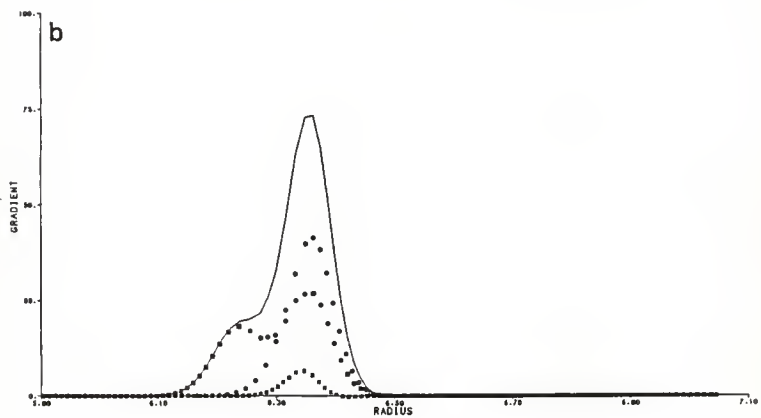
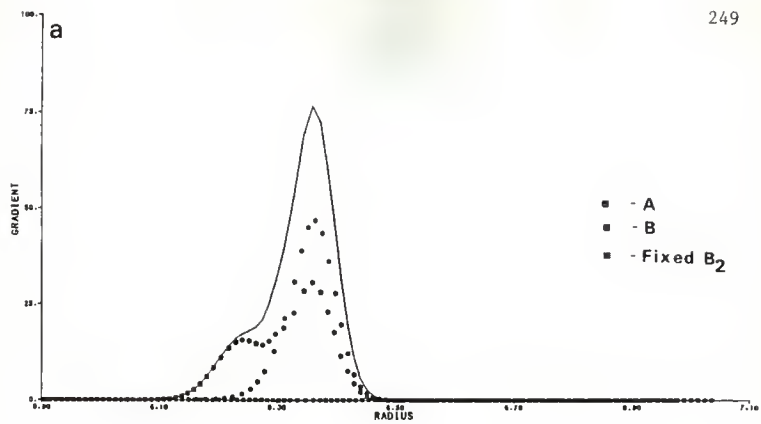
Dimer transport coefficients are the same as for AB

Rotor speed = 60,000 rpm.

Initial sharp boundary position (r_0) = 6.0 cm.

$\Delta t = 1357.91 \text{ sec}$

- a. no fixed B_2
- b. 0.5 mg/ml (of total C_{BT}) present as fixed B_2
- c. 1.0 mg/ml (of total C_{BT}) present as fixed B_2



Contamination of either A or B with fixed dimer decreases the average sedimentation rate of the leading boundary. The individual constituent and fixed dimer boundaries show that this decrease is due to the contribution of the slower dimer boundary to the total leading boundary rather than a change in the sedimentation rates of the leading reactive constituent boundaries.

The unusual appearance of a negative gradient in the non-interacting dimer profiles of these systems probably arises because of the large A and B gradients in that area, which would result in a sharp decrease in the effective sedimentation coefficient of the dimer, causing a pile-up of dimer behind the reaction boundary (ie. a Johnston-Ogston effect).

3.7.2 Crippled Monomer

Simulated profiles of preparations of an uncooperative AB_2 system with various amounts of inactive A and B monomer are shown in figures 64 and 65. With constituent A initially in excess ($C_{AT}=C_{BT}= 5.0$ mg/ml), as the fraction of crippled A monomer is increased, the crippled A boundary, which sediments at the same rate as the noncrippled A monomer boundary, becomes progressively larger, while the reactive A monomer boundary becomes progressively smaller. The net result is no effect on the trailing boundary size. Increasing the fraction of crippled B monomer (with A initially in

excess) increases the amount of excess A. This, along with the increase in the contribution, to the trailing boundary, of the crippled B monomer boundary, results in a sharp increase in the total size of the trailing boundary.

The presence of either crippled A or B reduces the size and average sedimentation rate of the leading boundary - probably by shifting the equilibrium of non-crippled components toward the smaller species (AB, A and B).

Since the presence of crippled species affects boundary sizes and positions, failure to recognize or consider their presence could lead to faulty interpretations of the observed schlieren patterns and make modelling very difficult. Fortunately the presence of fixed dimer can usually be detected in the schlieren patterns of the individual constituent samples and the fraction of dimer can be determined either directly from area measurements or indirectly by modelling and simulation. When the contaminant is crippled or inactive monomer, however, its presence is less likely to be recognized beforehand, as it has no effect on the schlieren patterns of the monomer samples. If the monomers are undergoing reversible self association then it might be possible to determine the presence and quantity of crippled monomer from modelling studies with the individual constituent preparations at different concentrations. If the amount of crippled monomer cannot be assessed prior to modeling the mixed system then erroneous models might be put forth for

Figure 64: Effect of Crippled A Monomer on the Boundary of an Uncooperative AB_2 System.

$$K_I = 1.0 \times 10^5 \text{ M}^{-1}$$

$$W_A = 100 \text{ Kd}$$

$$W_B = 100 \text{ Kd}$$

$$C_{AT} = 5.0 \text{ mg/ml}$$

$$C_{BT} = 5.0 \text{ mg/ml}$$

$$[A] = 5 \times 10^{-5} \text{ M}$$

$$[B] = 5 \times 10^{-5} \text{ M}$$

$$[B]/[A] = 1.0$$

Frictional ratios (f/f_0) for all species = 1.1

All self and cross hydrodynamic constants (k) = 0.01

Species transport coefficients are given in table 2

Rotor speed = 60,000 rpm.

Initial sharp boundary position (r_0) = 6.0 cm.

$\Delta t = 2155.51 \text{ sec}$

- a. no crippled A monomer
- b. 0.5 mg/ml (of total C_{AT}) present as crippled A monomer
- c. 1.0 mg/ml (of total C_{AT}) present as crippled A monomer

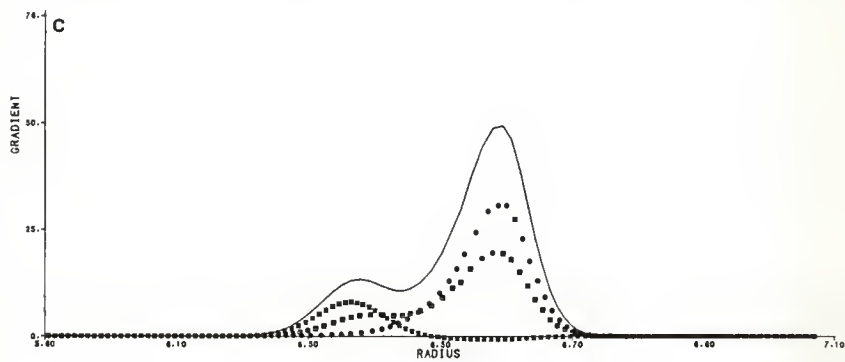
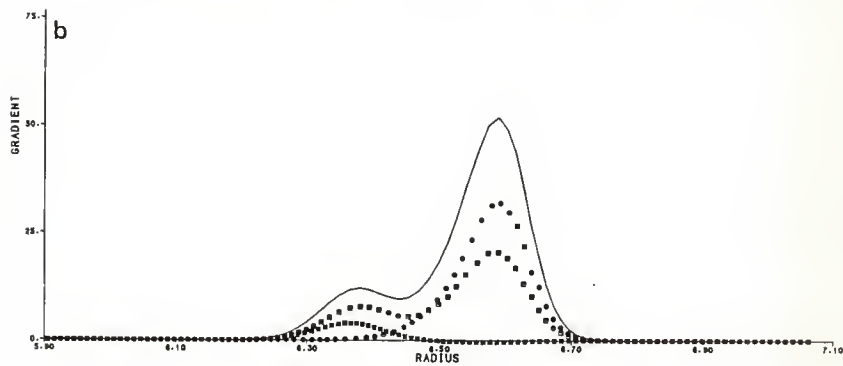
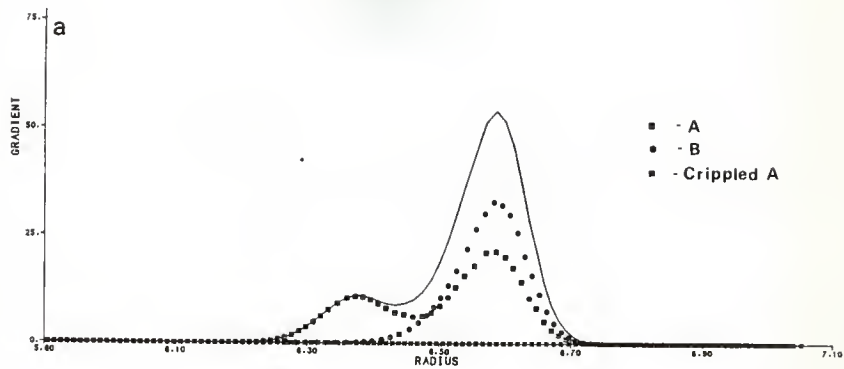


Figure 65: Effect of Crippled B Monomer on the Boundary of an Uncooperative AB_2 System.

$$K_I = 1.0 \times 10^5 \text{ M}^{-1}$$

$$W_A = 100 \text{ Kd}$$

$$W_B = 100 \text{ Kd}$$

$$C_{AT} = 5.0 \text{ mg/ml}$$

$$C_{BT} = 5.0 \text{ mg/ml}$$

$$[A] = 5 \times 10^{-5} \text{ M}$$

$$[B] = 5 \times 10^{-5} \text{ M}$$

$$[B]/[A] = 1.0$$

Frictional ratios (f/f_0) for all species = 1.1

All self and cross hydrodynamic constants (k) = 0.01

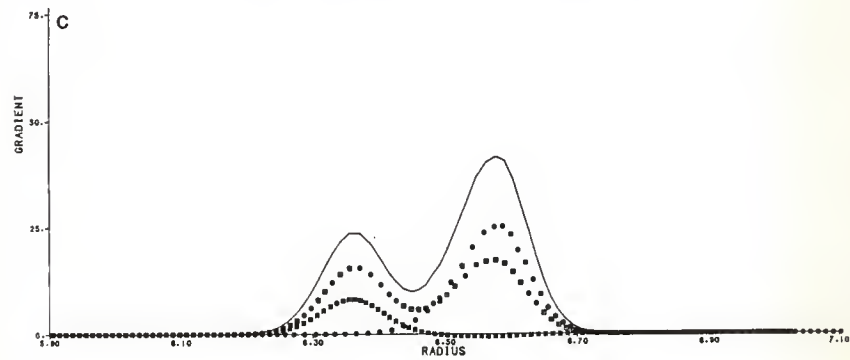
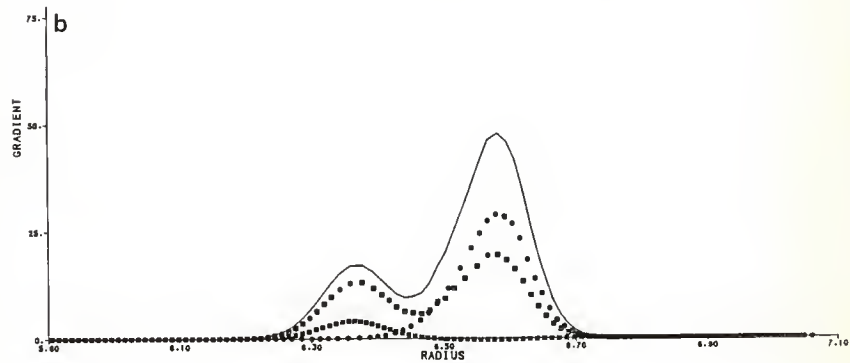
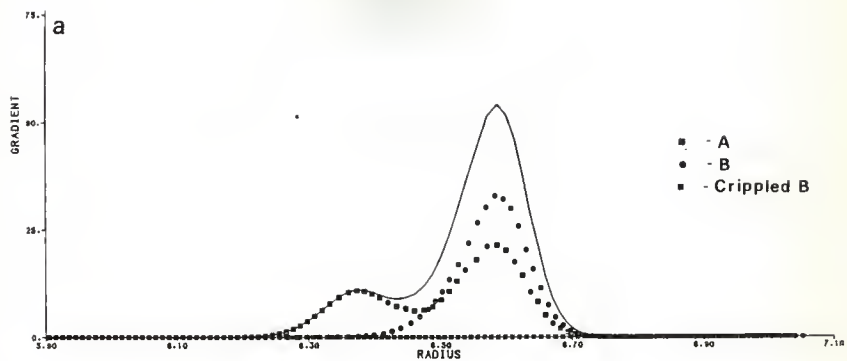
Species transport coefficients are given in table 2

Rotor speed = 60,000 rpm.

Initial sharp boundary position (r_0) = 6.0 cm.

$$\Delta t = 2155.51 \text{ sec}$$

- a. no crippled B monomer
- b. 0.5 mg/ml (of total C_{BT}) present as crippled B monomer
- c. 1.0 mg/ml (of total C_{BT}) present as crippled B monomer



the underlying reactive system. However, since the concentrations of crippled monomers vary linearly with the total concentrations and the distribution of active constituents among the various species does not, it seems unlikely that an erroneous reaction model (not accounting for crippled monomer) would give adequate matches to the real data at more than a few select constituent ratios.

Chapter IV

DISCUSSION

In general, we can conclude that, under many circumstances, it will be possible to distinguish between various plausible models for an AB_2 system by comparing simulated velocity sedimentation profiles of the suspected models with that of the real system. Specifically, when everything about a system that affects its behavior during velocity sedimentation (i.e. boundary shape),¹⁹ except for the values of the association constants, are known, then it should be possible to discover the values of the association constants by trial and error modelling and simulating.

It has also been shown that, in some instances, it will be possible to differentiate between AB_n systems with different overall stoichiometries (AB_2 , AB_3 and AB_4 ,). Specifically, if the (AB_n) system is noncooperative, and the stoichiometry and intrinsic association constant (K_I) are the only unknowns, then it should be possible to identify the correct stoichiometry and K_I simultaneously. In addition,

¹⁹ The important variables that contribute to the boundary shape for a rapidly relaxing AB_2 system are: 1. the association constants, K_1 and K_2 , 2. the molecular weights and partial specific volumes of the monomers, 3. the frictional ratios of each species, 4. the hydrodynamic dependencies of the sedimentation coefficients and 5. the concentrations of inactive species in the preparation used in the ultracentrifuge run.

it has been shown that cooperative AB_2 and AB_4 systems have boundaries that are generally different from one another, as well as from the boundaries of noncooperative AB_2 and AB_4 systems. Actually, strictly speaking, we have shown only that these distinctions can be made when the systems have a particular set of properties ($\bar{W}_A = \bar{W}_B = 100Kd.$, all $f/f_0 = 1.10$, all hydrodynamic constants, $k_{ij} = 0.01$, and no inactive contaminants or self association.), and it is not at all unlikely that systems with a different set of properties would be less distinguishable. Lower molecular weights and larger frictional ratios would be particularly likely to make modelling more difficult since both would tend to obscure the distinctive bimodal features of a migrating boundary.

Of course, as a general rule, the more that is already known about the system before attempting to model velocity sedimentation the more likely it is that such modeling studies will resolve the residual ambiguity and identify or confirm a single model as the correct one.

In particular, it is likely to be necessary to carry out thorough modelling studies with the individual constituents before attempting to obtain an unambiguous result for mixed systems.

Usually there will be some uncertainty about several of the variables other than the association constants, that influence sedimentation behavior, the most troublesome of

which, for our purposes, would probably be the aggregate frictional ratios, the concentrations of inactive species, particularly monomer, and the cross hydrodynamic dependencies. When these things are not known accurately it may be necessary to settle, in the end, for a range of possible models for the system, since these variables affect the same structural features of the gradient profile that reflect the values of the association constants (the heights, widths, and migration rates of the boundaries). It is therefore important that every effort be made to define plausible ranges that are as narrow as possible for all of the variables, including the association constants, before attempting to model the velocity sedimentation behavior of the mixed system. Thorough velocity sedimentation-modelling studies of the individual components should be completed first. The transport properties of the monomers, self-association constants, and the concentrations of inactive species will usually be easier to obtain from modeling studies with the monomers than they will from studies with the mixed system.

In practical situations, additional information is usually available from other techniques, particularly from such thermodynamic equilibrium techniques as sedimentation equilibrium, light scattering and osmometry. A correct physical description of a real system must be consistent with the results of both transport and equilibrium experiments. Neither category of data alone will usually suffice to define any but the simplest real system.

The present work has shown, however, that transport experiments can radically narrow the range of acceptable models for a real system. Fitting a real sedimentation velocity profile precisely in every respect - the number, velocity, height and width of subsidiary boundaries - is quite difficult to do. Fitting is particularly difficult when an acceptable model must be consistent with the behavior of the individual constituents and must describe the mixed system at several constituent ratios. That difficulty confirms the power of the simulation technique to distinguish correct from incorrect models.

REFERENCES

1. P. D. Jeffrey (1981) in "Protein-Protein Interactions", (C. Frieden and L. W. Nichol, Eds.) J Wiley and Sons, New York, pp. 213-256.
2. G. A. Gilbert, Discnss. Faraday Soc. 20, 68 (1955).
3. G. A. Gilbert, Proc. R. Soc. A250, 377 (1959).
4. G. A. Gilbert and R. C. Jenkins, Proc. R. Soc. A253, 420 (1959).
5. J. L. Bethune and G. Kegeles, J. Phys. Chem. 65, 1761, (1961).
6. J. L. Bethune J. Phys. Chem. 74, 3837, (1970).
7. J. L. Bethune and P. J. Grillo, Biochemistry 6, 796, (1967).
8. B. J. McNeil, L. W. Nichol, and J. L. Bethune, J. Phys. Chem. 74, 3846 (1970).
9. D. F. Oberhauser, J. L. Bethune, and G. Kegeles, Biochemistry 4, 1878 (1965).
10. G. Kegeles, L. Rhodes, and J. L. Bethune, Proc. Natl. Acad. Sci. USA 58, 45 (1967).
11. G. Kegeles, and M. L. Johnson, Arch. Biochem. Biophys. 141, 59 (1970).
12. G. Kegeles, and M. L. Johnson, Arch. Biochem. Biophys. 141, 63 (1970).
13. J. R. Cann and W. B. Goad, J. Biol. Chem. 240, 148 (1965).
14. J. R. Cann, Interacting Macromolecules, Academic Press, New York, 1970
15. W. B. Goad and J. R. Cann, Ann. N. Y. Acad. Sci. 164, 172 (1969).
16. J. R. Cann and W. B. Goad, J. Biol. Chem. 240, 1162 (1965).

17. J. R. Cann, Biophys. Chem. 1, 1 (1973).
18. J. R. Cann and N. D. Hinman, Biochemistry 15, 4614 (1976).
19. J. R. Cann and D. I. Stimpson, Biophys. Chem. 7, 103 (1977).
20. J. R. Cann and G. Kegeles, Biochemistry 13, 1868 (1974).
21. D. I. Stimpson and J. R. Cann, Biophys. Chem. 7, 115 (1977).
22. J. R. Cann and K. J. Gardiner, Biophys. Chem. 10, 211 (1979).
23. M. Dishon, G. B. Weiss, and D. A. Yphantis, Biopolymers 4, 449 (1966).
24. M. Dishon, G. B. Weiss, and D. A. Yphantis, Biopolymers 4, 457 (1966).
25. I. B. Billick, M. Dishon, M. Schulz, G. B. Weiss, and D. A. Yphantis, Proc. Natl. Acad. Sci. USA 56, 399 (1966).
26. I. B. Billick, M. Dishon, G. B. Weiss, and D. A. Yphantis, Biopolymers 5, 1021 (1967).
27. M. Dishon, G. B. Weiss, and D. A. Yphantis, Biopolymers 5, 697 (1967).
28. M. Dishon, G. B. Weiss, and D. A. Yphantis, Biopolymers 10, 2095 (1971).
29. D. J. Cox, Arch. Biochem. Biophys. 112, 249 (1965)
30. D. J. Cox, Arch. Biochem. Biophys. 112, 259 (1965)
31. D. J. Cox, Arch. Biochem. Biophys. 119, 230 (1967)
32. D. J. Cox, Arch. Biochem. Biophys. 129, 106 (1969)
33. D. J. Cox, Arch. Biochem. Biophys. 142, 514 (1971)
34. D. J. Cox, Arch. Biochem. Biophys. 146, 181 (1971)
35. D. J. Cox and R. S. Dale in "Protein-Protein Interactions", (C. Frieden and L. W. Nichol, Eds) J. Wiley and Sons, New York, pp. 173-211.
36. J.-M. Claverie, B. Drenx, and R. Cohen, Biopolymers 14, 1685 (1975).

37. R. Cohen and J.-M. Claverie, Biopolymers 14, 1701 (1975).
38. J.-M. Claverie, Biopolymers 15, 843 (1976).

SIMULATION STUDIES OF VELOCITY SEDIMENTATION
FOR MIXED ASSOCIATING SYSTEMS

by

GLEN MICHAEL DELOID

B.S., Kansas State University, 1980

A MASTER'S THESIS

submitted in partial fulfillment of the
requirements for the degree

MASTER OF SCIENCE

Graduate Biochemistry Group
Department of Biochemistry

KANSAS STATE UNIVERSITY
Manhattan, Kansas

1983

The shape of the migrating boundary produced by a reversibly associating system of macromolecules during velocity sedimentation in the ultracentrifuge is generally thought to be a fairly distinctive indicator of the reaction scheme (ie. stoichiometries and association constants) of the system. Computer simulation of velocity sedimentation may be useful in distinguishing between correct and incorrect reaction models when other techniques (eg. sedimentation equilibrium, light scattering, and osmotic pressure) give ambiguous results.

In the present work, velocity sedimentation in the ultracentrifuge was simulated for a variety of AB_n mixed-associating systems using the distorted-grid model of Cox. The predicted sedimenting boundary profiles of these systems were compared in order to evaluate their ability to differentiate among dissimilar systems. We have found that 1) among AB_2 systems boundary shape may be an unambiguous indicator of the values of the association constants K_1 and K_2 , and that 2) among uncooperative AB_n systems boundary shape may be an unambiguous indicator of the stoichiometry and association constant (K_I) of the system. In general, our results indicate that modelling studies of velocity sedimentation data can be a quite effective approach for distinguishing between various plausible models for a real interacting system.